Master's thesis

NTNU
Norwegian University of Science and Technology
Faculty of Engineering
Department of Energy and Process Engineering

Magnus Egerdahl

Integrated thermal system for hydrogen and ammonia driven cruise ship

Master's thesis in Mechanical Engineering
Supervisor: Armin Hafner
Co-supervisor: Muhammad Zahid Saeed
June 2022

NTNU
Kunnskap for ei betre verd

Magnus Egerdahl

Integrated thermal system for hydrogen and ammonia driven cruise ship

Master's thesis in Mechanical Engineering
Supervisor: Armin Hafner
Co-supervisor: Muhammad Zahid Saeed
June 2022

Norwegian University of Science and Technology
Faculty of Engineering
Department of Energy and Process Engineering

NTNU
Kunnskap for en bedre verden

Preface

This report summarize my master's thesis work at the Norwegian University of Science and Technology, Department of Energy and Process Engineering. The report is a continuation of the preliminary project written in autumn 2021. The work was is in collaboration with SINTEF. The aim of the work was to develop and evaluate thermal designs for hydrogen and ammonia driven cruise ships for increased efficiency and reduced emissions. I would like to thank Professor Dr. Armin Hafner, Muhammad Zahid Saeed and Cecilia Gabrielii for guidance and help throughout this master's thesis.

Norwegian University of Science and Technology
Trondheim, June 2022

Magnus Egerdahl

Abstract

The cruise ship industry is facing emission regulations due to climate change and global warming. Traditional fossil fuels consumed for propulsion and energy demands onboard cruise ships result in a high carbon footprint. Hydrogen and ammonia are therefore investigated as possible future marine fuels for environmentally friendly cruise ships. Along with eco-friendly and energy-efficient propulsion systems will effort towards thermal systems onboard have a significant impact on cruise ship emissions and energy efficiency. The refrigeration systems account for a large degree of emissions due to refrigerants of high global warming potential (GWP). CO_2 was therefore investigated as a refrigerant due to excellent thermophysical properties and low GWP. High temperature exhaust gas is wasted into the atmosphere with a large potential for thermal energy recovery. Waste heat recovery was therefore investigated with the possibilities of generating electricity in a bottoming power cycle and recovering heat for thermal demands onboard. Thermal boilers and auxiliary engines emit large quantities of pollutants during port stay. Thermal energy storage was therefore investigated storing thermal heat from waste heat exhaust gas and cold thermal energy from regasification of liquid hydrogen (LH_2), providing thermal demands with zero emissions. Cold recovery of LH_2 was also investigated for the potentials of reducing refrigeration system capacity.

This aim of this master's thesis was to investigate thermal systems of hydrogen and ammonia driven cruise ships for increased energy efficiency at reduced emissions. Two design cases was developed operating with hydrogen and ammonia as fuel. Simulation models using Dymola/Modelica was developed evaluating fuel saving and emission reduction of the proposed thermal designs.

The results from the CO_2 refrigeration models showed that the COP could be increased by 10.13% in a transcritical ejector cycle in comparison to a traditional subcritical R134a cycle. The proposed system not only increase efficiency but also operates with near zero emissions. Waste heat recovery using a CO_2 recuperative rankine cycle showed promising results, contributing as high as 14.48% of the total electrical demand in the hydrogen design case and 6.42% in the ammonia design case. This contributed to fuel saving and emission reduction. Heat recovery of exhaust gas was able to cover 100% of the heating demand in the hydrogen design case and 56.13% in the ammonia design case, significantly reducing emissions from thermal boilers. Integrating thermal energy storage (TES), the hydrogen design case could provide 100% of the heating demand during port stay whereas the ammonia design case was capable of providing 46.2%, significantly reducing pollutants amongst the harbour. Through cold recovery of LH_2, 17.22% of the cooling demand could be contributed reducing refrigeration system capacity, emissions and saving fuel. The results also found that 100% of the cooling demand could be provided at zero emissions recovering LH_2 in a cold thermal energy storage (CTES) tank of 57.1 m^3.

Sammendrag

Cruiseskipindustrien står overfor utslippsreguleringer på grunn av klimaendringer og global oppvarming. Tradisjonelt fossilt drivstoff som brukes til fremdrift og energibehov ombord på cruiseskip resulterer i et høyt karbonavtrykk. Hydrogen og ammoniakk utredes derfor som mulig fremtidige marine drivstoff for miljøvennlige cruiseskip. Sammen med miljøvennlige og energieffektive fremdriftssystemer vil innsatsen mot termiske systemer om bord ha en betydelig innvirkning på cruiseskipets utslipp og energieffektivitet. Kjølesystemene står for en stor grad av utslipp på grunn av kjølemedier med høy GWP. CO_2 ble derfor undersøkt som kjølemedie på grunn av utmerkede termofysiske egenskaper og lav GWP. Høytemperatur eksosgass slippes ut i atmosfæren med et stort potensial for termisk energigjenvinning. Spillvarmegjenvinning ble derfor undersøkt med muligheter for å generere elektrisitet i en rankine-syklus og gjenvinne varme for termiske behov ombord. Termiske kjeler og hjelpemotorer slipper ut store mengder forurensning under havneopphold. Termisk energilagring ble derfor undersøkt med lagring av termisk varme fra spillvarme eksosgass og kald termisk energi fra regassifisering av flytende hydrogen, da med muligheten til å forsyne termiske behov med null utslipp under havneopphold. Kaldgjenvinning av flytende hydrogen ble også undersøkt med tanke på potensialet for å redusere kjølesystemets kapasitet.

Målet med denne masteroppgaven var å undersøke termiske systemer av hydrogen- og ammoniakkdrevne cruiseskip for økt energieffektivitet ved reduserte utslipp. Det ble utviklet to designtilfeller som opererer med hydrogen og ammoniakk som drivstoff. Simuleringsmodeller med Dymola/Modelica ble utviklet for å evaluere drivstoffbesparelse og utslippsreduksjon av de foreslåtte termiske systemene.

Resultatene fra CO_2-kjølemodellen viste at COP'en kunne økes med 10,13% i en transkritisk ejektorsyklus sammenlignet med en tradisjonell subkritisk R134a-syklus. Det foreslåtte systemet øker ikke bare effektiviteten, men opererer også med nær null utslipp. Gjenvinning av spillvarme ved bruk av en transkritisk CO_2 rankine-syklus viste lovende resultater, og genererte så høyt som 14,48% av det elektriske behovet i hydrogen modellen og 6,42% i ammoniakk modellen. Dette bidro til drivstoffbesparelse og utslippsreduksjon. Varmegjenvinning av eksosgass var i stand til å dekke 100% av oppvarmingsbehovet i hydrogen modellen og 56,13% i ammoniakk modellen, noe som reduserte utslippene fra termiske kjeler betydelig. Ved å integrere lagring av termisk energi, kunne hydrogen modellen forsyne 100% av varmebehovet under havneopphold, mens ammoniakk modellen var i stand til å forsyne 46,2%, noe som betydelig reduserte forurensninger i havnen. Gjennom kaldgjenvinning av flytende hydrogen kunne 17,22% av kjølebehovet forsynes. Dette resulterte i redusert kapasitet i kjølesystemet og besparelse av drivstoff. Resultatene fant også at 100% av kjølebehovet under havneopphold kunne forsynes med null utslipp ved å lagre kulde fra flytende hydrogen i en termisk energitank på 57,1 m^3.

Contents

Nomenclature

HVAC	Heating, ventilation, and air conditioning
CO_2	Carbon dioxide
NO_x	Nitrogen oxide
SO_x	Sulphur oxide
TES	Thermal energy storage
CTES	Cold thermal energy storage
GWP	Global warming potential
COP	Coefficient of performance
$COP_{Ideal\ Ref}$	COP ideal refrigeration
$COP_{Ideal\ HP}$	COP ideal heat pump
η	Cycle efficiency
CFC	Chlorofluorocarbon
HCFC	Hydrochlorofluorocarbons
HFC	Hydrofluorocarbon
ODP	Ozone depletion potential
EES	Engineering equation solver
IHX	Internal heat exchanger
GHG	Greenhouse gas
HFO	Heavy fuel oil
LNG	Liquid natural gas
MDO	Marine diesel oil
IMO	International maritime organization
RPM	Revolutions per minute
ICE	Internal combustion engine
SI	Spark ignition
CI	Compression ignition
AF	Stoichiometric air-fuel ratio
LHV	Lower heating value
λ	excess air factor
WHR	Waste heat recovery
SRC	Steam rankine cycle
ORC	Organic rankine cycle
KC	Kalina cycle
LH_2	Liquid hydrogen
GH_2	Gaseous hydrogen
NH_3	Ammonia
MW	Megawatt
AHU	Air-handling unit
EER	Energy efficiency ratio
AB	Auxiliary boiler
PCM	Phase-change material
HTWH	High temperature water heater
HRSG	Heat recovery steam generator
CW	Cooling water
3WV	Three-way valve

List of Figures

List of Tables

1 Introduction

1.1 Background

Summer of 2019, the cruise ship industry was thriving in a growing market with hundreds of thousands of cruise tourists visiting Norway and exploring the world. As the Covid-19 pandemic struck the world, the cruise ship industry met a standstill. This led to a great opportunity for the cruise ship industry to take charge of the environmental footprint of the industry, and be part of the global environmental transition. The cruise ship industry is energy intensive, corresponding to 8% of the total energy consumption used for transportation in Norway. Traditionally, this large energy demand onboard the cruise ship is met through combustion of fossil fuels. This results in a high carbon footprint in the cruise ship industry.[1]

The international maritime organization (IMO) has therefore circulated guidance and proposed environmental restrictions in order to reduce emissions from cruise ships. One of these regulations include the reduction of greenhouse gas emissions by 50% by 2050, compared to emissions of 2008. Other restrictions include zero emission from cruise ships along EU harbour and ports by 2030. The Norwegian Parliament has also proposed the regulation of zero emissions from cruise ships and ferries in the World Heritage fjords. Efforts towards more environmentally friendly and zero emission cruise ships must therefore be investigated.[2]

The CruiZE project - Cruising towards Zero Emissions, started year 2020. The goal of the project precisely is to investigate the necessary energy efficient technologies for a more environmentally friendly cruise ship industry. The objectives are to investigate heating and cooling concepts enabling minimal emissions from cruise ships. This include thermal energy storage, propulsion waste heat recovery, HVAC, provision cooling and fresh water production.[1]

1.2 Objectives

In this master's thesis the following tasks are to be considered:

- Review of relevant literature e.g., Refrigeration system for cruise ship, thermal management of hydrogen and ammonia as a fuel for engines, and the potential for thermal energy storage.
- Describe and develop models representing the energy systems of a cruise ship
- Develop skills in Modelica/Dymola modelling environment.
- Perform simulations of the different parts of the energy system.
- Analyze and discuss the results in terms of system performance, energy consumption and thermal energy storage potential/demand.
- Write a report including chapters discussion, summary, and proposal for further work.
- Create a draft scientific paper related to the findings of the Master Thesis.

The first part of this master's thesis provides an overview of the comfort and energy demands onboard cruise ships. The thesis then provides a basic understanding of refrigeration systems and the implication of CO_2 as a working fluid for cruise ship. Hydrogen and ammonia is then studied as marine fuels for propulsion, utilizing internal combustion engines. Waste heat recovery in terms of thermal management of the marine fuels is at last studied with the integration of TES.

2 Background

This chapter will provide an overview of the topics investigated in this Master thesis. The literature provided in this section is a continuation of the preliminary project work of autumn 2021 which is expanded and improved.

2.1 Cruise ships

Cruise ships are among the most challenging engineering systems, requiring expertise from many different fields of study. Passengers onboard a cruise ship are provided a very high standard of living resulting in large power demands. Cruise ships are often equipped with luxuries such as spas, swimming pools, wellness centers, restaurants and bars. These services are provided while the cruise ship operates autonomous, where all power is generated onboard. The general forms of energy required onboard a cruise ship can be divided into mechanical, electrical and thermal energy.[3] What all these have in common is that all energy forms are provided through combustion of fossil fuels.

As environmental restrictions and climate change are pressuring the cruise ship industry to become more environmentally friendly, will operators have look to alternative fuels. The restrictions set to lower emissions include, reduction in carbon dioxide, and the pollutants nitrogen oxide (NO_x) and sulphur oxide (SO_x). Two of the alternative fuels that could meet the emission restrictions while maintaining the large power demand onboard are hydrogen and ammonia. These fuels and the methods of energy generation will be investigated throughout this master thesis.[4]

2.1.1 Energy systems

Figure 1 presents the traditional layout of the systems providing the three main energy demands of mechanical, electrical and thermal energy onboard passenger ships. The mechanical energy refers to the power required to propel the cruise ship during maneuvering and cruising by the use of diesel internal combustion engines (ICE's). The ICE's are then coupled to gearboxes regulating the propulsive power of the ship. Similar internal combustion engines can be found for electricity generation. Diesel auxiliary internal combustion engines are then coupled with generators to generate electricity onboard, with no connection to shore. As with the main ICE's, the mechanical efficiency of such diesel engines can be up to 50% while generator efficiency can be up to 95%.[5]

In the case of thermal energy requirements, are waste heat recovery and auxiliary boilers the most commonly used methods. Hot engine cooling water or waste heat from exhaust gas from main engines or auxiliary engines may be used to produce hot water at a desirable temperature of 90 °C for the heating demand. This concept requires no additional fuel consumption. When thermal demand is larger than energy provided from waste heat recovery, boilers are used. These providing thermal energy through combustion of fuels.[6] According to Baldi et al. will exhaust waste heat recovery fulfill almost 75% of total thermal energy demand, which leaves about 25% of the remaining demand to auxiliary boilers.[7] Boilers are typically fired using heavy fuel oils (HFO) with thermal efficiencies of about 80%.[3]

The cooling demands of air-condition and provision cooling are met by compression chillers. Compression chillers consuming large amounts of electricity generated by auxiliary diesel engines. For air-conditioning, the compression chiller cools water which is transported to decentralized ventilation units. These units are called air-handling units (AHU), and provide cool air to several cabins throughout the cruise ship.[8] The efficiency of the compression chillers have a

large impact of the total power consumption required to meet the cooling demands. Along with emission restrictions of combustion fuels for propulsion will refrigeration refrigerants also need to change. Refrigerants of high GWP and ozone depletion potential (ODP) must be changed for environmentally friendly alternatives. An attractive alternative working fluid for refrigeration systems onboard cruise ships is CO_2. The basic principle of a refrigeration cycles and the benefits of CO_2 will be examined in this thesis.

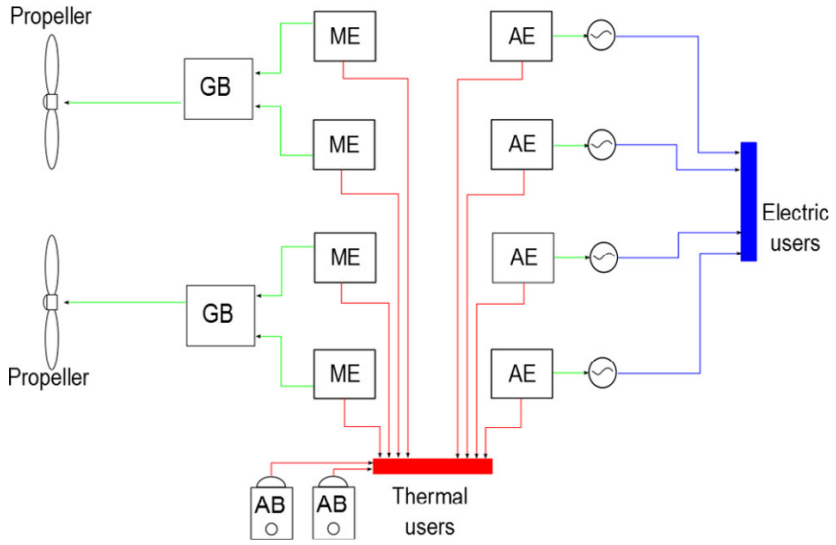

Figure 1: Schematic of energy systems onboard cruise ships [9]

Future energy systems of passenger ships tend towards so-called hybrid propulsion systems, interconnecting the main engines and auxiliary engines for electricity generation only. The internal combustion engines thus generate electricity for common electrical demand onboard the ship but also to electrical powered propulsive engines. Waste heat recovery of such systems then comes from one set of ICE's. The optimization of these energy systems will be further investigated throughout this thesis.[3]

2.2 Refrigeration cycles

2.2.1 Refrigeration history

During the pre-industrial era, people seeked cooling through natural means of ice and snow. The United States had an active role in harvesting natural ice from icy rivers and glaciers in northern states. Along with Norway providing ice blocks in Europe. The ice was transported to warmer countries like India by sailing vessels, insulating the ice using sawdust.[10] During the 1800's, the first mechanical refrigeration system was invented by an American inventor named Jacob Perkins. The first step towards modern refrigeration, Perkins developed a closed cycle utilizing the organic compounds such as ether, CO_2, and ammonia in a vapor-compression system. Due to the matter of high flammability and toxicity of refrigerants, the synthetic working fluid freon became the new standard refrigerant after the 1930's.[11] In 1985, scientists discover that the synthetic working fluids was harming the environment and ozone layer highlighting the necessity to phase out high ODP refrigerants. Today, refrigeration cycles have turned back to natural refrigerants such as CO_2.[12]

2.2.2 Refrigeration principles

Power cycles are based on the principle of heat being received in a working fluid at a high temperature, the working fluid expands and rejects heat at a low temperature. A net amount of work is then done by the working fluid. These cycles can be reversed where heat is received at a low temperature and rejected at a high temperature. Thus, a net amount of work is done on the working fluid through compression. These cycles are called heat pump or refrigeration cycles and are identical in principle, therefore often just referred to as a refrigeration cycle. The purpose of the cycles are to either provide cooling to a given space by extracting heat, or to provide heat at an elevated temperature.[13] The two main refrigeration cycles are vapor-compression and vapor-absorption.[14] This thesis will consider refrigeration vapor-compression cycles as presented in Figure 2.

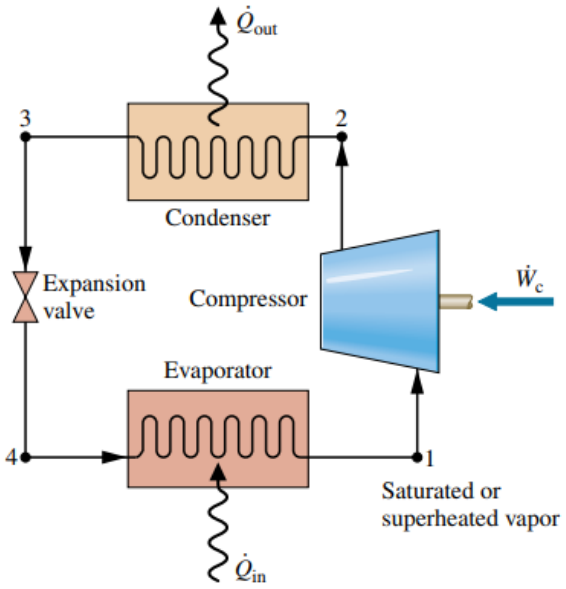

Figure 2: Ideal vapor-compression cycle [14]

Vapor-compression cycles are the most common refrigeration cycles for refrigerators and heat pumps today. As mentioned, the cycle is a closed-loop containing a working fluid, often called refrigerant. For an ideal vapor-compression cycle, certain assumptions must be made. The ideal cycle is based on the reverse Carnot cycle where irreversibilities for the compressor, condenser and evaporator are ignored. Assuming no pressure loss in the heat exchangers and zero heat losses to the surroundings. The refrigerant starts at the inlet of the the compressor as saturated vapor, then is compressed isentropically to a superheated state of high pressure and high temperature (1-2). At constant pressure, the refrigerant rejects heat to a heat sink, de-superheating and condensing the refrigerant to a saturated liquid (2-3). The refrigerant is then expanded in a isenthalpic irreversible throttling process into the two-phase vapor-liquid region accompanying an increase of specific entropy (3-4). Finally, the refrigerant absorbs heat from a source evaporating into a saturated vapor (4-1).[14]

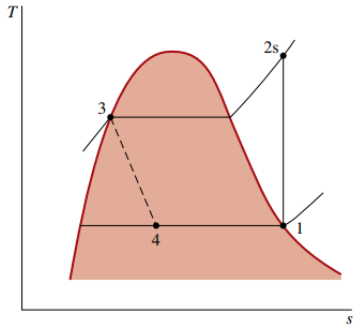

Figure 3: T-S diagram ideal vapor-compression cycle [14]

As seen from Figure 3, in the ideal-vapor compression cycle all processes except throttling process are internally reversible. For an actual vapor-compression cycle this is not the case. In reality the compressor is not internally reversible. This results in a increase in entropy during compression. In practice, the utilization of multi-stage compression with internal cooling can lower entropy increase.[15] For an ideal cycle, the refrigerant is compressed in the right-most two-phase region. This is called wet compression and is in practice avoided. This is due to the fact that liquid droplets can damage compressors. The refrigerant is therefore slightly superheated in the evaporator to ensure dry compression. Pressure drop is not to be avoided either in an actual cycle, resulting in increase of work in the compressor. All assumptions made for the ideal cycle influence the refrigeration performance.[14]

In order to express the performance of a refrigeration cycle, it is common to utilize a power factor describing the ratio between cooling output and input power. This dimensionless factor is called coefficient of performance (COP). Its is useful to calculate the COP of the ideal Carnot cycle as this will give the maximum theoretical performance of a system. As previously mentioned, a real cycle will encounter unavoidable irreversibilities in the system restricting the actual COP to never be equal or greater than ideal COP. Equation 1 and 2 represent the performance of a refrigeration cycle and heat pump cycle, respectively.

$$COP_{Ideal\ Ref} = \frac{Q_{41}}{W} \tag{1}$$

$$COP_{Ideal\ HP} = \frac{-Q_{23}}{W} \tag{2}$$

2.2.3 CO_2 as refrigerant

During the early 1900's carbon dioxide was among the most common refrigerants used for several applications such as air-conditioning and marine refrigeration. As a result of the introduction of synthetic refrigerants in the 1930's, CO_2 was slowly phased out by chlorofluorocarbons (CFC) and hydrochlorofluorocarbons (HCFC) until the 1960's. Over the last decades, the choice of refrigerants for marine applications has been through change as new environmental restrictions has taken place.[16] In 1974, observations of a hole in the ozone layer above Antarctica was made by Molina and Rowland. They discovered a direct connection between ozone layer depletion and refrigerants of CFC.[17] The discovery led to the Montreal Protocol in 1987. The protocol aimed to phase out CFC's and HCFC's by regulating use and production of such chemicals which have a direct impact on the ozone layer. CFC's has currently been phased out by all countries involved in the Montreal protocol. HCFC's have yet to be phased out by 2040. The discovery led to the increased use of hydrofluorocarbons (HFC). HFC's do not deplete the ozone layer but instead

contribute to global warming.[18] This discovery later led to the Kyoto Protocol in 1997, which precisely was initiated to regulate emissions for global warming.[19]

The latest regulations are F-Gas 517/2014. This regulation aims at reducing European supply of HFC's by about 80% within 2030 in comparison to average values of 2010. This goal can be achieved by reducing the average global warming potential for working fluids used today.[20] GWP is a index developed in order to compare global warming impact of various gases. This allows for a common unit of measure in order to estimate reduction in high GWP gases in order to meet regulation goals. CO_2 has by definition a GWP = 1 known as the reference point of all emitted fluids. The higher the GWP is, the larger impact the fluid has on global warming effect relative to CO_2.[21] R134a is one of the most dominant refrigerant for air conditioning on passenger ships today. In 2015, it was reported a total refrigerant leakage of 18.9% of refilled refrigerant for passenger ships in Europe. R134a has a GWP of 1300, which will contribute to global warming.[22] The low GWP and zero ozone depletion potential of the natural working fluid CO_2 is one of the main reasons for the renewed interest today.

Other refrigerants such as propane and ammonia (NH_3) are also great refrigerants considering GWP. However, due to the high toxicity of NH_3 and high flammability of propane is CO_2 the better alternative. CO_2 is classified as A1 safety class, which means that the refrigerant has low toxicity and no flame propagation.[23] In fact, CO_2 is non-toxic, non-flammable and chemically inactive. As a by-product of multiple industrial applications, CO_2 is cheap, readily available and naturally present everywhere in our environment. In 1988, Professor Gustav Lorentzen studied CO_2 cycles concluding excellent thermodynamic properties for CO_2.[24]

Bellos et al. states that CO_2 has a higher thermal conductivity and lower dynamic viscosity compared to other refrigerants. In terms of CO_2 as a transport medium, will CO_2 thereby encounter lower pressure loss and pumping power required resulting in a more compact design. CO_2 has a critical pressure and critical temperature of 73.8 bar and 31.1 °C, respectively. The high operating pressure thus lead to higher energy density. Higher energy density result in higher volumetric heat capacity allowing for sufficient cooling at a more compact design.[24] In fact, Kim et al. states that compressor displacement can be reduced by 80-85% when operating with CO_2 compared to NH_3.[16] Further, compression ratios are low compared to HFC systems. This result in greater isentropic efficiency in the compressors. CO_2 systems operate at a higher pressures which often is correlated with higher explosion risk. However, as CO_2 systems operate at smaller volumes will the overall explosion energy be much like that of systems with lower pressure.[19]

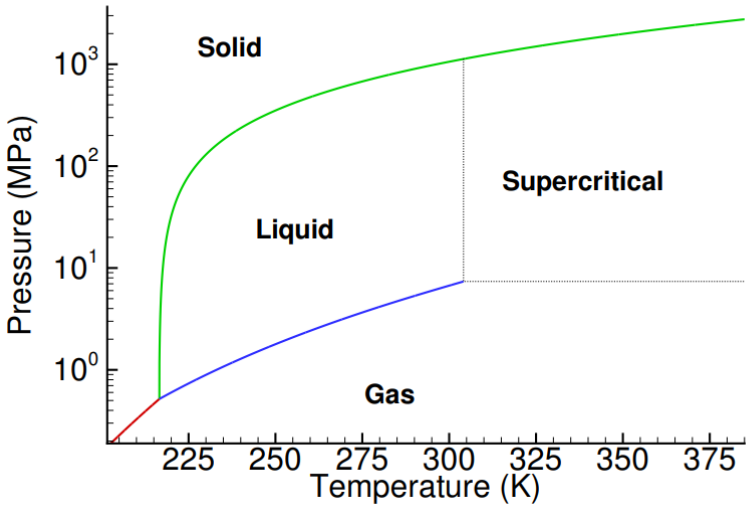

Figure 4: CO_2 Phase-diagram [25]

When operating with CO_2 as a refrigerant for vapor-compression cycles, there are many benefits. However, the critical point and triple point differ significantly from other refrigerants. Therefore, ambient conditions play a big role in CO_2 cycle efficiency compared to conventional systems. As mentioned, the critical pressure and critical temperature is 73.8 bar and 31.1 °C, respectively. Therefore, as ambient temperatures are near or above this low critical temperature, CO_2 is unable to undergo phase-change in a condenser. To be able to operate in such ambient conditions, the system must cycle through a transcritical process where heat rejection occurs in the supercritcal state as presented in Figure 4. A transcritical process operate at realitively high pressure differences. This leads to major efficiency losses during throttling.[19]

2.2.4 Transcritical heat rejection

In the supercritical region there is no liquid formation. In a traditional subcritical process, the high pressure side of the cycle is condensed in a condenser where heat sink temperature influence the condensation pressure and temperature. The refrigerant condenses at constant temperature inside the phase envelope. However, for a transcritical cycle the condenser is replaced by a gas cooler. The gas cooler cools the dense single phase gas in a gliding temperature profile.[19] The pressure is independent of the temperature and no saturation condition exist.[26]

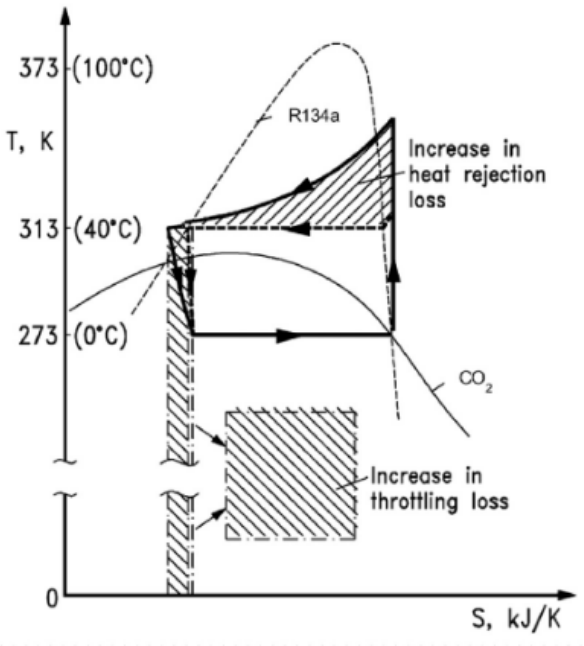

Figure 5: CO_2 and R134a comparison [26]

Yu et al. compares a transcritical CO_2 cycle with a subcritical R134a cycle in the same operating conditions. Heat is absorbed by evaporation of a refrigerant at low pressure. The study assumes equal evaporating temperatures and equal condensing temperature. The results show less efficiency in the CO_2 cycle. This is due to the larger throttling and heat rejection losses observed in Figure 5. The much larger average temperature of CO_2 compared to R134a during gas cooling results in the larger heat rejection loss when the heat rejected is not of interest. Throttling of CO_2 will also encounter a larger entropy increase. This is due to large pressure differences between gas cooler and evaporator. The gliding temperature during gas cooling will in this case not be beneficial compared to the conventional cycle, where R134a experience phase-change during condensation. However, for heat pumping processes and heat recovery processes the gliding temperature is beneficial.[26] As Figure 6 presents, the gliding temperature decrease of CO_2 will result in better matching temperature profiles, consequently, reducing heat rejection

loss. The pinch point of the supercritical heat rejection is then found near the inlet of the cooling medium. Therefore, capable of achieving larger temperatures in the cooling medium in the case of heating applications or heat recovery.

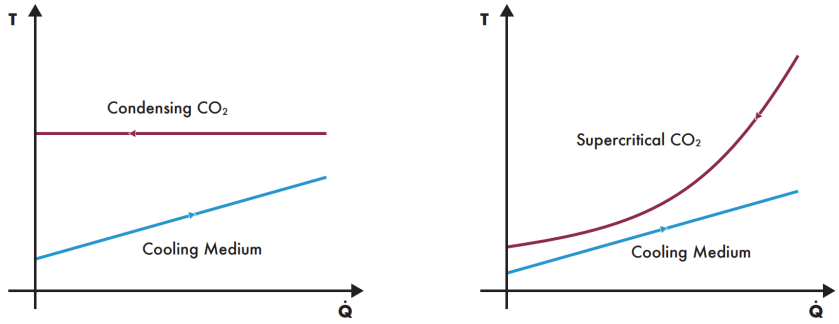

Figure 6: Subcritical and supercritical heat rejection [27]

Kim et al. states that heat rejection at gliding temperature is an advantage for heat pumps. In water or air heating applications, the temperature curves between cooled single-phase CO_2 and heated water will have a better match, thus reducing the thermodynamic losses. Heat rejection from CO_2 to water at a water inlet temperature 10 °C will ideally provide water in the range of 70-80 °C.[16] In terms of efficiency losses for CO_2 will the biggest challenge lie in high pressure throttling, as illustrated in Figure 5. Transcritical CO_2 cycles may operate at 5-6 times higher pressure compared to traditional refrigerants, leading to large entropy increase during throttling.[26] Though transcritical CO_2 cycles show lower efficiency in high ambient temperatures compared to traditional subcritical cycles, has a number of technologies been developed improving the efficiency. Making CO_2 a superior refrigerant for clean and environmentally friendly operations.

2.2.5 Evolution of carbon dioxide refrigeration cycles

So, CO_2 as a refrigerant is proven to have excellent thermodynamic properties such as high specific heat capacity, thermal conductivity, density, latent heat, and low dynamic viscosity compared to HFC's. Nonetheless, CO_2 cycles generally have lower efficiencies compared to HFC refrigeration cycles in warm ambient temperatures. As mentioned, this is due to heat rejection losses from the large temperature glide and high pressure throttling losses. There is therefore a necessity for modifications of the CO_2 cycle in order to reach COP equal or greater than HFC refrigeration cycles. According to Brown et al. a subcritcal R134a refrigeration cycle operating at ambient temperatures of 32.2 °C will have 21% higher COP compared to a basic transcritical CO_2 cycle. This performance gap further increases to 34% at 48.9 °C, as presented in Figure 7.[28]

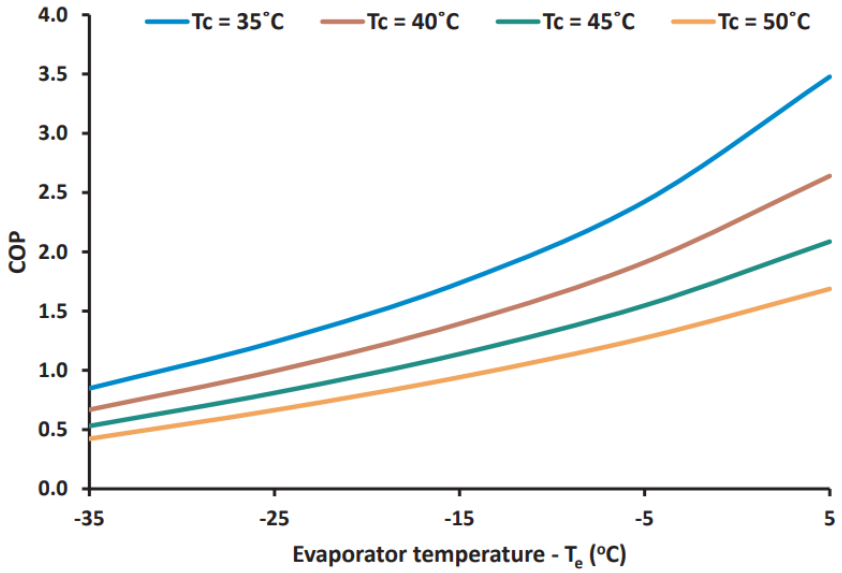

Figure 7: COP with respect to evaporator (Te) and gas cooler outlet temperature (Tc) [24]

After the Montreal Protocol in 1987, subcritical and transcritical CO_2 systems were brought back in the 1990's. However, due to low performance in comparison to HFC's, especially during high ambient temperatures, the first generation transcritical booster system was introduced early 2000's.

Transcritical booster system

In comparison to a simple transcritical CO_2 cycle, will the booster system operate with two-stage evaporation of medium temperature and low temperature. The booster system is also equipped with the corresponding two-stage compression. In addition to the two-stage concept is the booster system equipped with two additional control valves. The high pressure control valve regulates CO_2 pressure in the gas cooler and controls the CO_2 outlet temperature of the gas cooler. The flash gas by-pass valve (FGBV) regulates the pressure in the liquid receiver, regulating liquid distribution accordingly.[29] This transcritical CO_2 booster system requires 52% less annual electricity in comparison to a R404A refrigeration cycle, while simultaneously reducing environmental impact by 4%.[30] The schematic of the transcritical booster system is displayed in Figure 8.

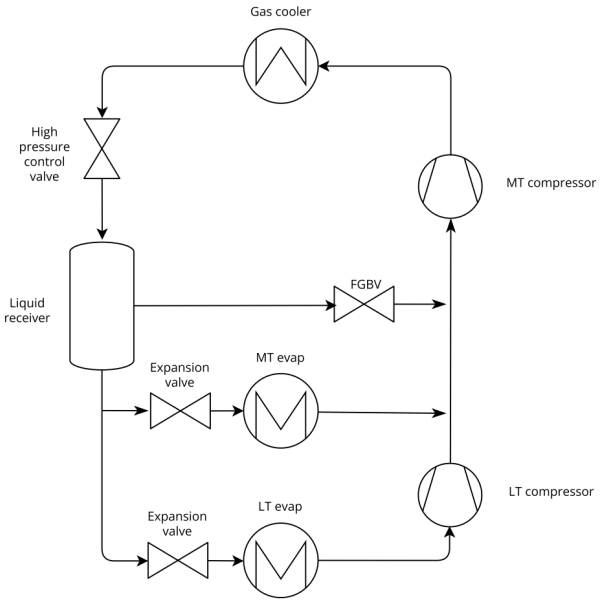

Figure 8: Transcritical booster system

Transcritical parallel compression system

In 2008 came the transcritical parallel compression system in Figure 9. Specifically designed to enhance efficiency of the system in warmer climates. When operating in warmer climates will the heat sink in the gas cooler be of higher temperature and the system will encounter a larger quantity of flash gas in the liquid receiver. Instead of dropping the pressure of the flash gas to meet suction pressure in the medium temperature compressor, the flash gas is instead further compressed to the discharge pressure. This is essentially what increases the efficiency of the system.[29] Gullo et al. states that annual electricity consumption can be lowered by another 3.6% in comparison to the booster system.[31]

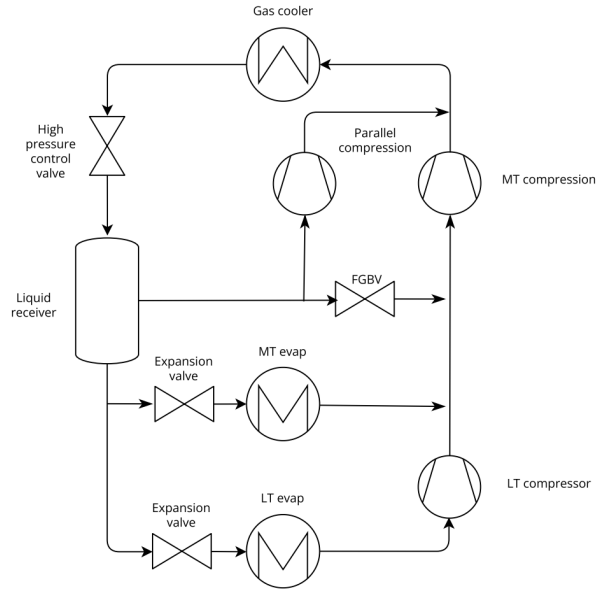

Figure 9: Transcritical parallel compression system

Transcritical ejector supported parallel compression system

The third and final generation is the transcritical ejector supported parallel compression system presented in Figure 10. First adapted in 2012, significantly increasing the efficiency of the transcritical CO_2 cycles. The main principle of the ejector is to convert the internal energy in the primary flow into kinetic energy, essentially converting the expansion process from an isenthalpic to near isentropic process. Through a suction line from the medium pressure side, secondary flow is mixed with the primary flow lifting the pressure of the secondary flow through Bernoulli's principle, as velocity increases pressure decreases. This causes a pressure lift of the secondary flow consequently reducing compressor work while increasing cooling capacity.[29] This technology is proven to save as much 22% on electricity consumption.[31] Today, the multi-ejector is the most attractive technology within CO_2 refrigeration cycles.

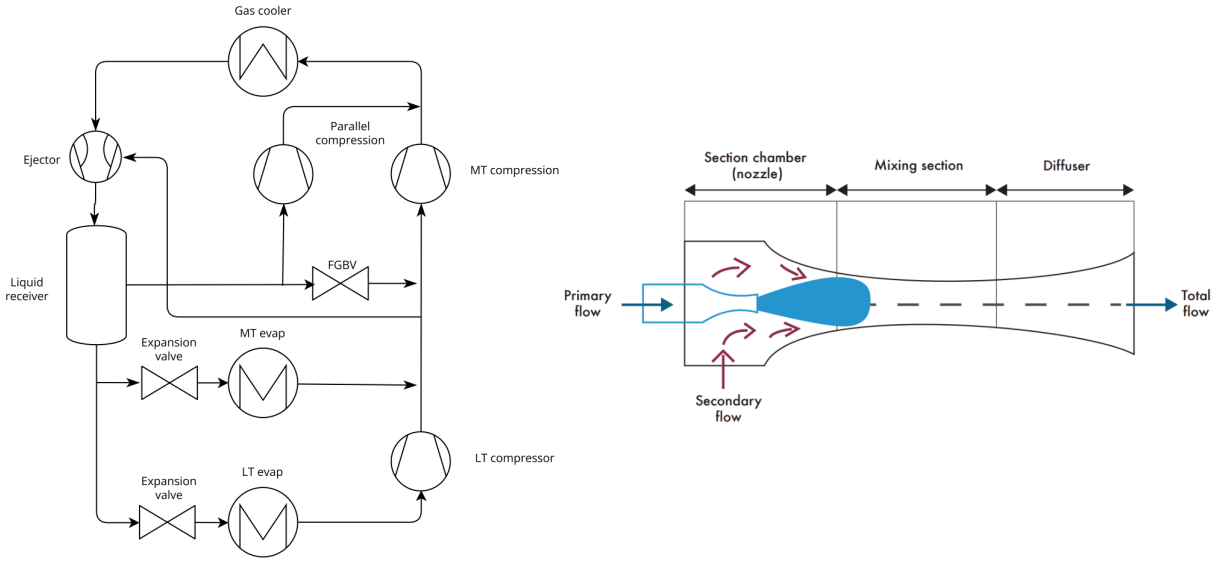

Figure 10: Transcritical ejector supported parallel compression system [29]

Other modifications include an internal heat exchanger (IHX), most common for subcritical cycles. IHX's are often installed in order to prevent flash gas in the expansion valve and to ensure adequate superheat before the compressors. However, a study by Bellos et al. compared multiple transcritical CO_2 refrigeration cycles and found substantial performance enhancement operating with a IHX. The developed models were analysed in Engineering Equation Solver (EES) and compared with experimental data for quality assurance. A simple transcritical CO_2 reference case was developed for comparison. The addition of a IHX resulted in a performance enhancement of 15% to the reference case. The IHX is then placed between gas cooler outlet and evaporator outlet. This will further cool the refrigerant before expansion valve, ultimately increasing the total refrigeration capacity of the system.[24] IHX also increase the superheat before the compressors, as a consequence increase the specific compression work. The ratio of refrigeration capacity and compressor work must therefore be optimized in order for IHX's to be advantageous.

2.2.6 Cruise ship air-conditioning

The most common method of air conditioning onboard passenger vessels is the use of a indirect system. The refrigeration unit then cools water which circulates around the passenger ship. The cooled water is then circulated in decentralized air handling units, providing cooled fresh air at the standard room temperature of 20 °C. The refrigeration unit typically cools the circulating

water from an inlet temperature of 12 °C to an outlet temperature of 7 °C. Alternatively, the direct system utilize the working fluid directly in cooling coils of the AHU, providing cooled air onboard. This method requires a larger quantity of working fluid and the additional piping and equipment suitable for the higher working pressures in comparison to circulating chilled water. Direct systems also experience greater rates of refrigerant leakage. Statistics of Swedish passenger ships show that annual leakage of filled refrigerant was reportedly as high as 62%, operating with HFC gases. Due to shorter refrigerant piping and more compact design of indirect systems the refrigerant leakage was lower at 21%. This clearly illustrates the importance of a environmentally friendly working fluid such as CO_2.[22]

2.3 Hydrogen and Ammonia as fuel for marine engines

As reductions in GHG emissions are becoming more essential regarding climate change, will the maritime sector experience a large transition. Current fuels of heavy fuel oils (HFO) will have to be replaced with more environmentally friendly alternatives. Liquid natural gas (LNG) has been introduced and gained much attention in past decades being consequently cheaper and emitting less pollutants due to the higher hydrogen to carbon ratio. Despite the fact that LNG emitt 25% less CO_2 and significantly less nitrogen oxide and sulphur oxide than HFO, will LNG not be the maritime fuel of the future. There have been several alternative fuels offered as potential replacements of high GHG fuels, two of the more prominent ones being hydrogen and ammonia.[4]

2.3.1 Properties of fuels

Hydrogen

In the near future, hydrogen in its purest form could be the solution used as either fuel for combustion engines or powering fuel cells for marine transportation. Hydrogen as a fuel for marine applications has been proven to work, however, currently developed for relatively short distances. With no carbon content, hydrogen propulsion has the potential of operating with zero emissions. In the case of fuel cells will water be the only by-product. However, combustion of hydrogen and air could lead to release of nitrogen oxide.[4]

The potentials of hydrogen as a clean fuel in the maritime sectors is gaining much attention with the drastically increasing renewable energy sources. Through electrolysis, hydrogen may be produced from renewable energy of solar power, wind power, and hydropower for environmentally friendly hydrogen production. For instance solar power, with a global potential solar energy of 48 000 TWh along the surface of the earth. This solar energy has to potential to easily cover energy demands of the shipping industry as an example, utilizing less than 0.5 TWh per year. The benefits of renewable energy sources are the even distribution and global accessibility in comparison to fossil fuels. Renewable energy sources do however require further developments in infrastructure and technology in order to be able to compete with less expensive hydrocarbon solutions.[32]

The most common methods of hydrogen production is from natural gas steam reforming and water electrolysis. Water electrolysis utilize electricity to separate hydrogen from oxygen in water. The process is highly efficient, however, technology is still in development so materials are currently expensive. Steam reforming stands for the majority of hydrogen production, reforming methane to hydrogen and CO_2. This method is effective however quite contradicting to the zero-emission label of hydrogen, as steam reforming is highly carbon intensive unless carbon capture is performed. Hydrogen should therefore only be considered carbon neutral when the method of production is carbon neutral.[4]

Ammonia

Today, the most common use of hydrogen is ammonia production. About 80% of all production of ammonia goes towards agricultural use as a fertilizer. The remaining use is for industrial manufacturing, refrigerant for refrigeration processes, water treatment, and cleaning solutions. Ammonia is also used as a fuel for heating and combustion engines. Ammonia is a carbon neutral alternative only releasing nitrogen and water at lower combustion temperatures. Of course only considered carbon neutral when produced from green hydrogen. Ammonia is also know for being a energy carrier of hydrogen. Ammonia can therefore alternatively be exploited directly in a combustion engine, used in high temperature fuel cells, or cracked to produce hydrogen. The volumetric energy density of liquid ammonia is considerably higher than that of liquid hydrogen. The main properties of hydrogen and ammonia versus conventional fuels can be seen in Table 1 below.[33]

Properties	Unit	Ammonia	Hydrogen	Hydrogen	Natural gas	Gasoline	Diesel
Storage		Compressed liquid	Compressed liquid	Compressed gas	Compressed liquid	liquid	liquid
Storage temperature	(K)	298	20	298	298	298	298
Storage pressure	kPa	1030	102	24821	24821	101.3	101.3
Autoignition temperature	(K)	924	844	844	723	573	503
Flammability limit	(Vol.%)	16-25	4-75	4-75	5-15	1.4-7.6	0.6-7.5
Min. ignition energy	mJ	8	-	0.02	-	0.14	-
Volumetric density	Kg/m^3	602.8	71.1	17.5	187.2	698.3	838.8
Energy density	MJ/m^3	11333	8539	2101	7132	31074	36403

Table 1: Properties of fuels [33]

2.3.2 Storage of fuels

Current fuels for marine transportation include oil-based fuels such as HFO and marine diesel oil (MDO). HFO is currently the most utilised fuel in marine transportation.[2] Also known as bunker fuel, HFO has a relatively low cost compared to cleaner sources of fuel as it is a by-product of crude oil refinery processes. As a by-product of crude oil, HFO include compounds such as nitrogen, sulfur and aromatics. With its higher sulfur content compared to MDO, combustion results in high levels of SO_x pollutant. However, with its high energy density its serves as an excellent alternative for long distance application due to lower required space for storage. Storage is relatively simple as large quantities of fuel can be stored for a long time without degrading of the fuel. This allows for opportunities to buy excess fuel in territories with cheaper prices.[4] The major drawback of HFO today is the large amounts of emission polluted with current technology. The 2020 report of IMO states that global marine transportation is accountable for about 2.89% of global GHG emission. As energy demands continuous to rise, these figures will increase in the years to come, making HFO not suitable to meet future emission regulations.[2]

Hydrogen

The production of hydrogen is challenging, yet may not the biggest bottleneck but rather hydrogen storage. Storage of hydrogen is very complex, and is one of the key challenges when operating with hydrogen in marine applications. The low critical temperature of 33 K makes storage in gaseous-form the easiest alternative. However, due to the lower volumetric energy density of 2101 MJ/m^3 for compressed hydrogen, will larger fuels tanks be required onboard a passenger ship in order to meet the energy demand in comparison to HFO.[4] Compressed hydrogen is typically stored at pressures of 70 MPa in the latest developments of type IV pressure vessels. These vessels are constructed using a polymetric liner supported by composite fibers which typically is carbon fiber.[32] By compressing the hydrogen, volume requirements

are reduced as volumetric density increase. At ambient conditions hydrogen has a volumetric density of 0.09 kg/m^3 and is increased to about 40 kg/m^3 at 70 MPa as presented in Figure 11. However, volumetric density does not increase linearly with increasing pressure. Compressed hydrogen will therefore not be a viable method of storage for large-scale applications in comparison to alternative fuels. The viability of these method are usually measured in terms of volume, weight and cost.[4]

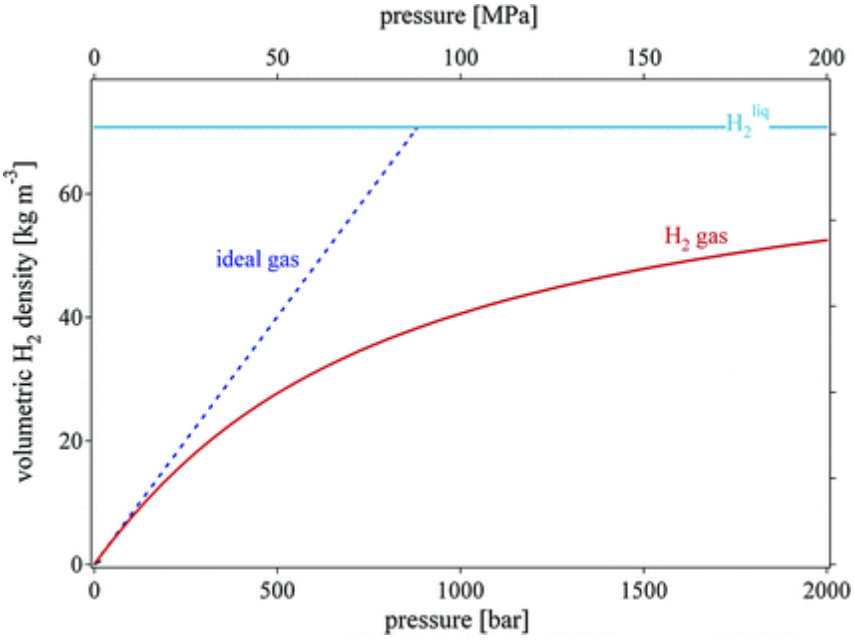

Figure 11: Hydrogen volumetric density as a function of pressure [34]

By liquefying hydrogen, less volume is required and the volumetric density is increased even further. However, this process requires substantially more energy and may increase capital cost up to 5 times compared to gaseous hydrogen (GH_2) storage depending on the scale. With a critical temperature of 33 K means that hydrogen must be cooled down to about -253 °C for liquid storage. This results in a volumetric density of about 71 kg/m^3, 775 times larger in comparison to hydrogen at ambient conditions. Liquefaction also increase the energy density. Liquid hydrogen has an energy density of 8539 MJ/m^3 in comparison to diesel with a value of 36403 MJ/m^3, clearly indicating the larger volume required in order to store liquid hydrogen at the same energy capacity.[32]

A study by Wang et al. review state-of-the-art storage methods of hydrogen on ships in terms of volumetric and gravimetric energy density in comparison to diesel/HFO. Table 2 illustrate the quantity of fuel required for a given mechanical power demand and the necessary storage volume. The diesel/HFO configurations shows to consume about 3.5 times the gravimetric quantity of fuel compared to hydrogen. LH_2 requires a storage volume ranging from 2-8 times whats required for HFO. Gaseous hydrogen requires an even greater volume at 5-20 times larger than HFO.

At -253 °C, liquid hydrogen stored in ambient conditions is equivalent to storing an ice cream in an oven, requiring thick insulation material. Significantly increasing the weight, volume and capital cost of the storage system. GH_2 with pressures up towards 70 MPa may require storage wall thickness 2 orders of magnitude greater than LH_2, due to hoop stress.[35] Even with super insulation, Boil-off gas generation may be in the order of 0.06% per day for an LH_2 storage tank of 20000 m^3.[36]

	Land-based vehicle	H_2-fuelled ship	Capesize bulk carrier
Power [kW]	90	441	15000
Diesel/HFO quantity [kg]	37-67 (Diesel)	101 (Diesel)	1843552-3688957 (HFO)
H_2 quantity [kg]	12.6-22.4	34	504000-1008000
Diesel/HFO tank size [m^3]	0.05-0.08 (Diesel)	0.12 (Diesel)	1818-3637 (HFO)
350 bar compressed GH_2 tank size [m^3]	0.53-0.94	1.42	21088-42176
LH_2 tank size [m^3]	0.18-0.32	0.486	7200-14400

Table 2: Vehicle fuel requirements [35]

The hydrogen liquefaction process is also quite energy intensive. Krasae-in et al. has calculated the energy consumption of a thermodynamically ideal liquefaction system. The ideal system requires 2.89 kWh/kg_{LH2}, corresponding to 8.67 % of the hydrogen LHV of 33.3 kWh/kg.[37] Aasadnia et al. has conducted a review of current large-scale liquid hydrogen production methods. The review concludes that current hydrogen liquefaction processes operate in the range of 12.5-15 kWh/kg_{LH2} (37.5-45%), and estimates that 5 kWh/kg_{LH2} may be achieved in the near future.[38] Compression storage will in this case be more efficient in terms of energy consumption with a consumption of 2.2 kWh/kg.[39] Compression storage will however not compete with liquid hydrogen in terms of volumetric density due to equipment pressure limitations as displayed in Figure 11.

Ammonia

Ammonia storage is much less energy intensive only requiring 10 bar to liquefy at ambient temperatures or a temperature of -10 °C at ambient pressure. Ammonia also has the advantage of much larger volumetric energy density of 11333 MJ/m^3 compared to LH_2, requiring less storage volume. Due to the higher density of ammonia, the gravimetric energy density will be lower than hydrogen resulting in higher total storage mass. Ammonia has also been considered as a hydrogen carrier. As a hydrogen carrier, ammonia will have the benefits of less complex storage and lower storage volume. The disadvantage being that this method would require additional infrastructure onboard the ship for ammonia cracking.

A study by McKinlay et al. investigate hydrogen and ammonia as long distance shipping fuels. The study compares the fuels in terms of fuel volume, required fuel quantity and cost to provide a specific energy demand of 9270 MWh for a cargo ship. Both fuels are assumed to operate with equal thermal efficiencies of 60% for the engines. Presented in Table 3, the study finds that ammonia requires half the storage volume compared to liquid hydrogen, were compressed hydrogen is almost 4 times as large. It is noteworthy to mention that the volumes provided are purely from the volume of fuel. Larger volumes operating with hydrogen are to be expected due to larger storage units for high pressure materials or cryogenic storage. The total storage mass required for both liquid and gaseous hydrogen is 464 tonnes of fuel. Ammonia requires 2959 tonnes, making up a large percentage of total ship mass. The increased weight operating with ammonia will have significant negative effects on the performance due to increased resistance in water. More energy will likely be consumed as a consequence, completing the same distance. The study also concludes over 4 times larger fuel cost operating with hydrogen compared to ammonia. These commercial prices are however expected to decrease upcoming years. This will have advantageous effects on the viability of hydrogen operations but will also reduce ammonia prices, as ammonia is made from hydrogen.[4]

	Diesel (HFO)	**Hydrogen (Gas @ 700 bar)**	**Hydrogen (Liquid)**	**Ammonia**
Efficiency	20-40%	40-60%	40-60%	30-60%
Required input energy [MWh]	23175	15450	15450	15450
Volume				
Energy density $[MWh/m^3]$	9.7	1.4	2.36	4.82
Total storage size $[m^3]$	2389	11036	6547	3206
% of cargo	1.77%	8.17%	4.85%	2.37%
Mass				
Energy density $[MWh/kg]$	0.0116	0.0333	0.0333	0.0052
Total storage mass [tonnes]	1998	464	464	2959
% of total	2.99%	0.69%	0.69%	4.42%
Price				
Fuel per voyage (£ Millions)	1.367	8.654	8.654	1.976

Table 3: Comparison of fuel volume, mass and cost to provide 9270 MWh [4]

2.4 Internal combustion engine

In the 1860's, the first internal combustion engine became reality. By utilizing chemical energy of fuels, mechanical power could be produced. Mechanical energy was produced through the concept of combustion of an air-fuel mixture in a cylinder, expanding over a piston providing the desired power output through a mechanical shaft. This engine is called reciprocating engine and is the most common concept of internal combustion engines.[40] Reciprocating engines can operate on what is known as four-stroke cycle or two-stroke cycle. The two cycles differ based on the amount of revolutions of the crankshaft per combustion in the cylinder. That indicates that the four-stroke engine requires four piston movements to complete its cycle, whereas the two-stroke only require two. Figure 12 illustrates the two-stroke cycle. In the first stroke, an air-fuel mixture is sucked into the chamber and compressed by the piston. The air-fuel mixture is ignited using spark ignition and expands until the gas exits the exhaust port completing the cycle. The two-stroke engines are common for operations which require low weight engines with high power density and high revolutions per minute (RPM). They also achieve simpler design compared to four-stroke engines, however, trade-off being the increased emissions due to release of non-ignited hydrocarbons. As the piston expands after ignition, exhaust gas may contain un-ignited fuel increasing pollution from 2-stroke engines.[41]

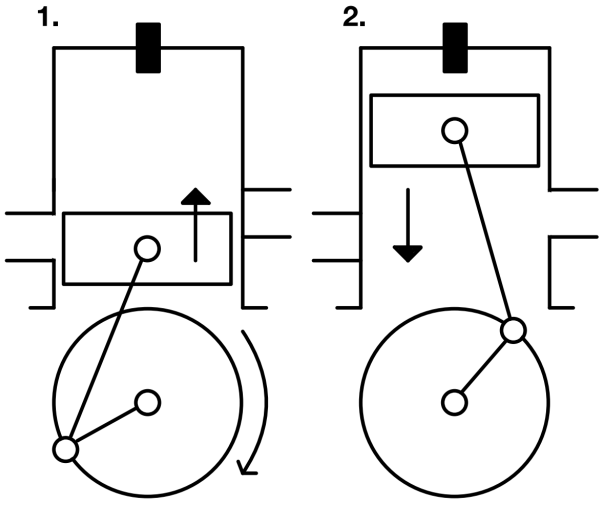

Figure 12: 2-stroke cycle

The operational strokes of the 4-stroke engine includes intake, compression, combustion and exhaust presented in Figure 13, respectively. The additional cycles separates the fresh air intake and exhaust residual in contrary to the two-stroke cycle. Resulting in better fuel efficiency and contributing to less emissions.[41]

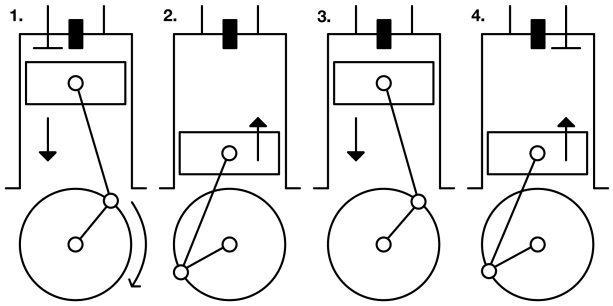

Figure 13: 4-stroke cycle

In addition to two-stroke and four-stroke cycles, ICE's are divided into two different ignition methods, spark ignition (SI) and compression ignition (CI). SI engines mix air and fuel in the combustion chamber before a spark plug ignites the mixture. This limits the compression ratio of the mixture to the auto-ignition limit in order to prevent combustion knock. Consequently, this limits the engine efficiency to about 35%.[42] CI engines do not require a spark plug and are based on the auto-ignition principle. Utilizing direct fuel-injection, fuel is injected into the chamber as air is compressed, and heated at a fuel-air ratio ensuring auto-ignition. As CI engines can operate under larger compression ratios, higher efficiencies can be achieved.[41] Internal combustion engines are not exclusively for oil-based fuels. With current technology, hydrogen and ammonia can be used to operate combustion engines, however, not without its difficulties.[4]

Marine transportation typically operate with marine diesel engines. The engines operate much like land-based transportation engines, however, differ significantly in size and achieve fairly high efficiency. Both operating with 2-stroke and 4-stroke engines, although 4-stroke is much more common. The marine engines are typically categorised in three speeds. Slow, medium and high. The speeds differ based on the operational purpose. Low speed engines, which typically are 2-stroke engines of 350 rpm or less, consume HFO fuel. Medium speed, in the range of 350-750 rpm, consume MDO and is most commonly operated as auxiliary engines. Meanwhile, at rpm of 750 and higher, high speed engines are most common for smaller ships and speed boats. During sea-going HFO is most common to power the engines, while MDO is more common during harbour stay operating auxiliary engines. Combustion of such fuels release emissions such as SO_x, NO_x, CO, and CO_2.[43]

In fact, research results have proven that 50% of NO_x along coastal regions and harbours are emitted from marine diesel engines. To invoke this issue the IMO initiated MARPOL Annex VI, set to regulate NO_x and SO_x emissions presented in Figure 14. The emission reduction technology to meet these regulation include alternative fuels, engine performance enhancement and post-treatment. The most effective methods of post-treatment of NO_x and SO_x are Selective Catalytic Reduction (SCR) and wet scrubbing, respectively.[44]

Studies have proven that such technology can reduce NO_x and SO_x emissions by 90-95%.[45][46] However, a study by Zhu et al. reported that even with effective technology of emission reduction, exhaust gas of high-sulphur content will not meet IMO tier III regulations with emission levels of 3.4 g/kWh NO_x. These regulations are in addition to the regulations set in terms of GHG emissions. In fact, the implementation of scrubbers onboard marine transportation have shown to increase power demand, ultimately increasing the amount of GHG emissions.[47] The marine

transportation industry will therefore seek to new alternative fuels, reducing SO_x, NO_x, CO, and CO_2.[48]

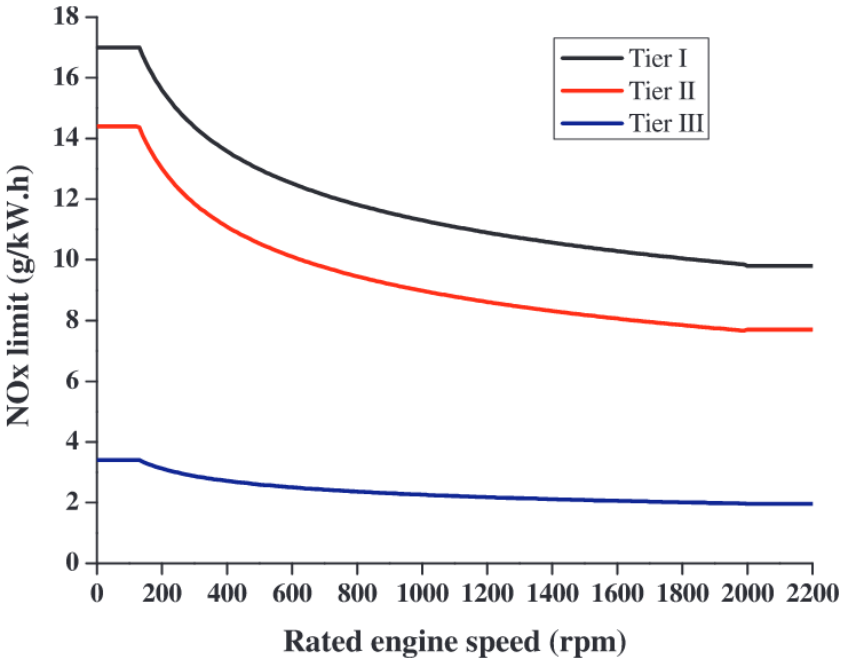

Figure 14: MARPOL Annex VI NO_x [44]

2.4.1 Hydrogen ICE

Hydrogen's clean burning properties are compelling reasons to evaluate hydrogen as an alternative fuel for ICE's. The use of hydrogen for ICE's can be operated with both SI and CI. With a flammability limit of 4-75%, the hydrogen-air mixtures can be ignited over a wide range. Hydrogen ICE's can therefore be operated with a lean hydrogen-air mixture, beneficial for fuel economy and reducing release of un-ignited fuel. Igniting hydrogen requires comparatively low energy, at one order of magnitude less that competing fuels such as diesel and gasoline. In this manner, hydrogen can be ignited at lean hydrogen-air mixtures without significant changes to available ignition components found in conventional diesel/gasoline ICE's.[49]

Hydrogen has an auto-ignition temperature of 858 K. This is considerably high in comparison to diesel which has a auto-ignition temperature of 503 K. The high auto-ignition temperature is beneficial in terms of CI engines as the compression ratio is determined by the auto-ignition temperature. Higher compression ratios result in greater thermal efficiencies. Hydrogen has an octane number of 130 which defines the fuels ability to withstand detonation under pressure. Diesel has an octane number of 30. Another factor enhancing the thermal efficiencies of hydrogen ICE's is the high flame speeds. At stoichiometric ratios, hydrogen ICE's approach near thermodynamically ideal cycle due to uniform mixture formation and near constant volume combustion. Hydrogen flame speeds are close to an order of magnitude larger than gasoline flame speeds.[49] The high flame propagation rates ensure short ignition duration, contributing to high power output efficiency even at lean air-fuel mixtures. During combustion, hydrogen has unique heat transfer charactersitics resulting in lower heat loss contributing to higher thermal efficiencies.[50] The major challenges of hydrogen ICE's include pre-ignition, knocking and NO_x emissions.[51] Hydrogen does not contain nitrogen, however at higher combustion temperatures thermal NO_x is formed from the nitrogen and oxygen in the air.

Nader R. Ammar has investigated the energetic and exergetic efficiency of a dual-fuel engine operating with diesel-hydrogen fuel mixture. Using the EES software package, the study proves

that brake thermal efficiency and exergy efficiency improved as the fraction of hydrogen increased. This is due to the enhanced combustion efficiency achieved due to hydrogen's favorable combustion characteristics. The improved thermal efficiency was notably better due to the lower heat transfer and near complete fuel combustion. These characteristics ultimately lead to higher exhaust gas temperatures in comparison to fuels of lower hydrogen fraction. As a result, NO_x emissions increased. Increasing up to 223% in comparison to pure diesel engine at 55.1 g/kWh NO_x, significantly higher than IMO regulations.[52]

A study by Radica et al. simulated a two-stroke marine diesel engine. The study aimed to investigate the emissions and performance of a low-speed engine of different diesel-hydrogen mixtures. The research investigates the potential of hydrogen additives to reduce NO_x emissions of diesel engines while meeting MARPOL Tier III regulations. As presented in Figure 15, effective efficiency decrease as the fraction of hydrogen increase. As with the study by Nader R. Ammar, the exhaust temperature increase as the fraction of hydrogen increase. The reduction in temperature through decreasing fuel consumption is therefore necessary to meet IMO regulation, however, decreasing efficiency.[53]

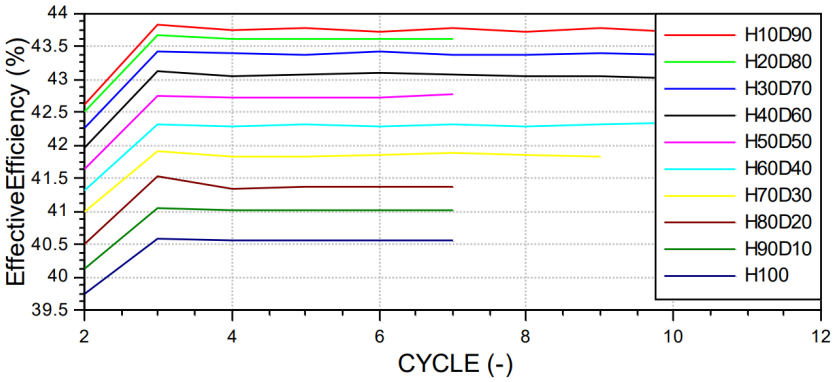

Figure 15: Effective efficiency diesel-hydrogen mixtures [53]

Elgohary has conducted a study regarding design of marine hydrogen internal combustion engines. The author defines the main requirements of power and RPM to be 3000 kW and 600 rpm, respectively. This allows for direct comparison to a well know diesel engine M32C by MaK. The engine cycle was simulated based on the Otto cycle. This allows for the assumption of a Otto constant volume process due to the high combustion rate of hydrogen. Further, assuming a cooling water loss of 30% the author is able to calculate the engine efficiency using thermodynamic equations along with qualitative assumptions.[54] The characteristics of the ICE's studied is presented in Table 4.

	Hydrogen	M32C
Power [hp]	4080	4080
Speed [rpm]	600	600
Cycle	4-stroke	4-stroke
CV of fuel [kJ/kg]	130000	42700
Efficiency	33%	47%
No. of cyclinders	6	6
Fuel consumption [h/hp.hr]	61.74	131.6
Max pressure [bar]	173.8	198
Brake mean eff. pressure	12.76	25.9
Stroke/Bore	60/40	48/32

Table 4: Comparison of hydrogen engine and M32C diesel engine [54]

The results from the thermodynamic design present a comparison of the hydrogen engine with the diesel engine with identical power outputs. This gives an engine efficiency of about 33% and an exhaust gas temperature of 485.8 °C. However, some clarifications must be made about the comparison. Hydrogen will reach a higher temperature during combustion, this leads to a larger cooling demand thus reducing the engine efficiency. Due to the higher calorific value of hydrogen compared to diesel, lower fuel consumption will be required to meet the power output demand. By achieving a larger engine efficiency, fuel consumption can be lowered even more. To compensate for lower engine efficiency, the hydrogen engine will require bigger engine dimension in order to match power output and RPM of diesel engine.[54]

Elgohary et al. later performed a case study comparing the use of a hydrogen engine with a M32C diesel engine on a RO/RO ship. The study considered the use of either pre-mixed hydrogen and air in the combustion chamber or direct injection of pure hydrogen. The analysis is based on the Otto-standard cycle looking at both two-stroke and four-stroke cycles. To minimize cost, the hydrogen is suggested to be utilized in an existing diesel engine. Hydrogen is injected directly into the chamber, igniting the fuel-air mixture using spark ignition. Unlike the previous literature study, this case study evaluates the use of hydrogen in diesel engine of identical engine dimensions as presented in Table 5.[51]

	Hydrogen	M32C
Engine speed (rpm)	775	600
Pressure ratio	9	12.8
Heating value of fuel (MJ/kg)	130	42.7
Bore (cm)	32	32
Stroke (cm)	42	42
Engine power (kW)	2700	2700
Thermal efficiency (%)	29.57	47
Specific fuel consumption (g/kWh)	93.46	178.98
No. of cylinders	6	6
Mean effective pressure (bar)	10.02	25.9
Compression pressure (bar)	75.57	84
Combustion pressure (bar)	132.4	124

Table 5: Comparison of hydrogen engine and M32C diesel engine [51]

The case study concluded that the best engine design is achieved with direct injection of hydrogen in a two-stroke cycle. The criterion are meet when hydrogen is injected into the chamber at a temperature of 127 °C and pressure of 3.7 bar. This results in a drastic decrease in fuel consumption compared to diesel even though engine efficiency only lie at 29.57%. This results in a fuel consumption of 93.46 g/kWh for hydrogen compared to diesel at 178.98 g/kWh. The required cooling water and air for the hydrogen engine are 67.83 kg/kWh and 13 kg/kWh respectively. Assuming a stoichiometric air-fuel (AF) ratio of 34.78 and excess air factor of 4 (λ). This resulted in a total exhaust flow of 13.1 kg/kWh.[51] Table 6 presents the hydrogen ICE characteristics from various literature studies.

Author	Power	η_{th}	T_{in}	P_{in}	T_{exh}	NO_x	Description
Nadar R. Ammar [52]	37620 kW	58%	-	-	575 K	55.1 g/kWh	2-stroke diesel DFE 40% hydrogen
Radica et al. [53]	6505 kW	40.5%	-	-	-	3.4 g/kWh	2-stroke diesel DFE 100% hydrogen
Seddiek et al. [51]	2700 kW	29.57%	127 °C	3.7 bar	700 K	-	2-stroke marine engine 100% hydrogen
Oh et al. [55]	7.4 kW	32.30%	-	5.5 bar	-	2.46 g/kWh	2-stroke marine engine 100% hydrogen
El-Gohary et al. [54]	4080 kW	33%	100 °C	4 bar	760 K	-	4-stroke marine engine 100% hydrogen

Table 6: Review of hydrogen ICE's

2.4.2 Ammonia ICE

Ammonia has the great advantage of simpler and much less energy intensive fuel storage. Ammonia has also been proven to be viable with internal combustion engines with minimal engine modifications. However, only a few researchers has investigated engine operations of pure ammonia.[56][57] Ammonia has the disadvantages of very high auto-ignition temperature, low flame speed, high ignition energy and narrow flammability limits as seen in Table 1. Making ammonia difficult to burn alone, but also inducing incomplete combustion in ICE's. Multiple studies has therefore been conducted operating with fuel mixtures of ammonia and ignition promoters such as hydrogen, gasoline, diesel and natural gas.[58][59] Due to the higher octane number of 130, ammonia has proven to be more suitable for spark ignition engines highly resistant to engine knock. However, for marine applications, compression ignition engines are more favorable as they can achieve higher capacities compared to spark ignition engines. The high compression ratio necessary can be a challenge combusting ammonia in compression ignition engines. Nevertheless, if compression ignition is achieved with ammonia, higher thermal efficiencies can be expected making ammonia engines superior to gasoline and diesel engines in terms of emissions. Higher compression ratios also means higher combustion and exhaust gas temperature. Ammonia has no carbon emissions but because of high nitrogen content, ammonia combustion can emit large quantities of nitrogen oxide. Emission control technologies are therefore essential for environmentally friendly ammonia operations.[60]

A study by Liu et al. performs a numerical investigation of emission and combustion characteristics of a low speed duel-fuel two-stroke marine engine running on ammonia and diesel pilot fuel. Using CFD, the study investigated both gaseous and liquid ammonia in a CI ICE in terms of engine performance, incomplete combustion and emissions of NO_x. The results of the study showed that the ammonia engine, whether supplied in liquid or gaseous form, can produce sufficient power in terms of marine applications and provide thermal efficiencies as high as 50%. The study also found that the supply method of liquid ammonia outperformed that of gaseous ammonia in terms of power, incomplete combustion and emitted ammonia. Through lean ammonia-air combustion mixtures, the results concluded an NO_x emission rate of about 6.8 g/kWh. This is however not sufficient in terms of Tier III regulations, but proves significant advantages in comparison to diesel and gasoline.[61]

The maritime transportation sector is yet a favourable contender of ammonia fueled ICE's as ships have less space constraints in terms of installing catalytic systems for the reduction of NO_x emissions.[62] Other methods of reducing NO_x emissions is by reducing exhaust temperature. As with hydrogen, will the majority of NO_x emissions come from thermal NO_x. Introducing ignition delay will significantly reduce NO_x emissions as exhaust temperature decrease, as a result the thermal efficiency decreased substantially.[63]

2.5 Waste heat recovery

This section presents the available waste heat sources onboard a marine ship operating with an internal combustion engine, and the possibilities of waste heat recovery for increased energy efficiency.

2.5.1 Waste heat sources

For the cruise ship industry, engines have a maximum energy efficiency of about 50%. The remaining heat from combustion in marine engines is lost to the environment through thermodynamic and mechanical processes such as exhaust gas, heat radiation, engine cooling and oil lubrication.[64] Each process of waste heat is distinct and varies in terms of quality and quantity.

The largest waste heat in terms of quantity and quality lies in the exhaust gas. The exhaust gas has great potential for waste heat recovery (WHR) as exhaust gas typically have a large mass flow and relatively high temperature. This potential waste heat can be recovered to enhance the ship efficiency, reduce emissions, generate electrical/mechanical power, heating services onboard and freshwater production. Many solutions for waste heat recovery are available. However, for marine applications additional challenges must be considered. WHR systems for marine applications must be able to obtain optimal performance under dynamic conditions.[65] Dynamic conditions include change in ambient temperatures but primarily variance in engine load. WHR systems add a large degree of complexity to marine applications. Challenges lie in integration of WHR to existing power units while maintaining reliable operation, small footprint, and being economically feasible.[66] The quality of the waste heat lies in the temperature of the source. Typically divided into low-, medium-, and high-quality waste heat as presented in Table 7.[66]

Quality	Temperature range (°C)
High	650 and higher
Medium	232-649
Low	232 and lower

Table 7: Heat quality classification [67]

For maritime applications, most waste heat opportunities are between medium and low heat quality. Typically, the temperature range of marine engine exhaust gas are about 300-500 °C. The temperature depends on the ambient conditions, engine load, fuel, but also the engine type. Diesel four-stroke engines typically have a nominal temperature range of 400-500 °C. Whereas two-stroke engines lie at a lower temperature of 300-350 °C. Waste heat recovery systems can be designed to utilize either a combination of different heat sources or a single heat source depending on energy demands and scale of ship.[66] Other potential waste heat sources include lubricating oil, engine cooling medium and scavenged air with temperature ranges of 60-75 °C, 70-125 °C and 100-160 °C, respectively. The low quality heat source of lubricating oil has rather low potential of waste heat in comparison to exhaust heat. However, studies have proven promising result utilizing lubricating oil in rankine cycles onboard an LNG carrier.[68] The engine cooling medium is also presented as a viable heat source mainly due to its simplicity and near constant delivery of heat, whereas the scavenge air is less reliable highly dependent on the engine load. The most promising waste heat source is exhaust gas, especially for power cycles generating electricity and providing heat. In fact, Mondejar et al. found that 10 to 15% of fuel savings can be obtained by exhaust waste heat recovery alone, utilizing an organic rankine cycle.[69] From a quantitative perspective, the recovery of both exhaust waste heat and engine cooling medium provides the largest potential for waste heat recovery with near 50% coverage of the fuels heating value. Figure 16 illustrates a typical sankey diagram of a marine engine, presenting the energy distribution of a fuel.

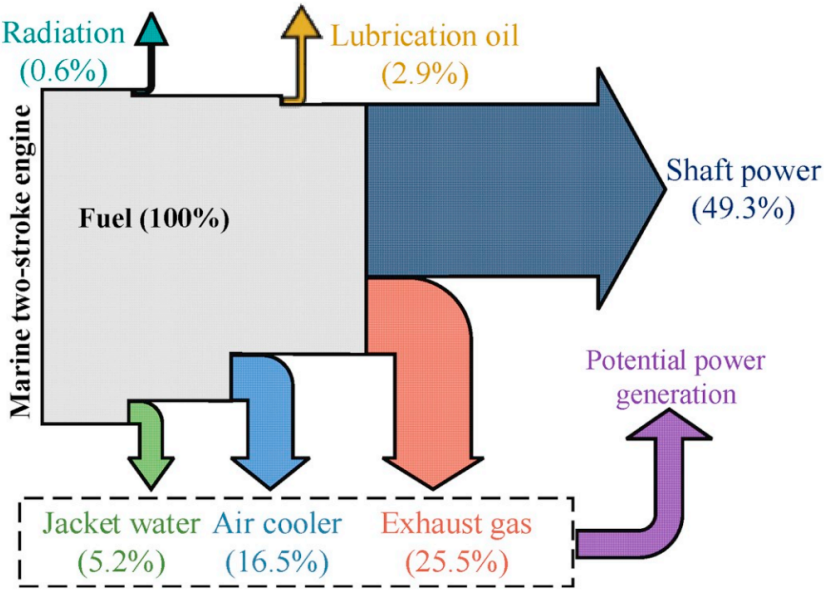

Figure 16: Sankey diagram marine ICE [70]

2.5.2 Power cycles

The three main technologies for power generation from waste heat recovery are thermoelectric generators, turbo-compounding and bottoming power cycles.[70] A summarized comparison is provided in Table 8.

	Advantages	Disadvantages	Potential fuel savings
Thermoelectrical generator	Silent operation, maintenance-free and lightweight	Cost ineffective and low efficiency	Normally less than 2.5%
Turbo compounding	Small size, low cost, and simplicity	Deteriorated engine performance and thermal load	3–5% at loads higher than 50%
Bottoming power cycles	High efficiency, flexible working fluid selection	High cost, large scale, and complex system structure	4–15% depending on system design

Table 8: Comparison WHR technologies [70]

Thermoelectrical generators, converts thermal energy to electrical energy through the Seebeck effect. The effect is based on the concept in which temperature difference between to non-similar electric conductors generate a voltage via a thermocouple. The voltage is generally very small but can be scaled up if large temperature differences are available. However due to low efficiency will thermoelectric generators not be able to compete with other technologies for marine applications.[71] Turbo-compounding is the method of utilizing turbines downstream of the exhaust in order to directly extract power either through coupling of a generator or direct transfer to the engine. Benefits of turbo-compounding is the small size and simplicity of the system compared to bottoming power cycles. Disadvantage being the lack of operational range providing small potential fuel savings at low engine loads. Conventional solutions to waste heat recovery often combine power turbines with Rankine cycles (RC) for maximum energy efficiency.[72]

The act of recovering waste heat in order to generate electricity is called bottoming cycle. The most know process of bottoming cycles is the Rankine cycle.[73] The Rankine cycle includes four main components such as expander, condenser, circulation pump and evaporator as illustrated in Figure 17. The cycle is a closed system with the option of operation with different working fluids depending on heat quality and demand.

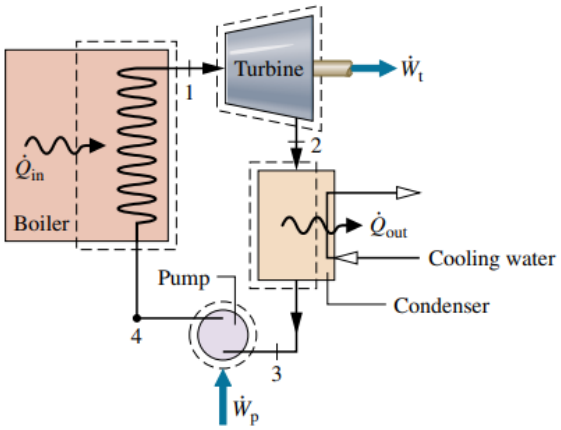

Figure 17: Basic Rankine cycle [14]

First, the working fluid with its elevated pressure is heated by the exhaust gas in a boiler to a superheated state. The steam working fluid expands over an expansion device (turbine) converting heat energy to work which can then generate electrical power. The working fluid is then discharged into the condenser at lower temperature and pressure going through phase-change from steam to liquid. Finally, the cycle is completed by pressure and temperature increase through a pump.[14]

The conventional Rankine cycle also know as the Steam Rankine Cycle (SRC) utilizes water/steam as working fluid. The SRC is successfully commercialized as waste heat recovering unit onboard ships due to the mature technology. SRC are traditionally used as auxiliary power generation but may also be used as the main propulsion of ships. Due to the relatively high evaporating temperatures of SRC, the WHR unit requires exhaust temperatures of about 350-370 °C. This criteria also limits the system to operation only above about 40% of main engine loads. Operation at lower temperatures would require larger, more expensive equipment making SRC less attrative considering the already large size compared to other power cycles.[70] Despite the high evaporating temperatures required, SRC's are non-toxic, non-flammable and low viscosity. They are also considerably safe and reliable. However, due to majority of waste heat from passenger ships being relatively low, will the efficiency be low.[66]

When heat source temperatures are lower, higher power output and efficiency may be achieved if using an organic fluid. These cycles are called Organic Rankine Cycle (ORC). The reason for the higher efficiency at lower quality heat sources is that ORC fluids have a lower latent heat of evaporation compared to water.[74] Organic working fluids may be chosen to best match the quality of the heat source. This usually means better efficiency of the system but may also reduce the size of the system. Due to the low boiling point of most organic fluids, ORC are efficient even at engine loads as low as 250 kW. SRC's usually require engine loads at about 20 times higher power output. Organic fluids such as benzene, toluene and R245fa may be used as working fluids for ORC. Which in turn means that some ORC system have a disadvantage considering that these fluids are flammable, toxic or not environmentally friendly.[70]

Another cycle of interest is the Kalina cycle (KC). A thermodynamic power cycle based on the use of a mixture of ammonia and water as working fluid for higher thermal efficiency. As with ORC, KC can operate taking advantage of lower temperature heat sources. The KC is a modified

rankine cycle. Modifications made to specifically take the most advantage out of the ammonia-water working fluid. The major advantage of KC compared to conventional rankine cycle lie in the heat exchange processes during heat rejection and heat absorption. The working fluid contains about 70% ammonia and remaining water. As the ammonia-water mixture is passed through the boiler and is heated up, ammonia vaporize before water. As volatile ammonia vaporize will the ammonia concentration decreases, thus, the saturation temperature of the working fluid will increase. This creates for a better match of temperature curves between working fluid and heat source as seen in Figure 18.[75]

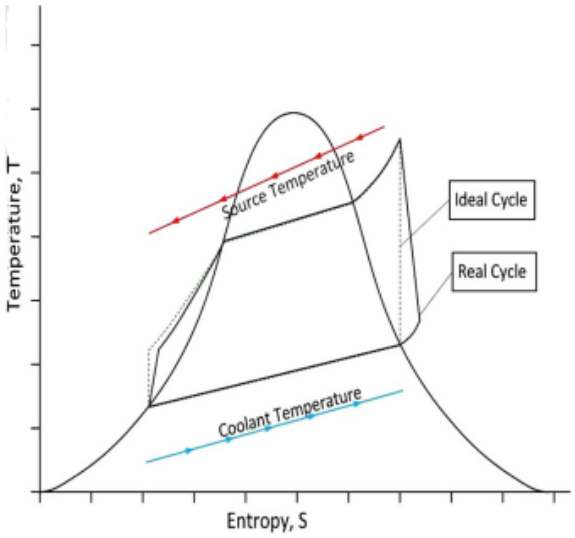

Figure 18: Kalina cycle [75]

One of the most attractive power cycle today is the CO_2-based power cycle, specifically the transcritical cycle. As mentioned, CO_2 has a long history within refrigeration and heat pumps. However, the history of CO_2 as a working fluid for power cycles is short. Given the advantages of CO_2 being non-toxic, non-flammable, environmentally friendly and having excellent thermodynamic properties makes CO_2 a great alternative for replacing less environmentally friendly solutions. The high density and volumetric heat capacity makes CO_2 power cycles a great alternative for marine applications, as design can be made quite compact. Additionally, the evaporator is replaced by a gas heater heating CO_2 with a gliding temperature profile, beneficial for reducing thermodynamic losses during heat exchange.

Due to the low critical temperature of CO_2, heat sink above 25 °C will not be sufficient for transcritical cycles for waste heat recovery.[66] For heat sink above sufficient condensing temperature, CO_2 power cycles will operate in supercritical state. The main difference between supercritical and transcritical lie in the state at which CO_2 rejects heat as seen in Figure 19. CO_2 power cycles which operate in supercritical state are known as supercritical brayton cycle. The brayton cycle operate much like the transcritical rankine cycle, however, pump and condenser is replaced compressor and gas cooler respectively. This is due to the working fluid only operating in supercritical state. High thermal efficiency can be achieved due to the unique thermodymanic properties of CO_2 in this state. Near critical pressure, CO_2 experience characteristics of both liquid and gas. Specific heat larger than gas and viscosity less that liquid. This adds to the advantage of low pressure loss and high volumetric heat capacity. Optimal placement of compression will thus be near critical point in order to take advantage of small compressibility factor and high density for low compressor power consumption.[35]

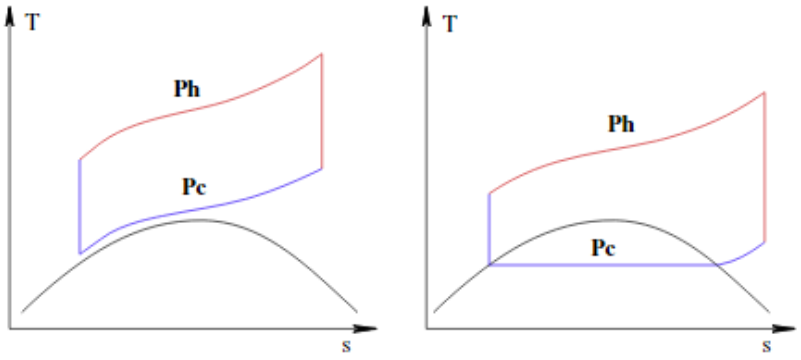

Figure 19: Supercritical (left) and transcritical (right) [76]

2.5.3 Hot water production

Onboard most cruise ships, the majority of thermal demands are met through waste heat recovery.[77] Exhaust gas economisers or high-temperature water heaters use the excess thermal energy of the exhaust gas to provide water at 90 °C for space heating or hot water production. Ideally, all excess thermal energy is to be recovered for maximum energy conservation. However, recovery is restricted by the sulphuric acid dew point causing corrosion and fouling on heat transfer area. At the dew point, typically in the range of 130-160 °C for HFO fuels, sulphuric acid of high-sulphur content exhaust gas start condensing in the water heater. Due to the absence of carbon dioxide and sulphur in fuels such as hydrogen and ammonia, will modern hydrogen and ammonia ICE's have negligible acid formation. As a result, more thermal energy may be recovered.

2.6 Rankine Cycle

This section provides an overview of the working fluids and components applicable in rankine cycles. The different configurations of rankine cycles will then be investigated in order to understand the principles of the power cycle. Finally, power cycles will be investigated for marine applications.

2.6.1 Working fluids

The choice of working fluid is crucial in terms of waste heat recovery using a rankine cycle. The working fluid must satisfy specific requirements in regards to a selection of criteria for waste heat recovery of marine ICE's as presented in Table 9. The thermodynamic properties such as critical temperature, decomposition temperature, specific heat, latent heat, and boiling temperature have a large influence on the RC performance. The working fluid must be selected based on the characteristics of the waste heat source. Other criteria are the safety and environmental impact of the fluid, such as toxicity, chemical stability, ODP and GWP.[78]

Description	Value	Reason
Critical temperature	Low	Easily realize transcritical cycle
Boiling temperature	Appropriate	Optimal thermal efficiency
Specific heat	High	Heat capacity
Latent heat of evaporation	Low	Evaporate at low quality heat sources
Heat transfer coefficient	High	Small-scale system
Thermal stability	High	Wide operational tamperature range
Viscosity	Low	Low pressure loss
Specific volume	Low	Larger mass flow rates
GWP	Low	Environmental impact
ODP	Low	Environmental impact
Availability	High	Commercialization
Cost	Low	economic viability

Table 9: Selection of criteria for RC working fluids [79]

As mentioned, the SRC is less attractive in terms of marine WHR due to larger scale and capital costs. The lower latent heat of evaporation for organic working fluids make ORC's more suitable, achieving higher thermal efficiencies at a smaller scale.[78] Isobutane (R600a) has recently received much attention considered as a potential replacement of environmentally hazardous refrigerants. Isobutane has a low GWP of 3, zero ODP impact, low toxicity and is considerably cheap to produce.[80] Isobutane has a critical pressure and critical temperature of 36.4 bar and 134.7 °C, respectively. With a low latent heat of evaporation of about 347 kJ/Kg, isobutane is an effective working fluid even at low quality heat sources.[81] A study by Darvish et al. compares optimum working fluids for ORC's based on an exergy analyses. The result show that isobutane has the highest thermal efficiency compared to working fluids such as R134a, R123, R245fa and n-pentane to name a few. The thermal efficiency represents the fraction of heat energy which may be converted to work in an expander.[82] This is also demonstrated in a study by Raghulnath et al., investigating maximum power output from ORC's operating with isobutane, R11, R12, R123, or R245fa. The result show that isobutane may produce about 36% more power compared to average power outputs of the other refrigerants.[83] Another study by Javanshir et al. investigates thermal efficiency of different working fluids of an simple ORC. The study consider a heat source of 250 °C achieving thermal efficiency of 17% with isobutane as working fluid.[84]

Astolfi et al. compared ORC's and CO_2 bottoming power cycles for low-medium quality heat source ranging from 200-600 °C. The study compared different configurations of ORC's and CO_2 based systems and found that ORC's are more suitable at temperatures of 350 °C and lower, while CO_2 was suitable for higher temperatures. This was reasoned by the limit of thermal stability of organic working fluids at high temperatures. Lighter compounds start decomposing, consequently degrading the thermodynamic performance. It was also concluded that solid particles of the organic working fluids may form, resulting in damage to turbine blades and increased fouling. In fact, isobutane has a maximum temperature limit of 300 °C.[85] With the added downside of high flammability, it is clear that CO_2 is more suitable for marine applications.

2.6.2 Components

Heat exchangers

In Rankine cycles, the waste heat energy recovered is used to generate electricity through turbine expansion of a working fluid. Thus, in order to maximize the potential energy recovery, component design of the pump, expander and heat exchangers must be optimized. The heat exchangers of interest include the evaporator, condenser, as well as the recuperator found in recuperative rankine cycles. Evaporators of rankine cycles operating with exhaust waste heat must be compatible with high temperatures, high pressure and fouling challenges. Important factors of evaporator design include heat recovery efficiency, heat transfer area, pinch point, pressure drop, size and system cost. The system cost is a function of the heat transfer area. By decreasing the pinch point, larger heat transfer area is required, thus, system cost increase. The lower pinch point result in higher heat recovery efficiency, however, induce larger pressure drops.[70] Motai et al. found that a pinch point of 5 °C produces 10 % more steam in the exhaust gas evaporator in comparison to a pinch point of 15 °C. The lower pinch point proves to increase the heat recovery efficiency but at the expense of larger capital costs. The study estimates a 2.3 times larger heat transfer area required when operating at the lower pinch point of 5 °C, concluding that the most sufficient pinch point is in the range of 15-25 °C for waste heat recovery.[86] Zheng et al. proves in a study that the thermal efficiency of a Rankine cycle may vary up to 7.91 % depending on the heat transfer area.[87] The design and layout of the heat exchangers is therefore crucial for optimal waste heat recovery.

The most common types of evaporators for waste heat recovery are shell-and-tube and plate-type heat exchanger. Waste exhaust heat from internal combustion engines onboard passenger ships typically have a temperature higher than 230 °C and volume flow rate of 50000 m^3/h.[69] Generally, shell-and-tube heat exchangers are more suitable for these operating conditions as materials are designed to withstand the high temperature and pressure under large volume flow rates. Shell-and-tube are more generally used in larger applications whereas plate-type for smaller applications.[88] The most simple configuration of the shell-and-tube heat exchanger is the single pass, counter flow heat exchanger displayed in Figure 20. Typically waste heat exhaust gas flows in the outer shell and the working fluids flows in the tubes. Baffles are then installed in order to induce turbulence and cross-flow on shell side, resulting in an increased convection coefficient improving overall heat transfer, however, at the expense of increased pressure loss.[89] Further heat transfer improvements introduce finned tubes for increased heat transfer area at an acceptable outer diameter. By adding multiple passes the convection coefficient can further increase as the velocity of the fluids increase. High velocities in the evaporator is generally desirable, resulting in high heat transfer coefficient but also helps prevent soot deposits.[70] Soot deposits also known as fouling, is one the challenges considered when designing heat exchangers. Partially combusted hydrocabons and soot particles build up on the surface of tubes and fins degrading heat transfer between working fluids. Heat exchangers are often designed such that cleaning is accessible.[78]

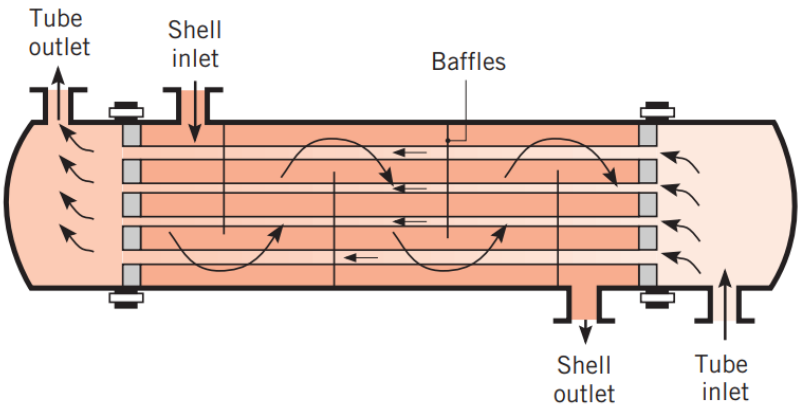

Figure 20: Shell-and-tube heat exchanger [89]

Plate-type heat exchangers are more compact and lightweight in comparison to shell-and-tube heat exchangers. They are constructed of many thin plates which are parallel to each other providing a large heat transfer area to volume ratio. The plates are bolted together sealed by gaskets. The plates are usually corrugated providing high turbulence in the fluid increasing heat transfer coefficient, capable of approach temperatures as low as 1 °C. The plates are usually constructed by stainless steel or titanium, which may easily be dismounted for cleaning. With a quite simple design, plate-type heat exchangers are the cheapest alternative where plates can easily be added or removed to meet heat transfer requirements.[90] The disadvantages, plate-type heat exchangers are limited to 2500 m^3/h and may not withstand pressures and temperatures above 40 bar and 250 °C, respectively. The limiting factors being gasket material and plate deformation. However, welded plates significantly increase pressure capabilities allowing pressure and temperatures of 80 bar and 500 °C, respectively.[69] Plate-type heat exchangers are therefore more common for condensers and recuperators. Another alternative is plate-fin or printed circuit heat exchangers. Highly suitable for waste heat recovery of marine applications, capable of 100 MPa and 800 °C. Mavridou et al. conducted a study of different heat exchangers for waste heat recovery of an heavy duty diesel engine. The study found that plate-fin heat exchangers required 66.5 % less volume and reduced pressure loss by 97.5 % in comparison to shell-and-tube.[91] Plate-fin heat exchangers have proven to have significant performance characteristics, however, typical trade-off being the difficulty of cleaning and potential clogging from sulphur content of exhaust gas.[78] Hydrogen and ammonia operation will then have a great advantage of no sulphur content in the exhaust gas. Illustrations of both plate-type and plate-fin is presented in Figure 21.

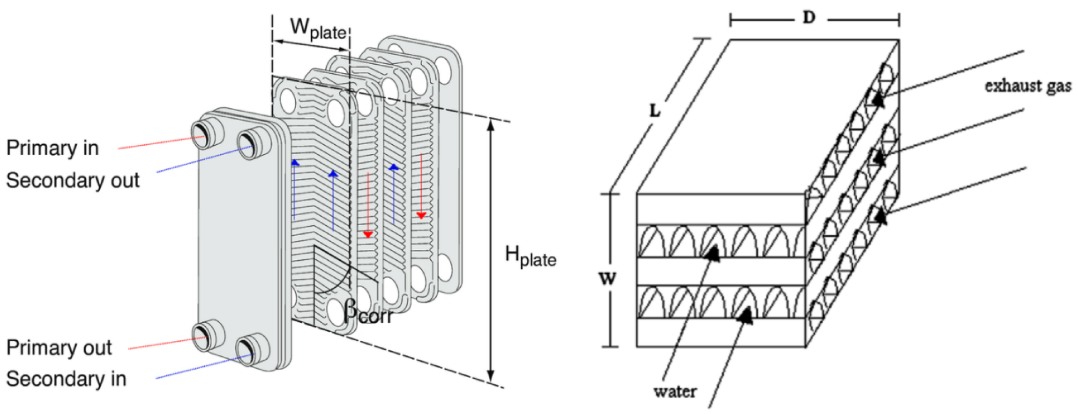

Figure 21: Plate-type (left) [92], plate-fin (right) [69]

Pump

In the case of a bottoming power cycle, the power required from the pumping process ideally represent only 10% of the power output from the expander. To achieve this pump-expander power ratio, the optimal pump must be chosen for the operation. The ideal pump for large scale waste heat recovery is the centrifugal pump, where efficiency is highly dependent on the pressure ratio. A study by Borsukiewicz-Gozdur found that the power ratio is correlated to the inverse of the working fluids critical temperature. Consequently, working fluids of higher critical temperature experience lower power ratios. Thus, SRC's may achieve greater efficiencies in comparison to ORC, as ORC operate with working fluids of lower critical temperature. Yet, pumps for ORC's still achieve an efficiency of 0.65-0.85.[93]

The pressure ratio will also have a significant effect on the thermal efficiency of a rankine cycle. Higher pump outlet pressures result in higher pump outlet temperature of the working fluid, thus providing a better temperature match between working fluid and heat source of high temperature. As a result, decreasing exergy destruction in the gas heater due to lower LMTD. Higher pressures also result in larger enthalpy differences in the expansion device, increasing thermal efficiency.[94] Transcritical CO_2 cycles has reportedly been operated with pressures as high as 350 bar for maximum thermal efficiency.[95]

Expander

The two most common types of expanders viable for rankine cycles are turbines and positive displacement machines. The latter includes rotary vane, screw, piston and scroll expanders, more common for power cycles of lower temperatures and low power output. Turbine expanders, with configuration of either mixed-flow, axial or radial, are more viable at power output of 100 kW and higher. With a temperature range of 120-350 °C in the working fluid, these expanders may achieve isentropic efficiencies as high as 90%.[69]

2.6.3 Cycle configurations

The basic power cycle is derived from the first and second law of thermodynamics. A power cycle is based on the concept of conversion of energy, which states that the net heat in a thermodynamic cycle must equal the net amount of work. A transfer of heat from a hot body to a system undergoing a thermodynamic cycle will therefore result in a energy conversion from heat to work, as presented in Figure 22.[14]

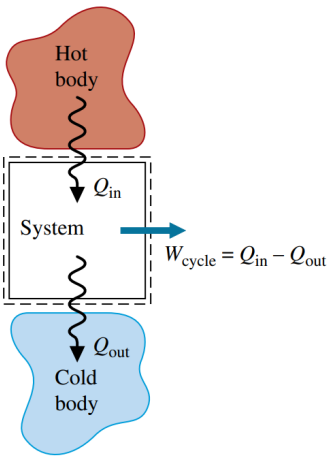

Figure 22: Cycle energy balance [14]

The net work is then the difference in heat energy entering and exiting the system. The thermal efficiency of the power cycle can be written as:

$$\eta_{th} = \frac{W_{cycle}}{\dot{Q}_{in}} = 1 - \frac{\dot{Q}_{out}}{\dot{Q}_{in}} \tag{3}$$

From equation 3 it is clear that the thermal efficiency will never be greater that 100% as long as heat energy is discharged into the surroundings. The goal of a efficient thermodynamic power cycle will therefore be to create a cycle with the least amount of heat loss to the surroundings. Further, given an ideal reversible power cycle, the maximum thermal efficiency can be expressed by the carnot efficiency of equation 4. The equation illustrates that, as the condensing temperature decreases and the evaporating temperature increases, the thermal efficiency of the power cycle will go towards 100%.[14]

$$\eta_{max} = 1 - \frac{T_C}{T_H} \tag{4}$$

Knowing this information is crucial for the basic understanding of an ideal power cycle, yet it is far more complicated with the actual power cycle. Integrating this concept to a subcritical non-superheated cycle leads to complications. Increasing the evaporating pressure does in fact increase thermal efficiency and work power output, however, due to the nature of the phase envelope will expansion of the working fluid lead to lower steam quality. This is demonstrated in Figure 23. Expansion at lower steam quality results in liquid condensate potentially damaging turbine blades resulting in decreased turbine efficiency. Likewise for the reduction in condensing temperature. This issue can be solved by superheating the working fluid, providing sufficient steam quality during expansion. Superheating the working fluid further increases the thermal efficiency as heat addition occurs at a greater average temperature.[14]

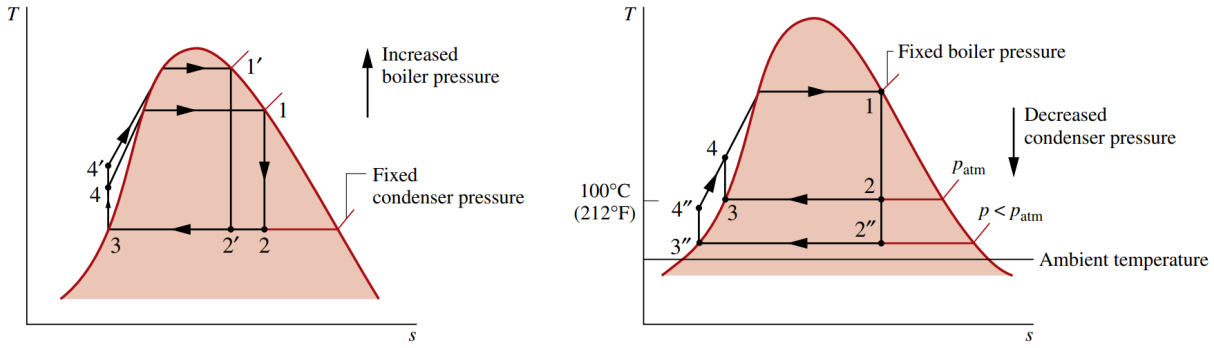

Figure 23: Effect of different operating pressures [14]

Further improvements include supercritical and reheat cycle. The reheat cycle expands the superheated steam in multiple stages. This methods preserves the higher thermal efficiency of the higher evaporation pressure while keeping the steam quality high. Supercritical, also known as transcritical, operates in pressure and temperature above the critical point. This allows for a further increase in the thermal efficiency, but at the expense of higher installation costs of equipment rated for higher pressures and temperatures. Figure 24 presents the combined supercritical reheated ideal cycle.[14]

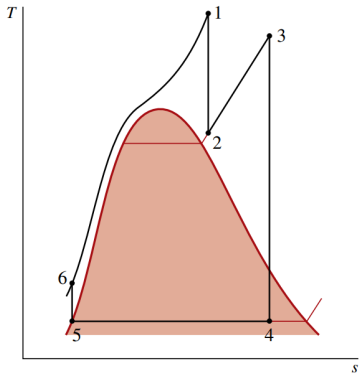

Figure 24: Ideal supercritical reheat cycle [14]

The of the most promising modification is the use of a recuperator. The recuperative cycle includes an additional heat exchanger situated between the pump and gas heater on the high pressure side and between the condenser and expander on the low pressure side as presented in Figure 25. The recuperator helps recover a larger fraction of the heat energy by pre-heating the high pressure working fluid using the excess heat energy at discharge of the turbine. The thermal efficiency of the power cycle is improved as the mass flow rate of the working fluid can be increased at the same thermal input, consequently increasing power output in the expander. Analysis show that the highest thermal efficiency is achieved at lowest obtainable pinch point in the recuperator, achieving the lowest possible heat rejection. The recuperative cycle will in theory have minimal impact on the capital costs of the system as the additional heat exchanger area will be compensated by the reduction in area of the gas heater and condenser.[85]

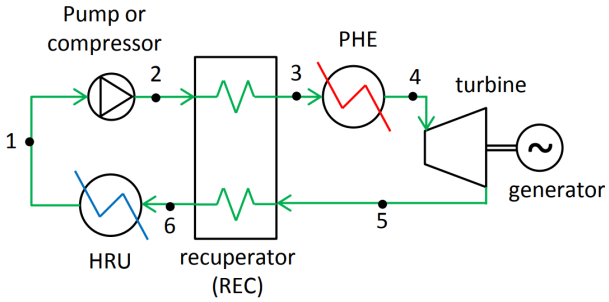

Figure 25: Recuperative cycle [85]

2.6.4 Marine applications

Zhu et al. has conducted a review presenting bottoming power cycles for marine engine waste heat recovery. The article presents opportunities of fuel savings in the range of 4-15% as seen in the Table 10. The study includes a thermodynamic comparison and a recommendation based on studies from the previous decade. For larger ships with marine engine outputs above 25 MW, the dual-pressure SRC with PT is suggested. The system is mature and environmentally friendly. KC's also operate well with high engine output. The disadvantages being the complex layout, the high operating pressures and risk of toxic leakage in machinery room. For smaller ships, ORC is superior compared to SRC and KC. The simple layout and excellent thermodynamic properties work well in marine applications. However, have a major disadvantage as refrigerants often are flammable, toxic and have a negative impact on the environment. CO_2 based power systems have energy potentials competitive with SRC and ORC. They are especially appealing for marine applications due to compact design.[70]

Configuration	Size	Cost	Maximum potential	Engine size
PT	Very small	Very low	3-5%	<15 MW
SRC	Large	Middel	4-8%	<25 MW
SRC plus PT	Large	High	8-11%	>25MW
ORC	Middel	High	5-15%	>250 kW
KC	Large	High	5-8%	-
CO2	Small	Middel	5-11%	>5 MW

Table 10: Comparison of different bottoming power cycles [70]

Zhang et al. has conducted a thermodynamic analysis of a transcritical CO_2 rankine cycle integrated with a ejector refrigeration cycle presented in Figure 26. The cycle is driven by exhaust gas from four 2750 kW diesel engines situated on a cruise ship with a capacity of 1800 passengers. The system is fitted with a three-way valve adjusting mass flow of CO_2 at inlet of turbine 1 and 2. This ultimately lets the system control output of heating, cooling and power depending on seasonal demand. By sending majority of refrigerant through turbine 1, electricity and hot water at 90 °C is produced. Typically for winter conditions. During summer operation, CO_2 expands through turbine 2 producing low temperature water at 45 °C and has the option to deliver cool air for air-conditioning at an evaporation temperature of 5 °C. The case study considered seawater temperatures ranging from -2 °C to 22 °C, implying that the low condensation temperature can be met. During summer mode the system is optimized to provide 499.26 kW cooling output and 133.57 kW net power output. While during winter mode, the system provides high temperature water heating and net power of 447.64 kW and 223.19 kW respectively. The result are compared to a commonly studied regenerative ORC utilizing R123 working fluid operating in subcritical state. The analysis conclude increased efficiency, but most importantly the advantage of operational flexibility with CO_2 cycle compared to the reference cycle.[96]

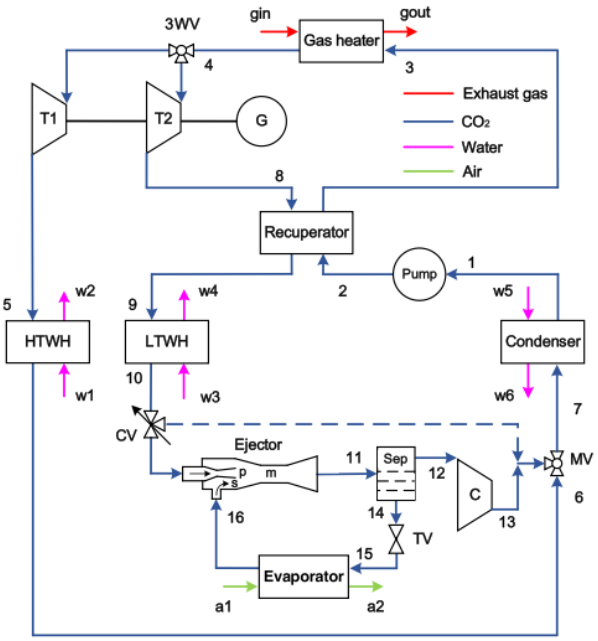

Figure 26: System layout Zhang et al. [96]

2.7 Cold Recovery

In the case of cruise ships utilizing LH_2 as fuel for engines, hydrogen will be stored onboard at a temperature of about -253 °C. In order to meet engine operational requirements, LH_2 must be pre-heated before injected into the engine. This cold energy associated with pre-heating of LH_2 can be utilized throughout the cruise ship for provision cooling or air-conditioning. Thus, reducing the overall fuel consumption of the cruise ship. As LH_2 cruise ship have yet to be developed, there is a lack of data considering cold recovery of LH_2 for marine applications. However, LNG stored at -162 °C utilize technology similar to that of LH_2 cold recovery. According to literature, only one cruise ship is operating with LNG but 33 are on order.[97] From a environmental perspective, there is good reason to believe that LH_2 will also play a big role in marine transportation. Therefore, cold energy recovery technology is attractive to further reduce emissions in the marine transportation industry.

Though the use of cryogenics onboard passenger ships have a relatively short history, the concept of regasification of LH_2 and LNG is well known. As hydrogen and natural gas is easier to transport in liquid state, customers will have to regasify LH_2 and LNG before distributed throughout the gas network. Regasification require a heat source in order to vaporize the cryogenic fuel, often with direct heat transfer from seawater or other heat sources. This method is complete waste of the cold energy along with mechanical power required to operate seawater pump.[98]

The largest importers of LH_2 and LNG is China, South Korea and Japan. Japan recovers and utilizes about 30% of all cold energy from LNG regasification. Among these plants is the Osaka gas plant, operating a cryogenic power generation system for 100% cold energy utilization.[99] LNG cold energy has also been implemented for cryogenic comminution and air seperation in South Korea. Numerous other processes are implemented such as hydrocarbon liquefaction, seawater desalination, dry ice production, refrigeration and cold energy storage. In regards to the demands of a cruise ship, will the process of cryogenic power generation, refrigeration and cold energy storage be of most interest.[98]

The benefits of cryogenic power generation is that the cold energy from LH_2 can further improve the overall efficiency of power cycles. Cold energy can either be used to decrease the inlet compressor temperature of a open brayton cycle or lower condensation temperature in rankine cycles reducing the optimum operating pressures. Due to the low condensation temperatures, even heat sources of low quality such as solar power, seawater and engine cooling water can be used for power generation. However, if large thermal efficiencies are to be achieved, heat sources of higher quality are preferable. CO_2 is then an excellent working fluid able to encounter larger temperature changes in comparison to organic fluids. This opens for opportunities of utilizing waste heat from exhaust gas as a heating source.[98]

Xia et al. has analysed a transcritical CO_2 rankine cycle utilizing solar power as heating source. The study concludes that the decrease of condensing temperature will further increase the exergy efficiency of the cycle.[100] Another study by Wang et al., analyzes a transcritical CO_2 rankine cycle with LNG heat sink and geothermal heat source. The study concludes that higher inlet temperature and pressure of turbine increase the overall energy conversion efficiency.[101]

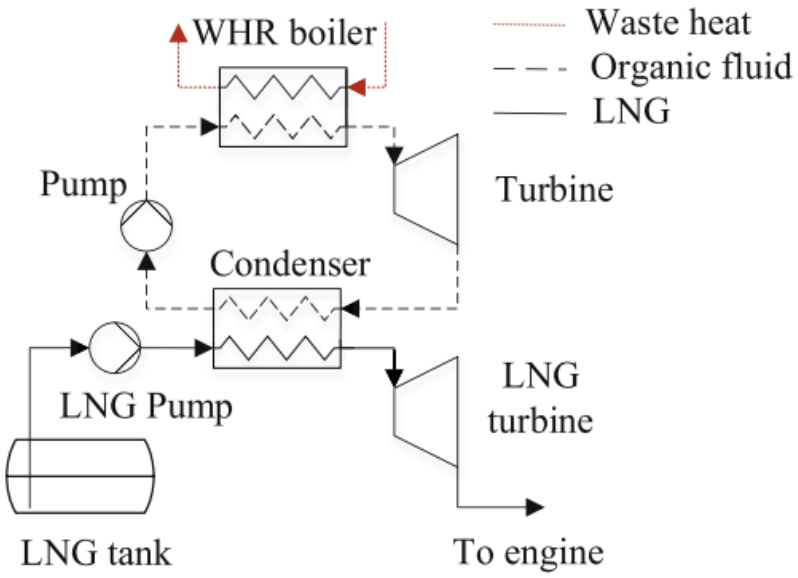

Figure 27: ORC configuration [8]

Baldasso et al. has numerically investigated an organic rankine cycle utilizing LNG and waste heat sources onboard a ship as presented in Figure 27. The ORC is integrated with a LNG direct expander as shown in the figure above. LNG is pressurized in a pump, evaporated in the condenser and finally expanded in order to produce power as the final stage of regasification. The study compares the net power output of the ORC utilizing different sources of waste heat and a selected working fluids. The heat sources investigated include glycol-water for HVAC, seawater, jacket cooling water and main engine exhaust gas. The ORC is limited to a pressure range 30 to 0.045 bar depending on the working fluid. This is to avoid freezing and thermal deterioration of the working fluids. This cycle will thus run in subcritical state. The ship operates with an engine rated at 8 MW. At an average load of 85%, the engine provides exhaust gas at a temperature of 365.4 °C and mass flow of 22.8 kg/s. This requires a total LNG consumption of 2700 kg/h.[8]

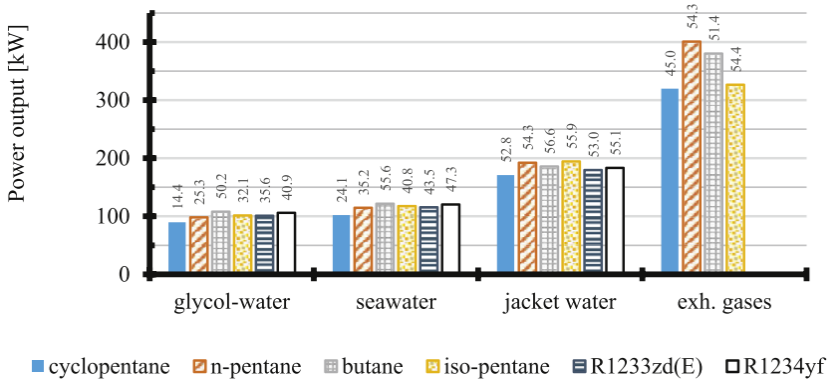

Figure 28: ORC power output [8]

The results show promising numbers. However, due to the low degradation temperatures of the working fluids will heat absorption from heat sources be limited. The temperature at boiler outlet only drops about 30.1 - 35.6 °C. Figure 28 above clearly illustrates this limitation as n-pentane, with highest degradation temperature, achieves the greatest power output. This limitation can be solved by utilizing CO_2 as working fluid. Glycol-water and jacket water achieve an estimated power output of 108 kW and 194.4 kW respectively. Jacket water is great source of heat due to the stable mass flow. Glycol-water is also a great alternative in warmer ambient conditions

where air-conditioning demand is high. The exhaust gas provide the largest power output of 400 kW. This results in a total fuel saving of 2.37%.[8]

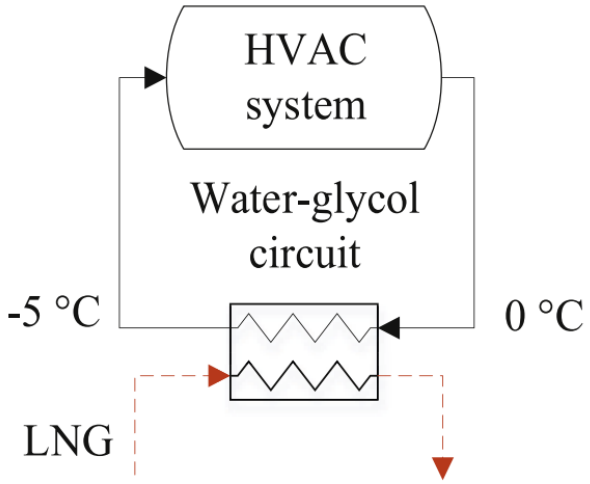

Figure 29: Water-glycol circuit [8]

Baldasso et al. also investigates LNG cold recovery with direct coupling to a glycol-water air-conditioning circuit. Glycol-water is cooled through regasification of LNG and provides cold energy to decentralized air-handling units onboard the cruise ship as illustrated in Figure 29. By providing cold energy from regasification of LNG to air-conditioning units, power consumption of HVAC chillers can be reduced. The performance of the cold recovery can measured by comparing cold recovery with existing marine HVAC systems for total power consumption reduction. The study assume a COP of 3 and 5 for existing HVAC systems. Auxiliary generators were assumed to consume 0.16 kg/kWh of LNG. The result clearly indicate that total fuel savings are dependent on the COP of the chillers. Warmer ambient temperatures lead to lower performance of the chillers, thus making cold recovery more attractive. The estimated fuel savings at a COP of 5 are 13.56 kg/h, 0.50% of total fuel consumption. Further increasing to 0.84% at a COP of 3.[8]

2.8 Thermal energy storage

Energy demands vary significantly on daily, weekly and seasonal basis. These demands may vary significantly from the energy supply of a marine application. By using thermal energy storage (TES) through operational strategies may these fluctuating demands be better matched by energy supply for optimal power consumption, better energy efficiency, operational flexibility and economic benefits. TES has received much attention regarding thermal applications such as commercial refrigeration within food processing, hotels, and transportation. Hotels, may use TES in order to lower the overall electrical demand but also the total discharge of electricity, also known as peak shaving. Charging the TES system before peak hours of electricity demand, reduce the peak discharge of electricity as seen in Figure 30. This enables strategic operations where TES can charge during hours of less expensive electricity and discharge at peak for economic benefits.[102]

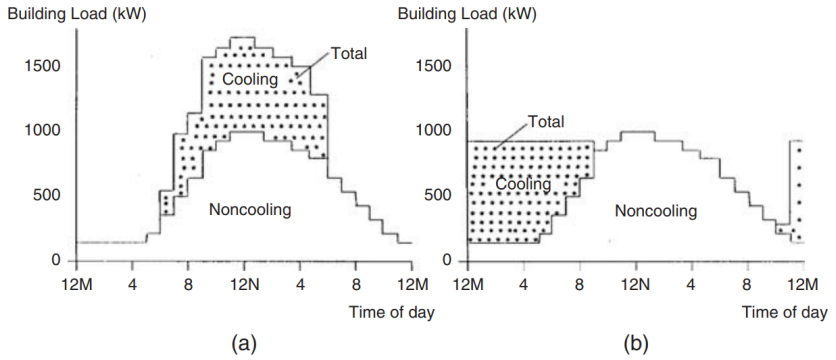

Figure 30: Peak shaving of electrical demand: (a) no TES (b) TES [102]

TES also helps reduce capital cost of refrigeration units, or other equipment providing thermal energy, through strategic charging. The three most common methods are full, near-full and partial storage presented in Figure 31. Through full storage, chillers can be turned of completely during peak cooling demands mid-day. This method is beneficial reducing the electricity costs, however, may not reduce capacity of refrigeration units. By operating partial storage, refrigeration units may be reduced substantially as the chillers continuously provide only about 60% of capacity. The final method and perhaps the most beneficial is the near-full storage. This allow for both a reduction in capital cost and electricity expenses.[102]

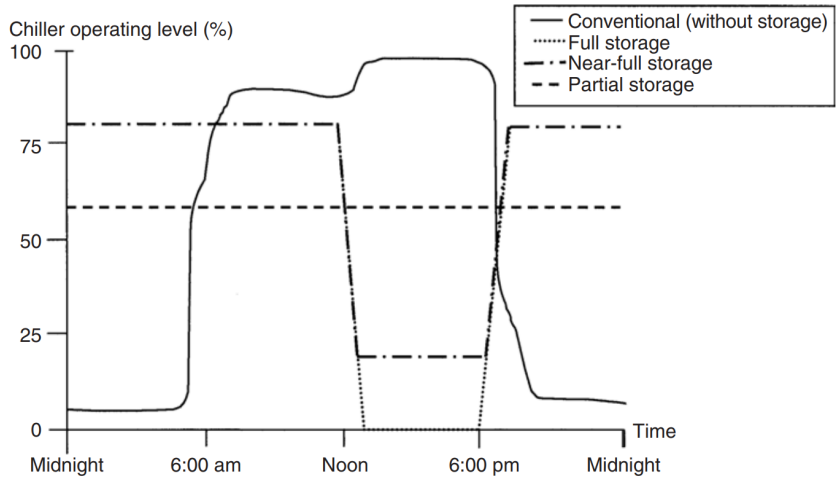

Figure 31: Charging strategies [102]

The coupling of TES with waste heat recovery onboard marine applications has large potentials from a environmental and economic perspective. Consumption reduction is achieved when excess waste thermal energy is stored and later discharged for cooling or heating demands during stand-by's or peak loads. During peak load demands, TES can be run parallel with heating and cooling equipment reducing the overall size and max power output required, thus, reducing costs.

2.8.1 Sensible

The methods of TES are sensible and latent. The concept of sensible TES is the temperature increase or decrease of a given material with no phase-change. The heat storage magnitude is dependent of material density and specific heat capacity. As the term implies, specific heat capacity indicates a materials ability to store thermal energy and resist temperature change.

The most common heat transfer medium of sensible TES is water. Water is readily available, non-toxic, inexpensive, and has a high specific heat capacity of 4.2 kJ/kgK. As a liquid, it obtains the benefit of being easily transferred through tubes using a pump. As an advantage, this allows liquids such as water to operate as both the heat transfer medium and storage medium. This reduces the amount of heat exchangers required and overall temperature lift in the TES system.[103] The limitations of water are the freezing and boiling points. To operate at higher temperatures, rock is a typical material for sensible TES. Rocks have a significantly lower specific heat capacity, however, the relatively high density and ability to operate at much larger temperatures compensate for the low heat capacity.[102] The amount of heat stored in TES materials can be calculated using the following equations:

$$Q_{sensible} = \frac{mc_p\Delta T}{3600} = \frac{\rho c_p V \Delta T}{3600}\ [kWh] \tag{5}$$

Another important parameter when considering materials for sensible TES is the rate at which heat is extracted or released. This is a function of thermal diffusivity or thermal conductance. Iron pellets have excellent thermal storage characteristics of high thermal conductivity and high heat capacity. Rocks and iron pellets are also considerably easier to store in comparison to liquids, considering the quality of thermal containers. Liquids require higher quality container to prevent leakage. The thermal containers must also be able to store thermal materials with minimal heat loss while maintaining a thermal gradient.[102] Materials of high energy density is preferred, as smaller volume storage units can be used and heat transfer area is reduced. From Table 11 it is clear that water has the highest energy density out of the selection. Water is also great for thermal stratification, also known as thermal layering, where hot and cold fluid is separated by a thermocline due to density differences of the temperature gradient.[104]

Material	Density (kg/m^3)	Specific heat (J/kgK)	Volumetric thermal capacity (10^6 J/m^3K)
Clay	1458	879	1.28
Brick	1800	837	1.51
Sandstone	2200	712	1.57
Wood	700	2390	1.67
Concrete	2000	880	1.76
Glass	2710	837	2.27
Aluminium	2710	896	2.43
Iron	7900	452	3.57
Steel	7840	465	3.68
Gravelly earth	2050	1840	3.77
Magnetite	5177	752	3.89
Water	988	4182	4.17

Table 11: Sensible TES materials at 20 °C [102]

2.8.2 Latent

Latent TES works by releasing or absorbing thermal energy through change in physical state of materials, also known as phase-change material (PCM). During charging, PCM absorbs thermal energy from a source undergoing phase-change. During discharging, the PCM once again undergoes phase-change releasing latent heat of enthalpy. The benefits of latent TES is the high energy storage densities and the low temperature range. During discharging of cold energy from ice for example, PCM temperature will rise linearily until phase-change. Then release cold energy at constant temperature through phase-change as presented in Figure 32.

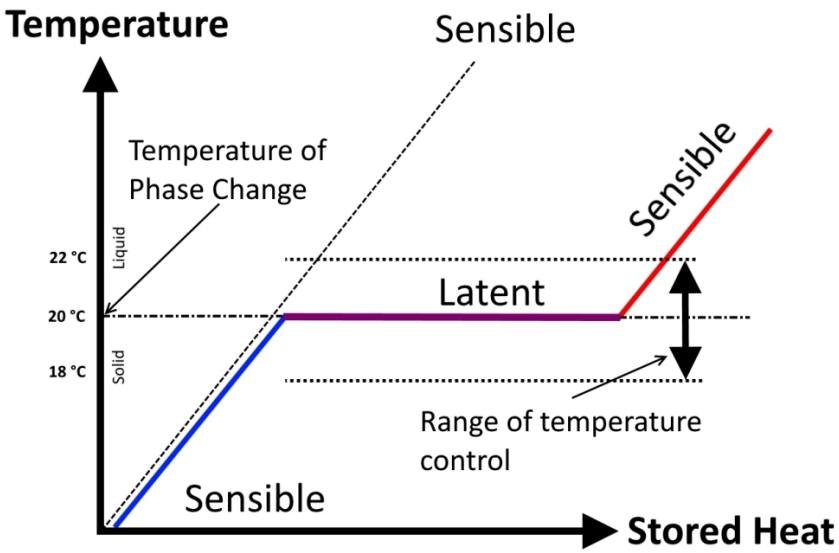

Figure 32: Principle of sensible and latent heat [105]

PCM absorb or release heat through phase-change from solid to liquid, liquid to gas, or vice versa.[106] The equation of latent TES can be expressed as:

$$Q_{latent} = \frac{m\Delta h_L}{3600} = \frac{\rho V \Delta h_L}{3600} \; [kWh] \tag{6}$$

The most common storage medium of latent TES is water-ice. With the advantageous attributes described earlier, it has a latent heat of enthalpy of 335 kJ/kg at the phase-change temperature of 0 °C. Heating water at 0 °C to 12 °C requires about 50.2 kJ of thermal energy, heating ice at 0 °C to 12 °C requires about 385 kJ. This comparison illustrates the significant capacity latent TES holds in the case of ice, 7.6 times higher than sensible TES. This larger energy density of latent TES greatly reduces the required storage volume. In fact, sensible TES of water requires four times the volume of latent TES to achieve same thermal energy capacity.[102] A selection of common PCM's for latent TES are shown in Table 12.

Material	Melting temperature (°C)	Latent heat of enthalpy (MJ/m^3)
Water-salt solution	-100 to 0	200-300
Water	0	330
Clathrates	-50 to 0	200-300
Paraffins	-20 to +100	150-250
Salt hydrates	-20 to +80	200-600
Sugar alcohols	+20 to +450	200-450
Nitrates	+120 to +300	200-700
Hydroxides	+150 to +400	500-700
Chlorides	+350 to +750	550-800
Carbonates	+400 to +800	600-1000
Fluorides	+700 to +900	>1000

Table 12: Latent PCM materials [107]

2.8.3 Thermal Energy Storage passenger ships

The most common method of providing thermal energy onboard a cruise ship is through waste heat recovery of exhaust gas. During port stay, waste heat from exhaust gas is not sufficient to meet thermal demand as the ships main engine is not operated, therefore, HFO boilers are used. The EU is proposing that all cruise ships must operate with zero-emission technology in European ports by 2030. This means that cruise ships will have to find new innovative solutions to use thermal energy during port stay. Port stay typically varies up to 10 hours. The required thermal demand of such time slots can be up to 6 MW and similarly for electrical demand. Cruise operators are introducing shore power during port stay, providing electricity. This may drastically reduce emissions as auxiliary engines will not operate. However, it is not as easy to get thermal energy from shore.[108] Alternatively, electrical boilers may be used but are often energy intensive with low efficiency. The shore power capacity will then increase which is already limited in many ports. The majority of emission are emitted during sea-going, however, emissions during port-stay has the most effect on cities and humans. TES has become more standard in the industrial sectors, many studies have been performed developing solutions for the mismatch of demand and supply energy. However, hardly any research has been put towards TES in the marine transportation sector.[109]

A study by Baldi et al. was performed with the aim to partially fill this gap of lacking knowledge. The study investigated a merchant ship with two main engines with an overall power rating of 7.68 MW, three auxiliary engines of about 2 MW and two auxiliary boilers providing steam at a total of 28000 kg/h during port stay. During sea-going, auxiliary boilers provide 1400 kg/h of steam while the main engines supply heat and power for propulsion. Excess heat from the exhaust gas during sea-going was stored in cylindrical storage tanks containing thermal oil as presented in Figure 33. Water as heat transfer medium was also considered however require about 10 bar of pressure to avoid evaporation. Assuming an heat exchanger coefficient of 40 W/m^2K, heat exchanger area of 70 m^2, exhaust gas specific heat capacity of 1.08 kJ/kgK, the study concluded that 1000 m^3 storage tank was sufficient to cover 70 % thermal demands during port stay with thermal oil of 100 °C. By further increasing the storage tank to 2500 m^3, 90% of thermal demand could be covered. Although increasing the storage tank helps reducing emissions will heat loss and capital cost increase. Further increasing the temperature of the thermal oil allows for smaller storage volumes.[109]

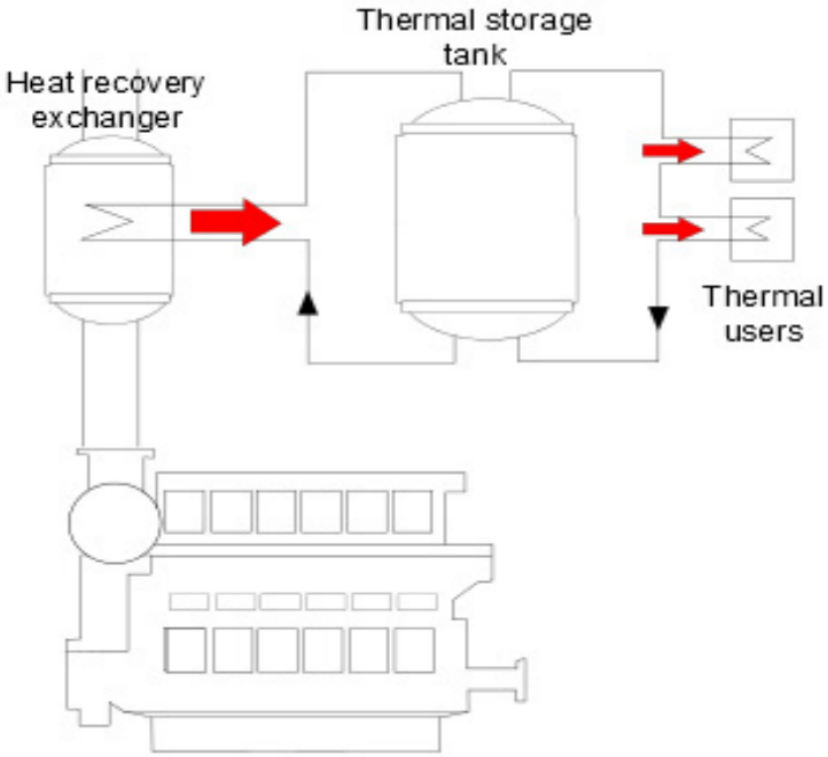

Figure 33: TES layout merchant ship [109]

During port stays of long duration's, electricity can be provided from shore. However, not during short stays. Andreasen et al. has investigated waste heat recovery using an organic rankine cycle with thermal energy storage during short port stay. During cruising, majority of waste heat from hot exhaust gas is used to charge TES system and remaining is used for power generation of ORC. During port-stay, the TES system is discharged in order to provide power from the ORC. This ensures a lower power demand from auxiliary generators which reduce release of emissions amongst the city. See Figure 34. The study investigated a stratified storage tank operating with thermal oil capable of temperatures as high as 345 °C at ambient pressure. The study considered an hypothetical ferry operating with two LNG powered engines of 8 MW power output each. The waste heat exhaust gas result in a thermal oil temperature of 310 °C. This thermal oil was used to provide electricity to the ship from an ORC during port stays ranging from 20-60 minutes. The study concluded that an stratified tank of 82.1 m^3 was capable of providing about 82% of the required 1 MW of electricity during port stay. The TES system reduces annual CO_2 emissions by 8%, corresponding to a daily reduction of 5.4 ton CO_2. The TES system also reduces emissions such as CO, SO_x and NO_x.[110]

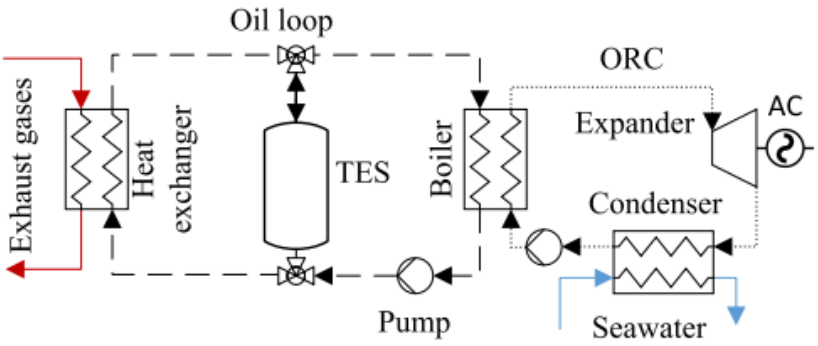

Figure 34: TES system Andreasen et al. [110]

2.8.4 Cold Thermal Energy Storage

Cruise ships do not experience the fluctuating electricity prices in the same way as a supermarket. The objectives of cold thermal energy storage (CTES) for ships will therefore be peak shaving for reduced refrigeration unit capacities, backup cooling capacity, or the possibility of reducing emissions during port stay. An experimental study by Tan et al. investigate cold energy storage of LNG in a refrigerated vehicle. Liquid natural gas is regasified by passing through a copper tube in a cold storage unit containing water. The cold liquid natural gas freezes the water around the copper tubing. During discharging, air is then blown about the cold storage unit providing cold air. The concept is illustrated in Figure 35.[111] The concept completely eliminates the necessary cooling output from a refrigeration system, thus saving fuel. The same concept may be used contributing to the cooling demand onboard cruise ships in the case of LNG or LH_2 operations.

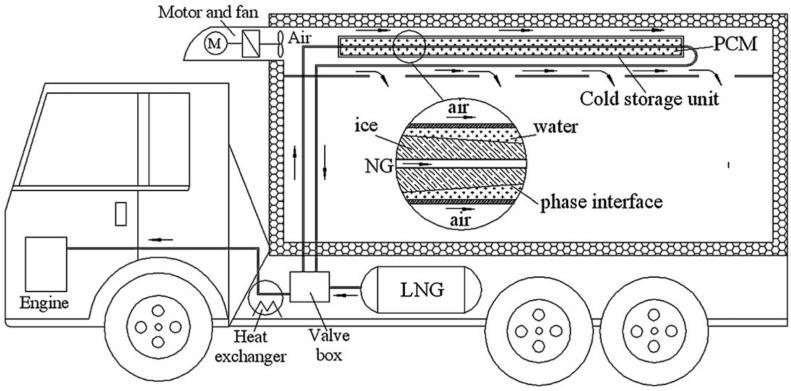

Figure 35: Cold TES refrigerated vehicle [111]

A study by Saeed et al. investigate the potentials of LNG cold utilization of a LNG fishing vessel. The study examines the possibility of charging a cold thermal energy storage tank through vaporization of LNG. A water-based PCM was then analyzed with a phase-change temperature of -6 °C. The study investigates charging of different volume storage tanks at various LNG mass flow rate. The study found that about 176 kWh of cold energy could be charged in about 13 hours. This CTES system may then be used for assisting the refrigeration systems onboard for chilling fish, increasing system performance.[112]

3 System Design

This chapter will describe the design case of a cruise ship operating on hydrogen or ammonia. The objectives of this thesis is to design and simulate different thermal systems in order to increase energy efficiency, reduce fuel consumption, reduce emissions and investigate the possibilities of zero emissions during port stay. The thermal systems will be analysed and compared for optimum performance.

3.1 Reference case

For this master's thesis, a case study created by Baldi et al. was used as a reference case to evaluate the potentials of reducing fuel consumption and emissions onboard cruise ships.[9][3] The ship of the case study is 176.9 m long and has a width of 28.6 m, which classify the ship as medium sized with a total passenger capacity of 1800. The case study presents a cruise ship operating daily voyages between Stockholm, Sweden, and Mariehamn, Finland, in the Baltic sea. Figure 36 presents the typical daily operational profile of the cruise ship. The ship departures the port of Stockholm at 18:00 and cruises the Stockholm Archipelago until reaching open sea at midnight. The ship continuous cruising at 05:00, arriving in Mariehamn at 07:00 for a one hour port stay. The cruise is then set back to Stockholm at 08:00, arriving at 15:00 for a three hour port stay until the next voyage.[9]

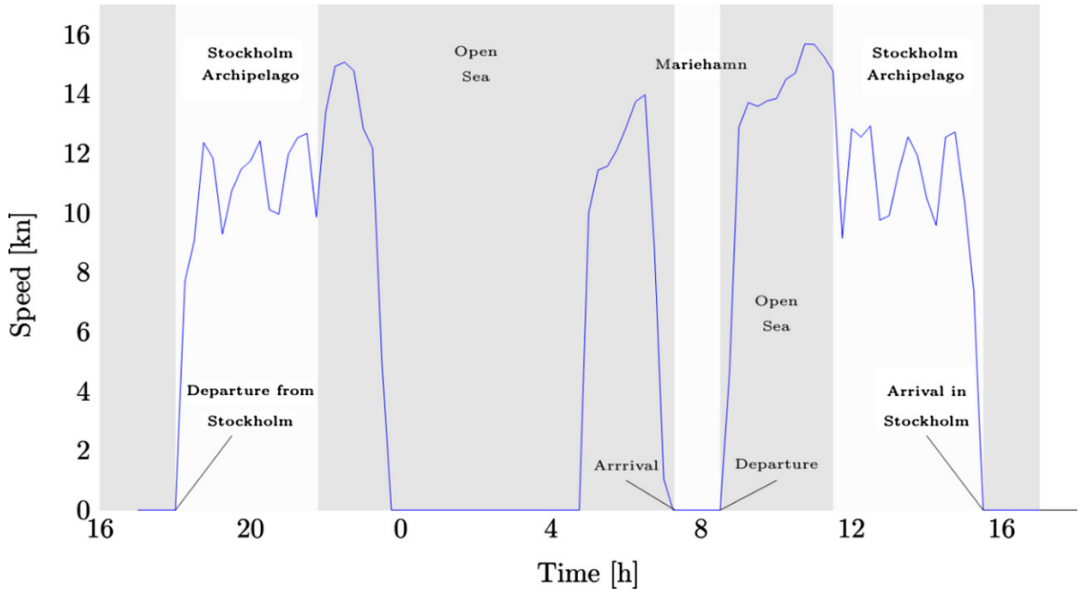

Figure 36: Typical ship operational profile [9]

The cruise ship offers passengers onboard access to restaurants, bars, nightclub, pools and saunas. This requires both thermal energy and electrical energy along with the mechanical energy required for propulsion. This results in the four main categories of power demands, specifically mechanical, electrical, heating and cooling. The mechanical power for propulsion is met by four 4-stroke diesel engines with a power rating of 5850 kW each. The four engines make up for two separate propulsion lines which consists of a gearbox and propeller as presented in Figure 37. The electrical demand is provided by operating four auxiliary diesel engines of a rated power output of 2760 kW each. The electrical users include refrigeration units which provide the cooling demand onboard. The refrigeration unit has a maximum cooling power output of 2000 kW with an energy efficiency ratio (EER) of 3.5. The average cooling demand is near constant for the case study with a cooling demand of about 1000 kW. All engines are equipped

with heat recovery steam generators (HRSG), providing heat to thermal users. Two additional marine-oil auxiliary boiler with a thermal output of 4500 kW each are also equipped, with a thermal efficiency of 80% operable during peak heating demands or during port stay.[9]

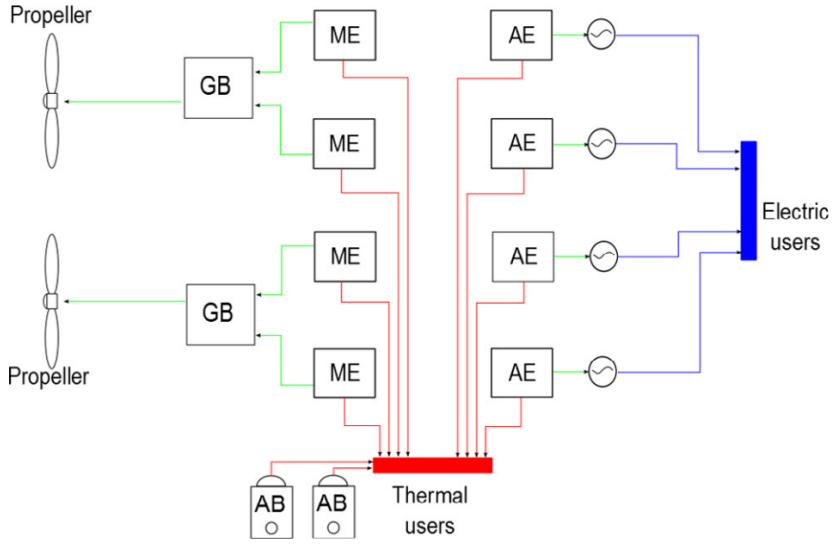

Figure 37: Reference case system layout [9]

The reference case provides specific energy demands based on onboard measurements but also under certain assumptions. The propulsive power demand is estimated, with a uncertainty of 6%, using dedicated sensors on the main engines, determining fuel rack position and speed. The electrical demand is measured directly onboard. However, the thermal demand are assumed based on the assumption that demands are similar to that of hotels. The assumption is estimated to have an uncertainty of 10%.[9] This results in the plot provided in Figure 38, representing the energy loads required during a cruise during summer conditions.

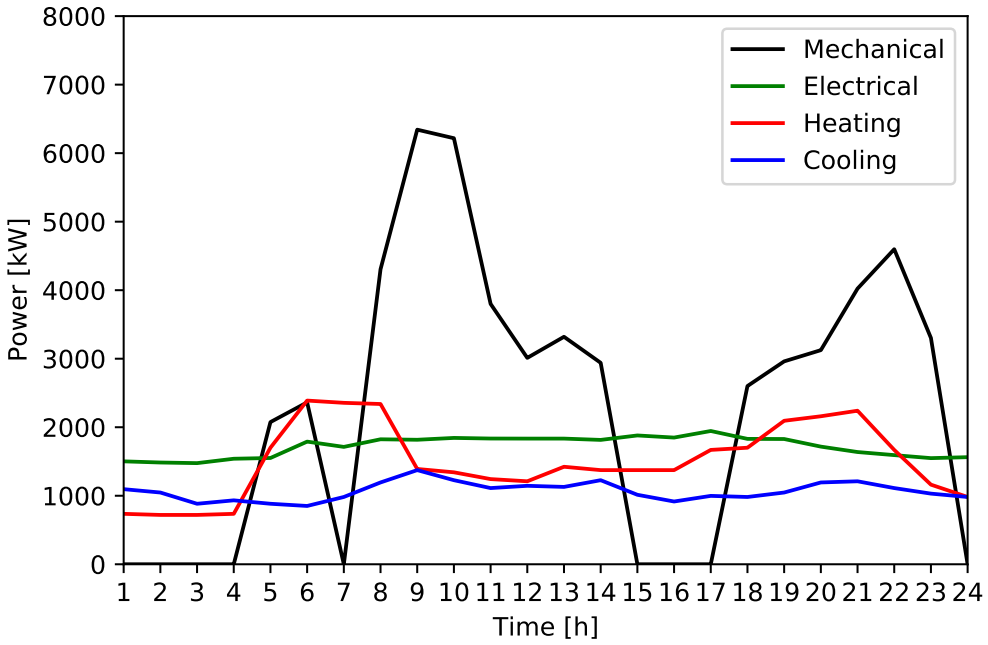

Figure 38: Energy loads

During cruising, the main engines provide mechanical power for propulsion while the auxiliary engines provide the electrical power. Both engine types recover excess heat from exhaust gas to thermal users such that the auxiliary boilers (AB) operate with minimal load. However, during port stay most of the thermal demand must be met through operation of the auxiliary boilers as the main engines are shut off. This results in a significant release of emissions along harbours given that auxiliary boilers operate through combustion of marine oil along with the combustion of marine diesel in the auxiliary engines. Further developments and research within the cruise sector is crucial to meet the environmental restrictions in the near future.

3.2 Design case

The objectives of this master's thesis was to investigate possibilities of increasing energy efficiency and reducing emissions of cruise ships. Figures 39 and 40 present the proposed system layouts of the design cases of this master's thesis. As majority of the power demands are provided from the main engines and auxiliary engines, will replacing these engines with more environmentally friendly alternatives have a significant impact on overall emissions. Hydrogen and ammonia was therefore investigated as an alternative fuel for cruise ship propulsion and auxiliary power generation. Therefore, two design cases have been considered in this study, operating with hydrogen and ammonia. This includes fuel storage, engine performance and the possibilities of waste heat recovery from excess waste heat from the internal combustion engines.

The waste heat exhaust gas of the main engines were investigated for potential electricity generation. Operating bottoming power cycles, energy efficiency of the cruise ship can be increased by generating electricity which reduce fuel consumption of the auxiliary engines. After the bottoming power cycle, exhaust waste heat recovery was also investigated for high-temperature water heating (HTWH), providing thermal demands onboard the ship. The integration of TES in the waste heat recovery unit was also investigated for the possibility of storing excess heat, matching fluctuating heating demand and providing thermal energy during port stay, with zero emissions.

CO_2 refrigeration units were also investigated for both design cases, providing cooling onboard with low-emission and high energy efficiency. Further, waste heat recovery of cold thermal energy from liquid hydrogen has also been examined for the possibility of reducing refrigeration capacity or reduce fuel consumption of auxiliary engines. Finally, for the hydrogen design case, cold thermal energy storage was examined for the potential of providing cooling demand with zero emissions during port stay.

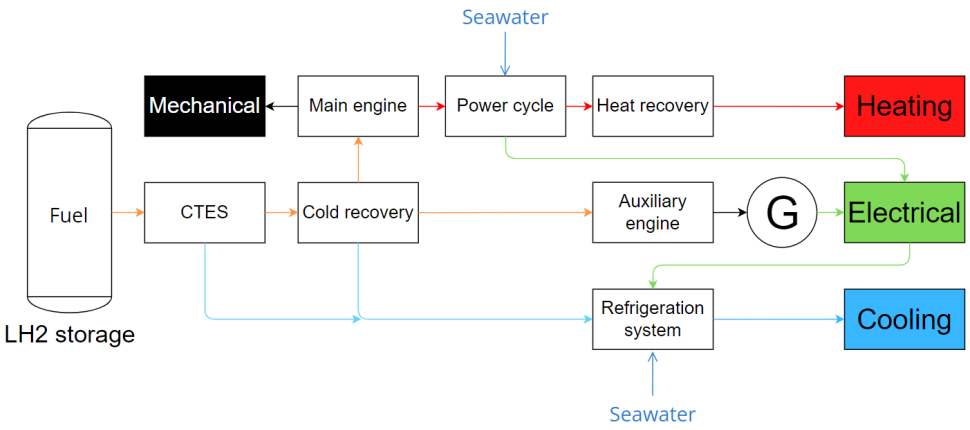

Figure 39: Hydrogen design case

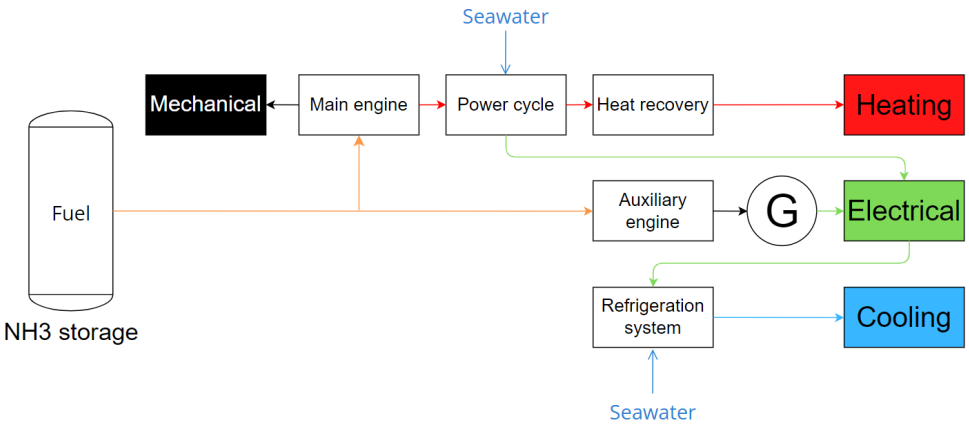

Figure 40: Ammonia design case

The thermal systems were designed and simulated on the basis of the energy demands obtained from the reference case, representing the operational profile during summer conditions. For summer conditions, the thesis assumed an ambient temperature of 25 °C and seawater temperature of 20 °C.

Objectives

The following tasks are to be considered:

- Investigate hydrogen and ammonia marine internal combustion engines
- CO_2 refrigeration systems
- Waste heat recovery of exhaust waste heat for increased energy efficiency
- Cold recovery of liquid hydrogen
- TES for zero emission energy utilization during port stay

3.3 Hydrogen and ammonia marine engines

From the literature study it is clear that both hydrogen and ammonia are promising alternative fuels for marine engines. Both fuels have the potential to achieve great thermal efficiencies, yet both are limited due to the increased NO_x emissions. Based on the literature study, the thermal efficiency (η_{th}), fuel injection temperature (T_{in}), fuel injection pressure (P_{in}), energy-based NO_x emissions and exhaust temperature (T_{exh}) are assumed for both engines of hydrogen and ammonia and presented in Table 13. The engine parameters are assumed to be valid for both the main engines and the auxiliary engines.

Fuel	η_{th}	T_{in}	P_{in}	NO_x	T_{exh}
Hydrogen	35%	80 °C	3 bar	3.4 g/kWh	400 °C
Ammonia	40%	25 °C	10 bar	3.4 g/kWh	400 °C

Table 13: Engine parameter's

3.3.1 Fuel storage

Liquid storage has proven to be the better alternative for both fuels. Liquid hydrogen will then be stored at a pressure and temperature of 3 bar and -248.5 °C, respectively. Liquid ammonia is then stored at ambient temperature of 25 °C and pressure of 10 bar. Knowing the sum of the total mechanical and electrical power demand throughout the voyage and the thermal efficiency of the internal combustion engines, can the total energy input from the fuel be calculated from the following equation:

$$\text{Required fuel input energy} = \frac{\text{Energy demand}}{\eta_{th}} \; [kWh] \tag{7}$$

Further, the total fuel storage volume and fuel storage mass can be calculated knowing the volumetric and gravimetric energy density of liquid hydrogen and liquid ammonia obtained from Table 3 in the literature study.

$$\text{Total fuel storage volume} = \frac{\text{Required fuel input energy}}{\text{Volumetric energy density}} \; [m^3] \tag{8}$$

$$\text{Total fuel storage mass} = \frac{\text{Required fuel input energy}}{\text{Gravimetric energy density}} \; [kg] \tag{9}$$

3.3.2 Fuel consumption

The total fuel consumption of the internal combustion engines are calculated from assumptions and data attained from literature studies presented. Given the lower heating value of the fuel (LHV) and the thermal efficiency (η_{th}) of the ICE, can the mass flow rate of the fuel consumption be calculated from the following equation as a function of the power output (P_{out}):

$$\dot{m}_{fuel} = \frac{P_{out}}{\eta_{th} * LHV} \; [kg/s] \tag{10}$$

Further, knowing the optimal stoichiometric air-fuel ratio (AF) along with the excess air factor (λ), can the mass flow rate of air required be calculated from the following equation:

$$\dot{m}_{air} = AF * \lambda * \dot{m}_{fuel} \; [kg/s] \tag{11}$$

Finally, the summation of the mass flow rates result in the total exhaust gas flow rate:

$$\dot{m}_{exhaust} = \dot{m}_{fuel} + \dot{m}_{air} \; [kg/s] \tag{12}$$

The following data of Table 14 is used to calculate the total fuel consumption and exhaust mass flow rate of the respective internal combustion engines:

Fuel	η_{th}	LHV	AF	λ
Hydrogen	35%	130 MJ/kg	34.78	4
Ammonia	40%	20 MJ/kg	6.0466	1.4

Table 14: Engine parameter's [113][114]

The total fuel consumption and exhaust mass flow rates are presented in Figure 41. These values are further used in the calculations of potential waste heat recovery from the main engines.

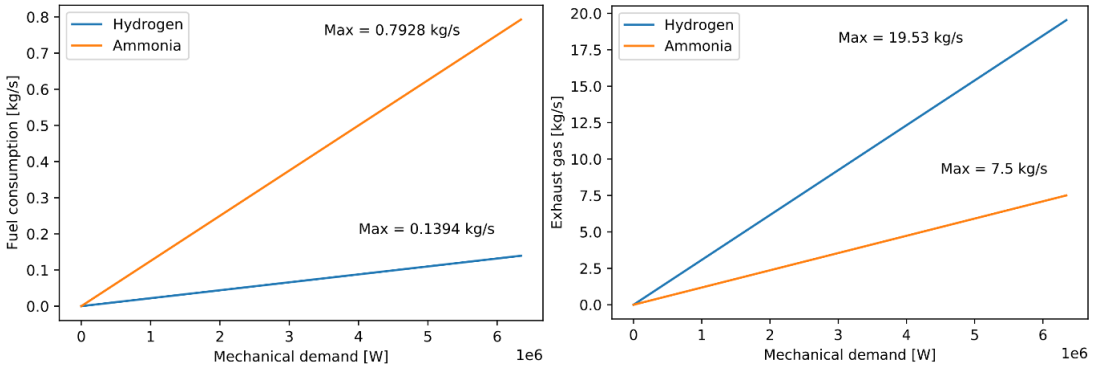

Figure 41: Mass flow rates of fuel and exhaust gas

3.4 CO_2 refrigeration cycle

The reference case provides cooling from a refrigeration unit with an EER of 3.5. The EER defines the ratio of cooling output in British thermal units (Btu) per hour to the compressor power input in watt. 1 Btu per hour is equal to 0.293 W. EER of 3.5 is therefore equivalent to a COP of 1.03. From the literature presented, it is clear that the equipped unit performs significantly worse than state of the art refrigeration units. Refrigeration units onboard marine applications have also proven to represent a large degree of total emissions, about 18.9% of leakage of all refilled refrigerant. As the most common working fluid of R134a has a GWP = 1300, will refrigerant leakage have a significant impact on global warming. This master's thesis will therefore investigate CO_2 refrigeration units for high performance and low emissions cooling onboard cruise ships.

3.4.1 System description

The reference case presents a cooling demand with an average of 1000 kW. For simplicity, this demand is assumed constant throughout the whole voyage given the low fluctuations in cooling output as seen in Figure 38. The system was designed to operate as an indirect system. The refrigeration unit then cools water which circulates in decentralized AHU's. Water is cooled to a temperature of 7 °C, which can be utilized to provide cool air in the cruise ship. Multiple configurations of CO_2 refrigeration units were investigated and compared to the more traditional refrigeration unit of subcritical R134a. The latter being a simple cycle, internal heat exchanger cycle and ejector cycle. For the sake of illustration will only the most promising configuration be displayed in Figure 42, being the transcritical ejector cycle. CO_2 has a critical pressure and critical temperature of 73.8 bar and 31.1 °C, respectively. Using seawater in the gas cooler of 20 °C should subcritical operations be attainable. However, as CO_2 refrigeration units struggle more in warmer climates was the gas cooler exit temperature set to 35 °C. Thus will the CO_2 refrigeration system be investigated in transcritical operation.

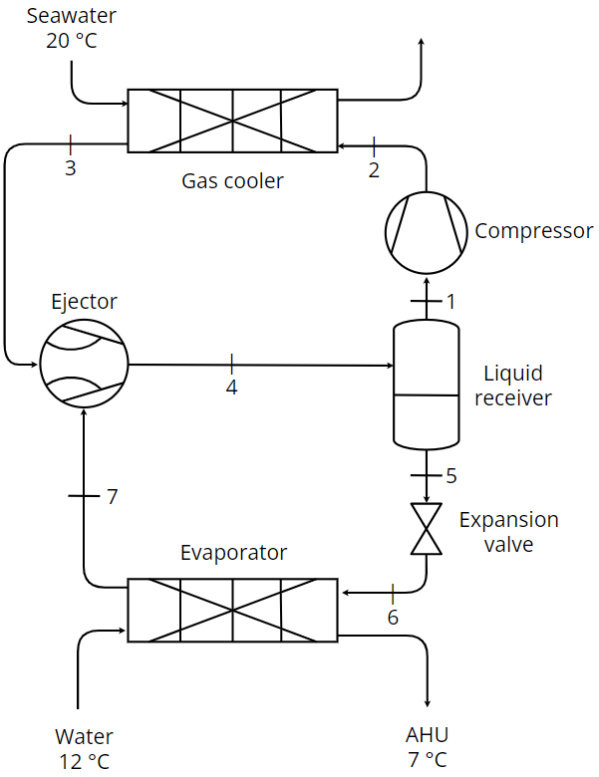

Figure 42: Transcritical ejector cycle

At the vapor outlet of the liquid receiver, vapor CO_2 is compressed to the high side pressure. High pressure and high temperature vapor then rejects heat in the gas cooler to seawater with a gliding temperature profile. Transcritical CO_2 is then expanded in a ejector into the intermediate pressure stage entering the liquid receiver. From the liquid outlet of the liquid receiver, CO_2 is expanded in an expansion valve before evaporating at low side pressure providing cooled water to AHU's. The ejector then lifts vapor CO_2 back to the intermediate stage completing the cycle. The performance of the refrigeration systems were expressed using the COP, the ratio of cooling output and required compressor work as provided below.

$$COP = \frac{\dot{Q}_{Cooling}}{\dot{W}_{Comp}} \; [-] \tag{13}$$

3.5 Exhaust waste heat recovery

As briefly explained in the design case, one of the objectives of this thesis was to investigate the possibilities of increasing energy efficiency by generating electricity and recovering waste heat contributing to heating demands. From the literature study it was clear that waste heat sources from marine ICE's have a great potential for waste heat recovery. The exhaust gas presented the greatest potential with a relatively large mass flow rate and medium heat quality of 400 °C. This thesis has evaluated the possibility of first recovering waste exhaust gas through electricity generation of a bottoming power cycle, then recovering excess waste heat contributing to heating demand onboard the cruise ship. The two design cases of hydrogen and ammonia operation has therefore considered two alternative waste heat recovery scenarios, to alternate the ratio of electricity generation and heating demand contribution.

The first scenario, maximum electricity generation of the bottoming power cycle (RC) was prioritized where excess heat is recovered for heating demand contribution. The second scenario,

heat recovery for maximum thermal contribution was prioritized. The study then investigated the possibility of contributing to 100% of heating demand, through HTWH and TES. Electricity generation was then regulated to achieve the objective of scenario 2. The waste heat recovery strategy is illustrated in Figure 43.

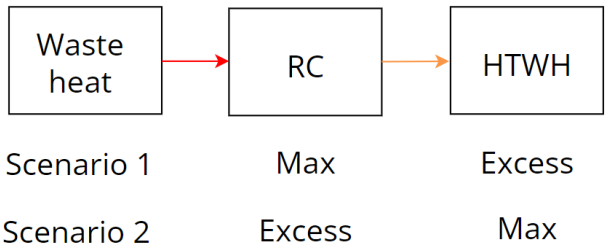

Figure 43: Waste heat recovery strategy

3.6 Bottoming power cycle

Bottoming power cycles were found to be the most reliable and efficient method of waste heat recovery for marine applications. The objective presented in this section is to simulate the waste heat recovery of exhaust gas from hydrogen and ammonia internal combustion engines. The goal was to recover waste heat energy using a rankine cycle. The rankine cycle was investigated for electricity generation, reducing the overall fuel consumption and increasing cruise energy efficiency. From the literature study, the recuperative rankine cycle was found to be the most promising configurations. In this study, the recuperative rankine cycle was compared to a subcritical isobutane cycle and simple transcritical CO_2 cycle in terms of thermal efficiency. The optimized recuperative cycle was then utilized in the reference case for electricity generation onboard the cruise ship.

3.6.1 Working fluid

The choice of working fluids has a large influence of the overall thermal efficiency of the rankine cycle for a given heat source quality. The two working fluids of interest were CO_2 and isobutane. From literature study, its has been made clear that CO_2 has excellent thermodynamic properties, is cheap, easily obtainable, and environmentally friendly. Isobutane has also demonstrated to be a great alternative for marine applications. Proven to obtain better thermal efficiencies than many other alternative organic working fluids. However, isobutane has the downside of thermal instability at higher temperatures and is highly flammable. CO_2 is therefore chosen as the working fluid for this simulation work and is compared to the simple subcritical isobutane cycle.

3.6.2 System description

Figure 44 presents the system layout of the recuperative power cycle used for exhaust waste heat recovery. The exhaust gas from the marine engines superheat the working fluid at a temperature of 400 °C. For simplifications, it was assumed that the exhaust gas had a constant temperature independent of engine load. The superheated high pressure working fluid is then expanded in a turbine generating electricity onboard the cruise ship. After the turbine, the high temperature low pressure working fluid enters the recuperator exchanging heat to the pump outlet flow preheating the working fluid. In the condenser, the working fluid is condensed using seawater at a temperature of 20 °C. The working fluid then passes through a liquid receiver ensuring liquid-phase flow to the pump, which completes the cycle lifting the working fluid back to high pressure before preheating in the recuperator.

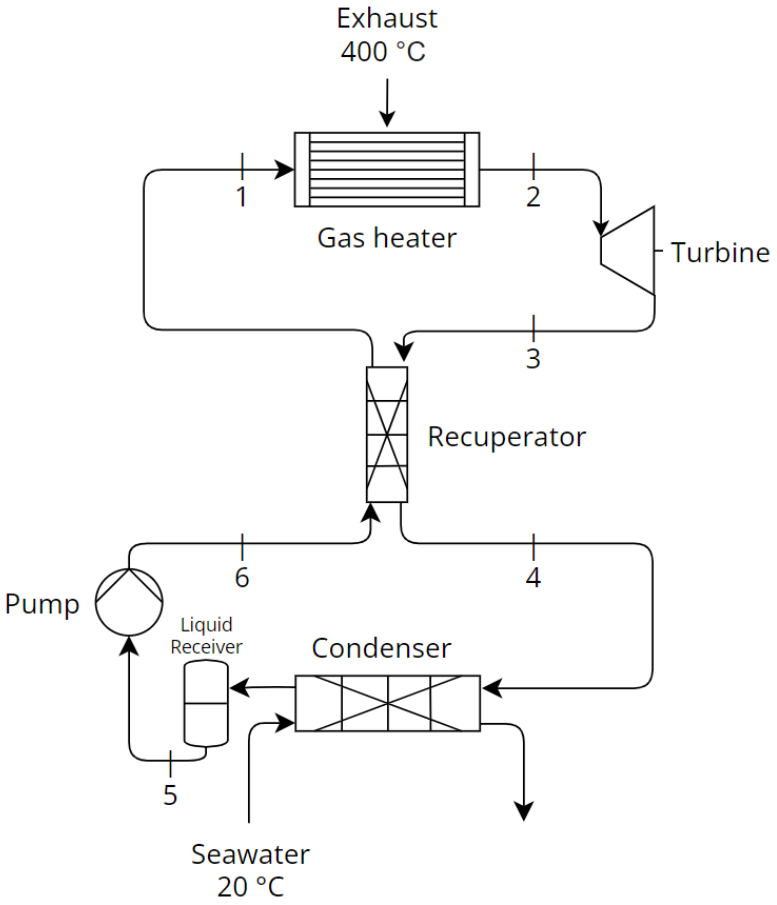

Figure 44: Recuperative rankine cycle

CO_2 has critical temperature of 31.1 °C critical pressure 73.8 bar. With a seawater temperature 20 °C, the cooling source is sufficient to condens CO_2 in the condenser. However, this results in a transcritical rankine cycle due to the low critical temperature of CO_2. The high-pressure side will then operate in supercritical state as explained previously in the literature study. To evaluate the performance of the power cycle, the total heat input is compared to the net power output of the system. The heat input from the waste heat exhaust gas can be calculated knowing the mass flow rate of the working fluid ($\dot{m}$) and the specific enthalpy at inlet (h_1) and outlet (h_2) of gas heater.

$$\dot{Q}_{in} = \dot{m} * (h_2 - h_1)\ [kW] \tag{14}$$

The power output of the turbine and power consumption of the pump can be calculated from the following equations:

$$W_{Turb} = \dot{m} * (h_2 - h_3)\ [kW] \tag{15}$$

$$W_{Pump} = \dot{m} * (h_6 - h_5)\ [kW] \tag{16}$$

Finally, the thermal efficiency (η_{th}) of the rankine cycles is defined as the ratio of net power output and total heat input from exhaust gas.

$$\eta_{th} = \frac{W_{Turb} - W_{Pump}}{\dot{Q}_{in}} \; [-] \tag{17}$$

The thermal efficiency was then optimized based on the high-side pressure and recuperator effectiveness for comparison of the different configurations. From the literature study it was found that the greatest thermal efficiency was obtained at the lowest pinch point in the recuperator. This recuperator effectiveness was calculated from the following equations:

$$\varepsilon_{rec} = \frac{T_3 - T_4}{T_3 - T_6} \; [-] \tag{18}$$

3.7 Heat recovery

After electricity generation in the transcritical recuperative RC, exhaust waste heat is recovered contributing to the heating demand onboard the cruise ship. An indirect system is designed, as presented in Figure 45, providing thermal energy through high temperature water heating with the possibility of integrating TES. The indirect system utilize Therminol D-12 as the heat transport medium at a temperature of 120 °C. Therminol D-12 is low cost, has low toxicity and has an operational temperature range from -94 to 230 °C.

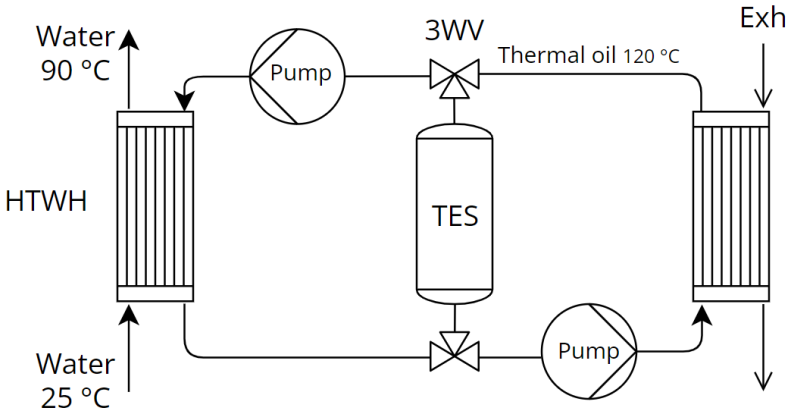

Figure 45: Schematic heat recovery

3.7.1 HTWH

Therminol D-12 is heated to 120 °C through heat exchange with exhaust gas. Water with an inlet temperature of 25 °C can then be heated to 90 °C from circulating thermal oil of 120 °C, contributing to the heating demand onboard. Traditionally this heat energy is provided by auxiliary boilers. The reference case presented an auxiliary boiler with an efficiency (η_b) of 80% operating with a marine HFO with LHV equal to 40.7 MJ/kg. The contribution of waste heat recovery in terms of emission reduction can then be calculated knowing the fuel consumption of the boiler and total heat recovery rate of the HTWH ($\dot{Q}_{HTWH}$).

$$\dot{Q}_{HTWH} = \dot{m}_{water} * (h_{out} - h_{in}) \; [kW] \tag{19}$$

$$\dot{m}_{AuxBoiler} = \frac{\dot{Q}_{HTWH}}{\eta_b * LHV} \; [kg/s] \tag{20}$$

Emission reduction is then found by multiplying the total fuel consumption of the HFO auxiliary boiler by the fuel-based emission factors provided in Table 15.

Emission type	Emission factor
CO_2	3.114 [kg/kg fuel]
SO_x	0.0508 [kg/kg fuel]
NO_x	0.031 [kg/kg fuel]

Table 15: Fuel-based emission of HFO [2]

3.7.2 TES

The heating demand of a cruise fluctuates from day to day depending on ambient conditions and the amount of passengers onboard. The heating demand is not correlated to the potential waste heat recovery of the ICE's either. Thermal energy should therefore be stored when excess heat energy is recovered, preventing waste heat when recovered heat surpasses heating demand. This opens the possibility of discharging during peak demands or port stay. During port stay, the heating demand is traditionally only provided by auxiliary boilers as the ICE's are shut off. The integration of TES thus also enables the possibility of provide heating during port stay with zero emissions.

As recovered heat surpasses the heating demand, thermal oil is directed into a thermal storage tank controlled by a three-way valve (3WV) as presented in Figure 45. A cylindrical insulated storage tank has been considered as the storage device of the thermal oil. The thermal oil was assumed to hold a uniform storage temperature of 120 °C considering the difficulty of modeling stratification effects. The Dymola simulation software used in this study does not support the use of a dynamic three-way control valve. Therefore, as excess heat surpasses the heating demand, the quantity of thermal oil directed to the thermal storage tank was calculated by hand. The hourly quantity of thermal oil stored in the storage tank was then calculated using the following equations:

$$m = \frac{\dot{Q} \cdot 3600}{C_p \cdot \Delta T} \; [kg] \tag{21}$$

The total amount of stored thermal oil is then a function of the amount of excess heat surpassing the heating demand. During port stay, the total heating demand is 4417 kWh for the 3-hour standstill. Assuming a temperature range from 120 to 27 °C in the thermal oil and an average specific heat capacity of 2.304 kJ/kgK, will the theoretical storage mass of thermal oil be 74210.35 kg to cover the heating demand during the port stay. With an average thermal oil density of 723.2 kg/m^3, will a storage tank with a total volume of 102.61 m^3 be sufficient for the port stay alone. With respect to the two scenarios defined and the two design conditions of hydrogen and ammonia, will the study evaluate the necessary TES storage volume to store excess heat surpassing the heating demand. This stored heat could then be used to further contribute to heating demand or cover heating during port stay.

Charging-discharging

The HTWH recovers thermal energy from exhaust gas contributing to heating demand onboard the cruise ship. When recovered thermal energy surpassed the heating demand of the cruise ship will the TES system start charging. During port stay or when heat recovery is not sufficient, will the TES tank discharge, heating water to 90 °C as illustrated in Figure 46.

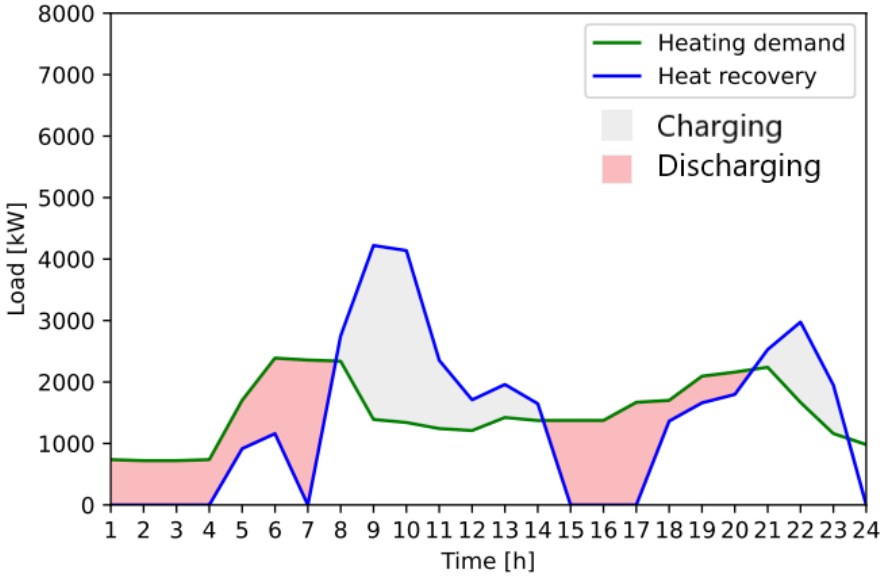

Figure 46: Charging-discharging TES

3.8 Cold recovery

The objective presented in this section was to evaluate the potential of recovering cold energy from regasification of LH_2 when operating with hydrogen ICE's. A numerical model has been created in order to calculate the total fuel savings achieved supplying cold energy recovered from regasification of LH_2 to the HVAC system onboard.

3.8.1 System description

Liquid hydrogen is stored onboard at -248.5 °C with a pressure of 3 bar. Based on relevant literature study, it was assumed that the hydrogen internal combustion engines require hydrogen fuel injection at conditions of 80 °C and 3 bar. Hydrogen must therefore be vaporized through heating in order to meet the engine operational criteria. The circulating water from the decentralized AHU's was then used to regasify the liquid hydrogen. Presented in Figure 47, water enters the first heat exchanger at a temperature of 12 °C and is cooled to 7 °C through regasification of LH_2. Gaseous hydrogen was then further heated to 80 °C using engine cooling water at 90 °C. The cold energy was then circulated back to decentralized AHU's onboard the cruise ship which can be exploited to deliver cool air during the summer season. The cooled engine water was directed back to the ICE's for engine cooling. The cold energy recovered to the AHU's can then help reduce the overall fuel consumption related to power required by the refrigeration units or potentially reduce the necessary refrigeration capacity of the units.

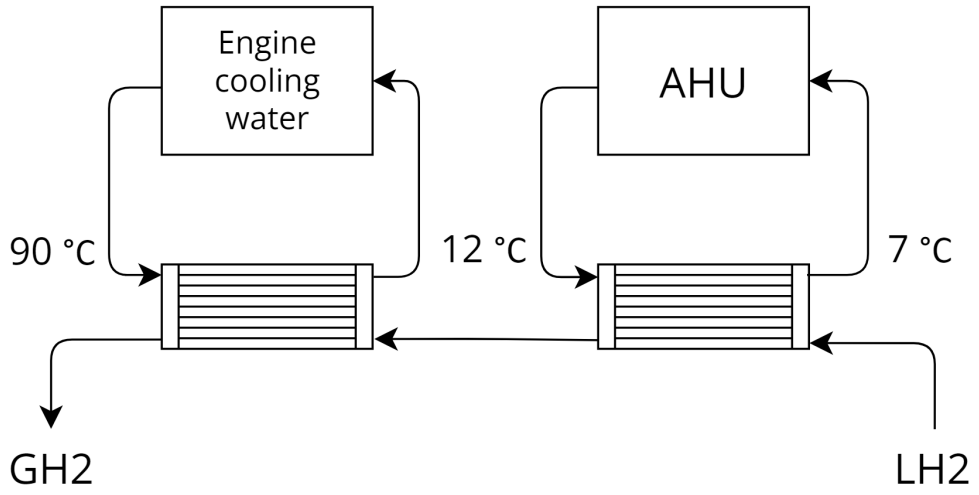

Figure 47: Schematic cold recovery

Knowing the mass flow rate of liquid hydrogen, $\dot{m}_{LH_2}$, and the difference in specific enthalpy at inlet (h_{in}) and outlet (h_{out}) of the first heat exchanger can the total heat transfer rate be calculated. The heat transfer rate ($\dot{Q}_{Cooling}$) is the rate at which cold energy is recovered and provided to the AHU's.

$$\dot{Q}_{Cooling} = \dot{m}_{LH_2} \cdot (h_{out} - h_{in}) \; [kW] \tag{22}$$

The electricity ($\dot{EL}$) saved will then be the amount of electricity required to cover the cold energy recovered otherwise provided by the refrigeration unit. Saved electricity can then be calculated knowing the COP of the refrigeration unit:

$$\dot{EL} = \frac{\dot{Q}_{Cooling}}{COP} \; [kW] \tag{23}$$

In order to further determine the amount of fuel saved must the fuel consumption of the auxiliary engines be calculated based on the required fuel to generate the saved electricity. Using the engine parameters provided earlier and the lower heating value of the fuel, can the fuel consumption ($F_{AuxEngine}$) of the auxiliary engines be calculated assuming a generator efficiency of 95% (η_g):

$$F_{AuxEngine} = \frac{3600}{LHV \cdot \eta_g \cdot \eta_{th}} \; [kg/kWh] \tag{24}$$

Finally, the fuel savings from the cold recovery was calculated as following:

$$Fuel_{savings} = \dot{EL} \cdot F_{AuxEngine} \; [kg/h] \tag{25}$$

3.9 Cold thermal energy storage

An alternative to the cold recovery through regasification of liquid hydrogen is to implement cold thermal energy storage. This allows cold thermal energy to be stored and later discharged during port stay. By providing cooling during port stay through cold energy storage, combustion engines may be shut off emitting zero emissions. The concept is an alternative solution with respect to the environmental restriction of zero emissions in EU ports.

3.9.1 System description

During seagoing, the liquid hydrogen for the main engines was regasified through charging a latent PCM cold thermal energy storage tank. During port stay, the CTES tank may be discharged providing full coverage of the cooling demand. The CTES tank was discharged by cooling water circulating from the AHU's as presented in Figure 48.

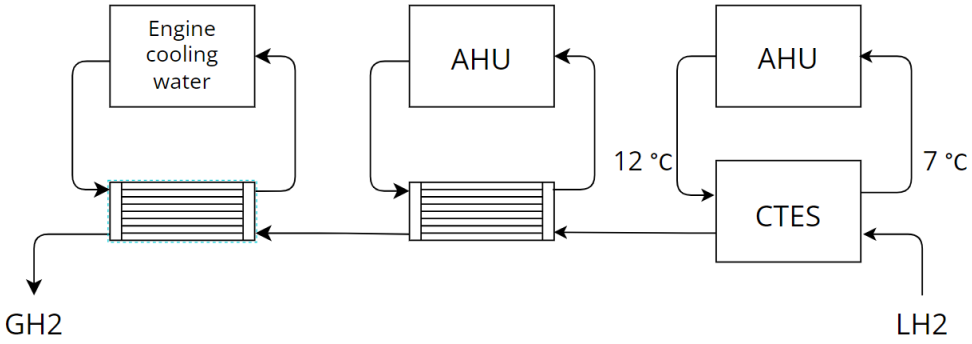

Figure 48: Schematic cold recovery with CTES

PCM

Water was chosen as PCM for this application. Water is cheap, clean and has great thermal properties. With a density of about 1000 kg/m^3 and specific heat 4.17 kJ/kgK, water has a high volumetric thermal capacity. More importantly for latent TES, water has a high latent heat of fusion of 335 kJ/kg at 0 °C, ensuring high TES capacity per unit mass.

Design

The CTES tank is based on the tube in tank concept which is a static system. The heat transfer fluid (HTF), liquid hydrogen, then flows through a tube inside the tank containing the PCM forming layers of ice around the tube. During discharging, water from the AHU's flows through a separate tube melting the PCM. This is only achievable when operating with a double bundle tube in tank system as presented in the simple sketch of Figure 49.

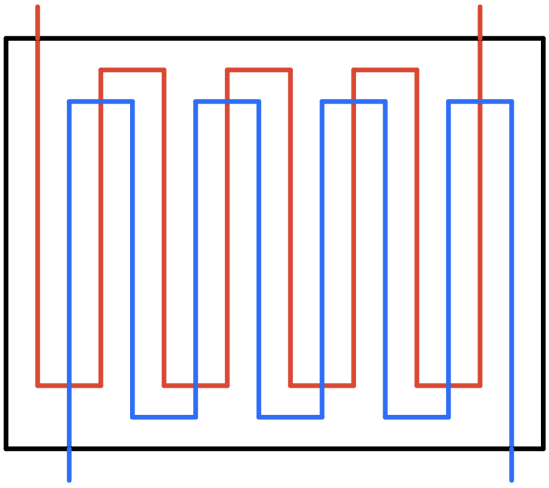

Figure 49: Double bundle tube in tank TES system

The objective of the CTES was to provide the cooling demand during port stay. During the 3-hour port stay in Stockholm, 2928 kWh of cooling demand is required. The total volume of ICE to provide the necessary cooling demand can then be calculated from the following equations:

$$V = \frac{3600 \cdot Q_{latent}}{\rho \cdot \Delta h_L} \; [m^3] \tag{26}$$

With an ICE density of 917 kg/m^3, the total volume of ICE required to provide 2928 kWh is 34.31 m^3 or 31465 kg. However, this was the ice alone. The required volume was expected to be much larger considering internal heat exchange volume and outer insulation.

Charging-discharging

Discharging the CTES system was only considered during the 3-hour timeframe of port stay. The CTES system was designed such that 2928 kWh of cold thermal energy is provided within the 3-hour time frame independent of the hourly cooling demand. Charging the CTES system was more complicated, as the freezing is a function of the engine load. Charging starts after complete discharge during port stay in Stockholm as illustrated in Figure 50. Assuming zero thermal losses, the CTES system is charged through regasification of liquid hydrogen going to the main engines. The CTES system is designed to achieve full charge before the port stay, with minimal subcooling of the ice.

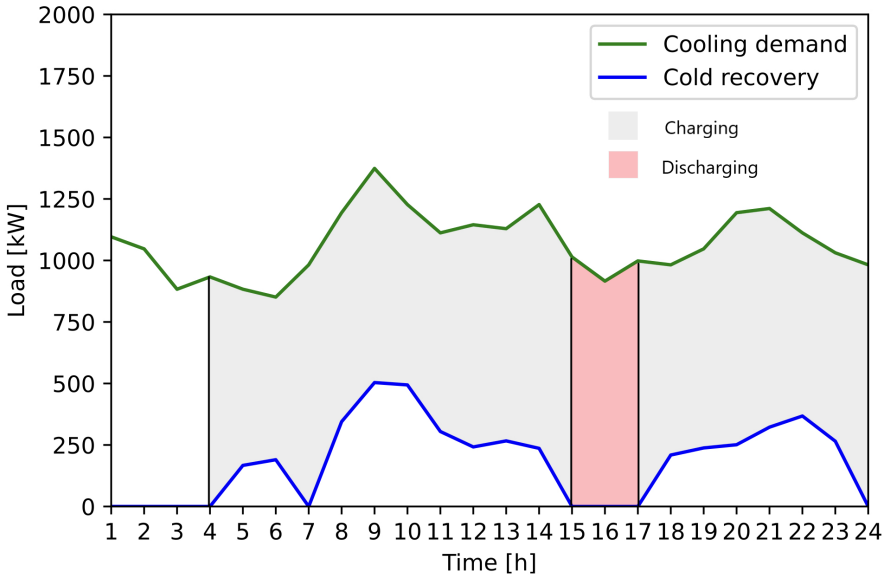

Figure 50: Charging-discharging CTES

4 Simulation

This section presents the simulation software and simulation models developed for energy analysis of the thermal systems, designed based on the system conditions presented in section 3.

4.1 Simulation software

Dynamic simulation models has been created using the software Dymola. Dymola operates with a simulation environment based on the Modelica modeling language. The libraries used for simulation are provided by TLK-Thermo GmbH. Four libraries are used. TIL 3.11 for components such as pumps, heat exchangers, turbines and for process control using PI controllers. TIL Media 3.11 for refrigerants. TIL FileReader 3.9.2, implementing data for dynamic simulations. Finally, TIL AddOn PCM storage 3.11 for simulation of thermal energy storage. TLK DaVE has also been used for plotting Dymola results in the form of P-H and T-S diagrams.

In order to simplify the numerical simulations a number of assumptions were made. All models were simulated as one big unit. More realistically, multiple units run in parallel in order to provide the specified capacity. The same goes for model components such as compressors and pumps. The models also assume no pressure loss and adiabatic behaviour, with no heat loss.

4.2 CO_2 refrigeration cycle

Multiple configurations of a CO_2 refrigeration system has been simulated in Dymola for performance comparison. The transcritical cycles include a simple cycle, IHX cycle, and ejector cycle. All configurations deliver a constant 1000 kW of cooling, cooling circulating water from 12 °C to 7 °C provided to decentralized AHU's. For simplifications, the evaporation of CO_2 was simulated using a simple tube with a constant heat rejection of 1000 kW assuming a pinch point of 5 K in the evaporator. It was assumed that 5 K superheat was sufficient to avoid damage to the compressor. After compression, supercritical CO_2 is cooled in a stainless steel plate heat exchanger. A PI controller regulates the mass flow of seawater such that 35 °C is achieved at outlet of the gas cooler. 35 °C was chosen to simulate warmer ambient climates. The COP of the configurations was then calculated such that the units could be compared in terms of system performance. The common system characteristics is presented in Table 16.

Characteristics	Value
Temperature cooling water [°C]	20
Compressor isentropic efficiency	0.8
Pinch temperature difference gas cooler [K]	15
Pinch temperature difference evaporator [K]	5

Table 16: Refrigeration system characteristics

4.2.1 Simple transcritical cycle

Figure 51 presents the simulation model of the simple transcritical cycle. At the outlet of the gas cooler, CO_2 has a temperature and pressure of 35 °C and 79.87 bar, respectively. The working fluid then expands into the two-phase region. The effective flow area of the expansion valve was regulated such that 5 K of superheat is achieved after evaporation. The evaporation temperature was then set to 2 °C, sufficient to provide cool water at 7 °C with a pinch point of 5 K. The evaporation temperature was set as a function of the low-side pressure, given that evaporation occurs at constant pressure and temperature. The evaporation pressure was set to 36.75 bar by regulating the volumetric displacement of the compressor using a PI controller.

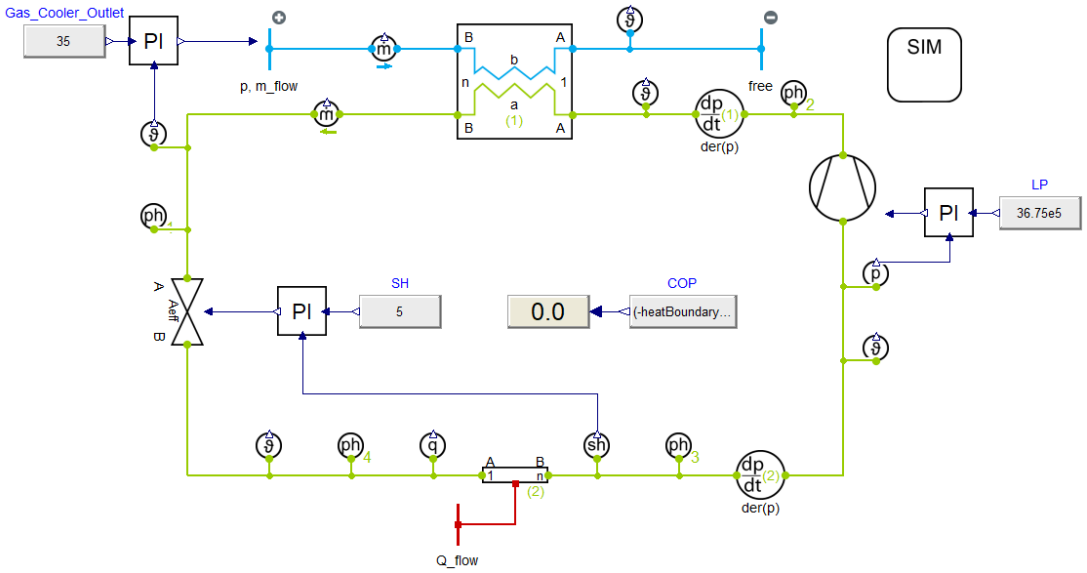

Figure 51: Simple transcritical cycle

4.2.2 Transcritical IHX cycle

Figure 52 presents the simulation model of the transcritical IHX cycle. The CO_2 has an outlet temperature and pressure of 35 °C and 82.54 bar, respectively. Similar to the simple cycle, low-side pressure was regulated such that evaporation temperature was set to 2 °C. Given the internal heat exchanger, will 1 K superheat after the evaporator be sufficient as the working fluid was further superheated in the internal heat exchanger. The internal heat exchanger was designed to achieve an effectiveness of 0.9. The recuperator thus increases the refrigeration capacity with minimal increase in compressor work.

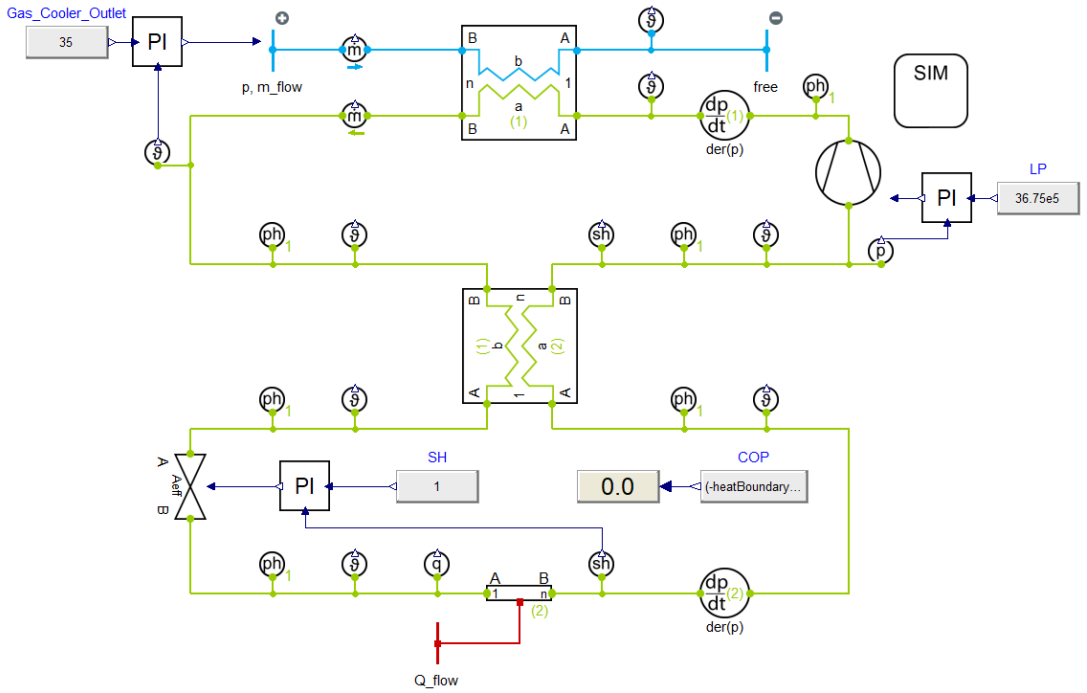

Figure 52: Transcritical IHX cycle

4.2.3 Transcritical ejector cycle

Figure 53 presents the simulation model of the transcritical ejector cycle. This cycle operates with a high-side pressure of 83.69 bar. The working fluid expands to the intermediate pressure stage of two-phase flow before entering the liquid receiver. Using a PI controller, the intermediate pressure stage was regulated adjusting the volumetric displacement of the compressor. As a result, regulating the evaporation temperature to the desirable temperature of 2 °C. The intermediate stage was set to 42 bar. Further, liquid CO_2 expands to the low-side pressure from the liquid receiver ensuring 1 K superheat after the evaporator. With an ejector efficiency of 0.3, the ejector achieves a pressure lift of 5.26 bar from low-side pressure of 36.74 bar. Furthermore, a PI controller has been used to ensure a filling level of 0.5 in the liquid receiver by adjusting the effective driving flow area of the ejector. Thus ensuring a flow balance in the system. Finally, an IHX with an effectiveness 0.178 was installed to ensure 5 K superheat at the inlet of the compressor.

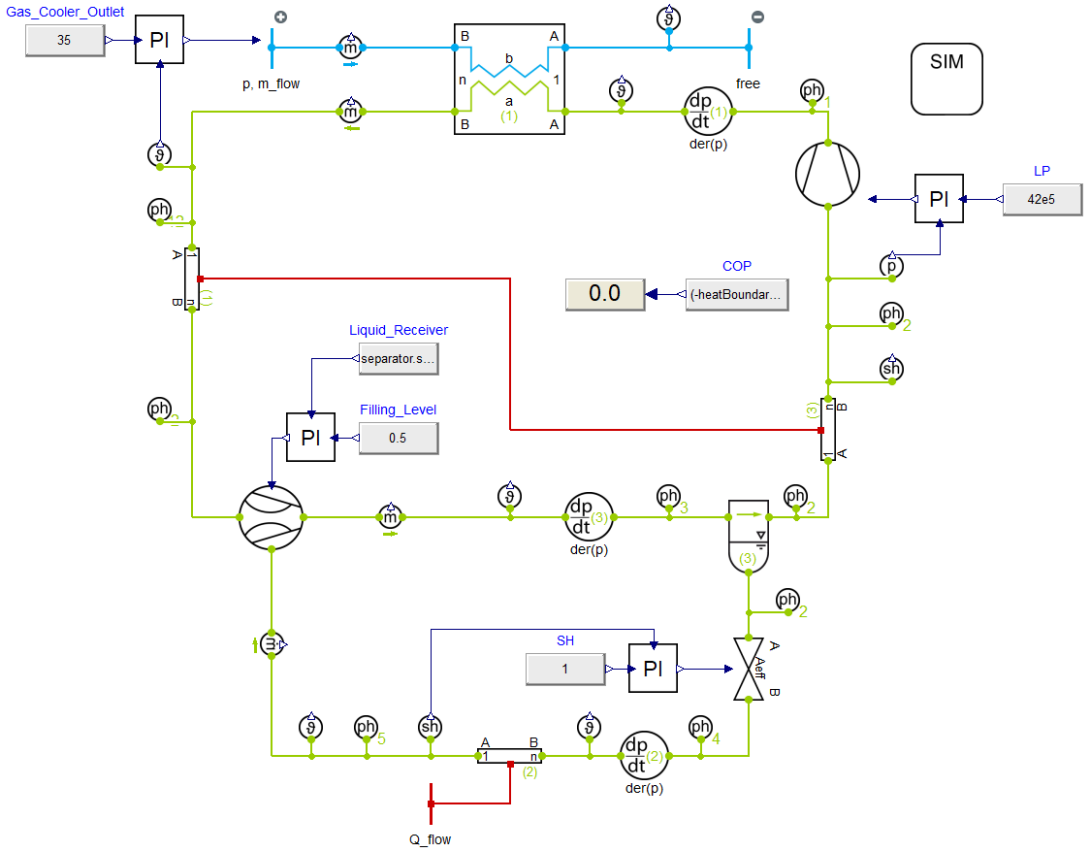

Figure 53: Transcritical CO2 ejector cycle

4.3 Bottoming power cycle

The power cycles investigated include a simple transcritical RC and a transcritical recuperative RC. Both power cycles contain similar components such as gas heater, condenser, turbine and pump. The characteristics of the components are defined in Table 17 based on literature provided in section 2.6.2. The gas heater is a plate-fin heat exchanger which superheats the CO_2 working fluid through heat exchange with exhaust gas of the main engines. For system optimization, the gas heater was designed to operate at a pinch of 25 K.

The optimal heat exchanger area was not examined in this study and therefore likely overdimensioned for the sake of maximum cycle performance. The exhaust input parameters were loaded

using a TIL FileReader, reading data obtained from section 3.3.2. The condenser is a plate heat exchanger, condensing CO_2 using seawater of 20 °C. The mass flow of sea water was controlled by a PI controller, ensuring a pinch point of 5 K. With a condensation temperature of 25 °C, the condensation pressure was set to 64.34 bar. To ensure pure liquid CO_2 entering the pump, a liquid receiver of 0.7 m^3 was installed.

Characteristics	Value
Temperature exhaust gas [°C]	400
Temperature cooling water [°C]	20
Pump isentropic efficiency	0.8
Turbine isentropic efficiency	0.9
Generator efficiency	1
Turbine speed [Hz]	50
Heat transfer area gas heater [m^2]	4.09 $\cdot 10^5$
Pinch temperature difference gas heater [K]	25
Pinch temperature difference condenser [K]	5

Table 17: Rankine cycle characteristics

The working fluid flow rate was manually adjusted using the pump. Higher flow rate increases the net power output of the RC, however, reduces the thermal efficiency and available heat recovery for HTWH. For system optimization, the mass flow of the working fluid was set such that a pinch point of 25 K was achieved in the gas heater. In scenario 1, the mass flow was set for maximum electricity generation. In scenario 2, where heat recovery was prioritized, the mass flow was set appropriately to maximize electricity generation while ensuring 100% coverage of the heating demand in the waste heat recovery unit.

4.3.1 Simple Transcritical RC

Figure 54 presents the simulation model of the simple transcritical RC. Using a PI controller, the intake volume of the turbine was regulated such that high-side pressure may be controlled. From literature study it is clear that higher pressure is beneficial in terms of thermal efficiency. The high-side pressure was therefore set to 180 bar.

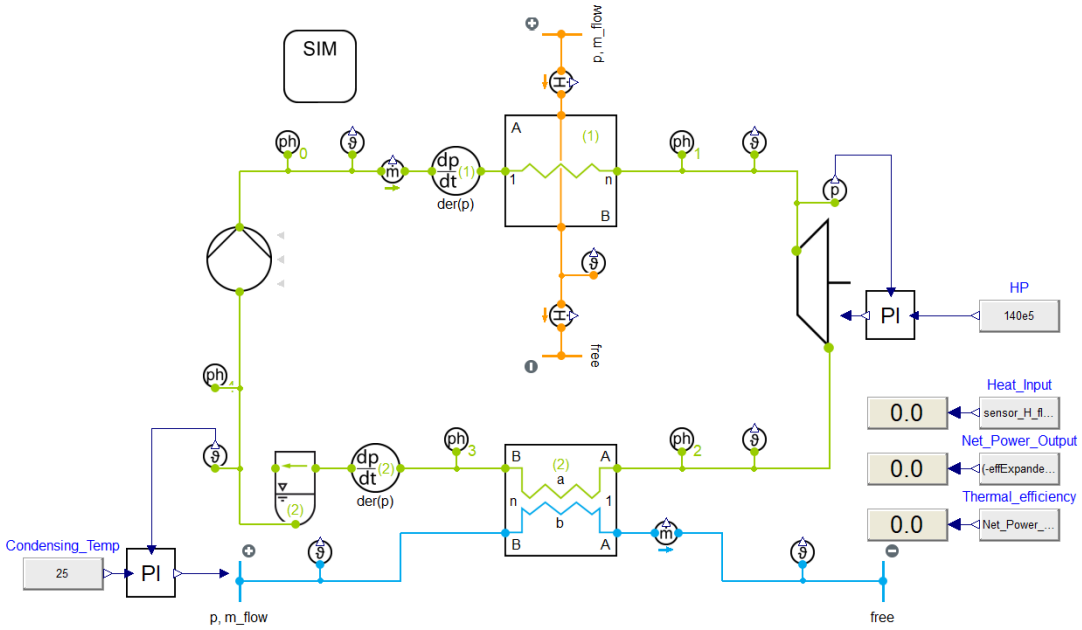

Figure 54: Simple Transcritical RC

4.3.2 Transcritical recuperative RC

The recuperative cycle of Figure 55, as the simple cycle, operates with a high-side pressure of 180 bar. With an additional heat exchanger, the working fluid is pre-heated before the gas heater, reducing LMTD during heat addition. The recuperator is a plate heat exchanger designed to have a recuperator effectivness of 0.9, found to be the optimal value with minimal increase in system heat transfer area.

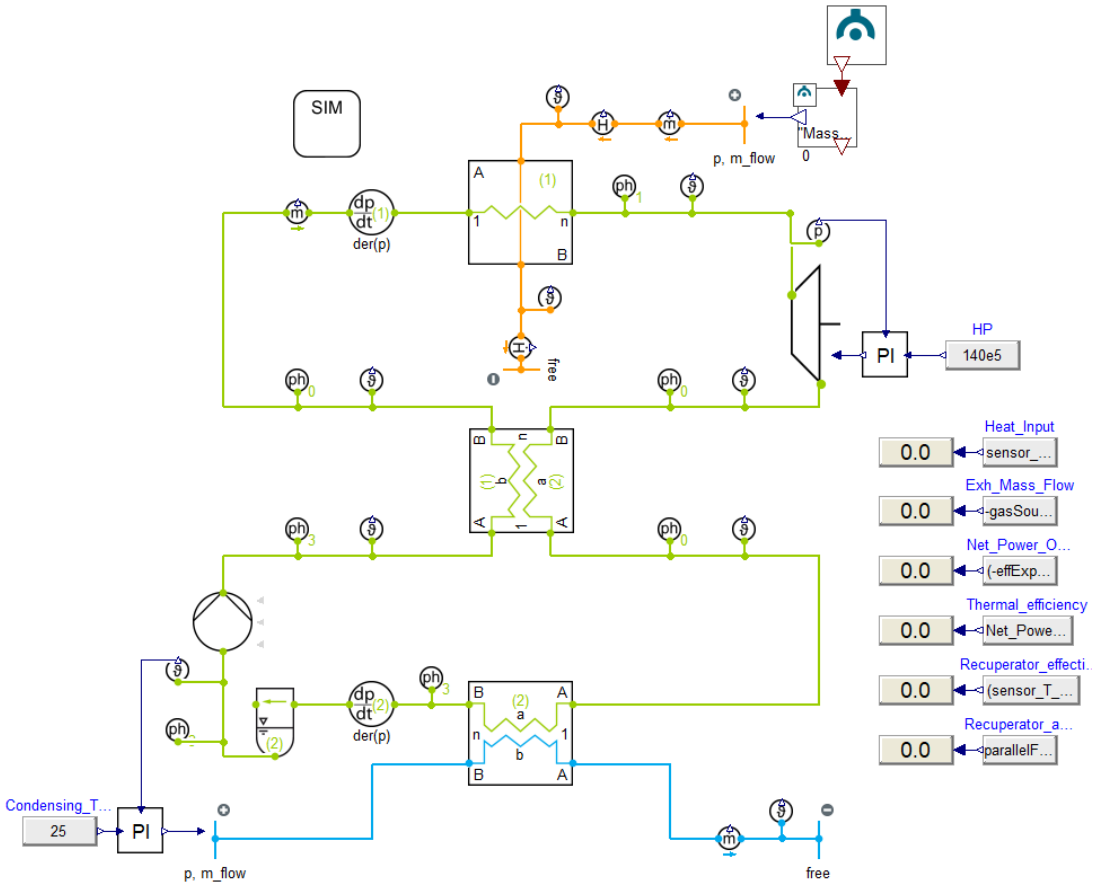

Figure 55: Transcritical recuperative RC

4.4 Heat recovery

4.4.1 HTWH

After electricity generation in the power cycle, excess waste heat exhaust gas was used to contribute to the heating demand onboard the cruise ship. Figure 56 presents the simulation model for heat recovery. TIL FileReader has been used to read input data at outlet of the power cycle. The heating of Therminol D-12 has been simulated by tube to tube heat transfer. The rate of heat transfer was determined such that exhaust gas exit temperature did not sink below 120 °C. The combustion of ammonia or hydrogen does not lead to sulphuric acid formation, however, nitric acid formation may take place due to high combustion temperature. For conservative measures, 120 °C was therefore set as a lower boundary at exit of exhaust waste heat recovery. A PI controller adjusted the rate of mass flow of therminol circulating in the system such that 120 °C was achieved. Further, through heat exchange in a plate heat exchanger. Water was heated to 90 °C, once again controlled by a PI controller. The plate heat exchanger was designed to operate with a minimum approach temperature of 2 K.

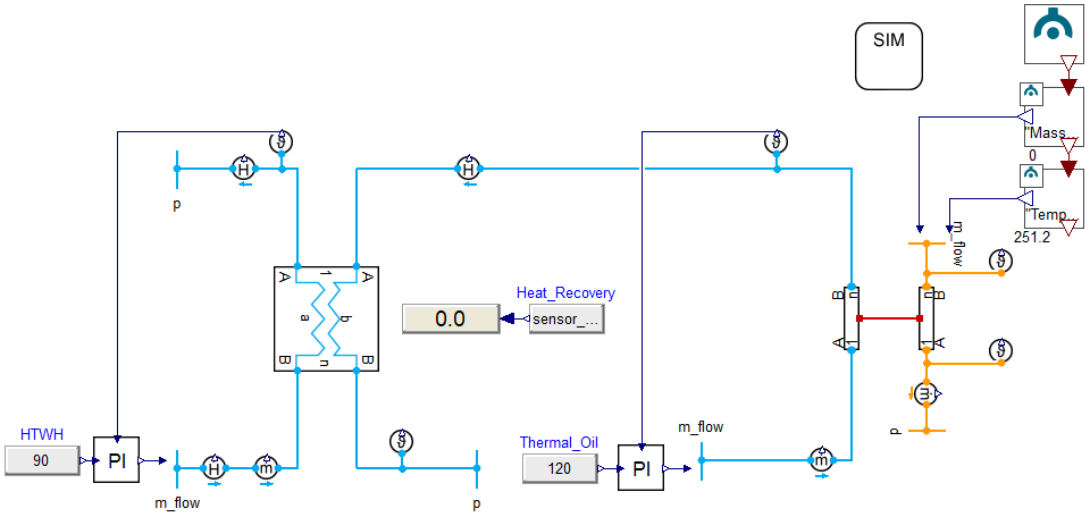

Figure 56: HTWH simulation

4.4.2 TES

Dynamic sensible thermal storage was not possible to simulate in the simulation software Dymola. A simulation model presented in Figure 57 has therefore been developed only considering TES discharging, validating the quantity of thermal oil required to cover 100% of the heating demand during port stay. As previously mentioned, 4417 kWh of heating is to be provided during port stay. The simulation model thus investigates the necessary mass flow rate of therminol in order to provide 4417 kWh of high temperature water of 90 °C.

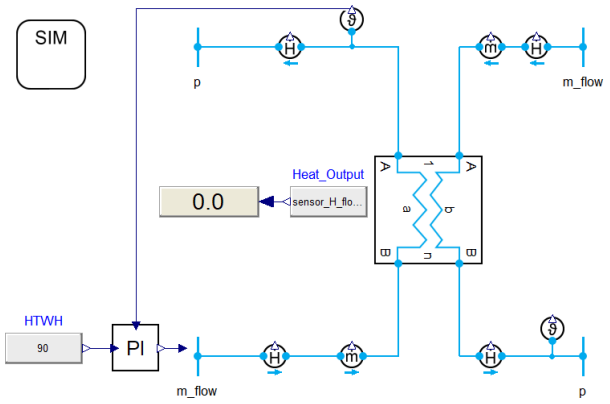

Figure 57: Therminol D-12 TES discharging model

4.5 Cold recovery

The LH_2 cold recovery was simulated on a dynamic basis, presented in Figure 58. TIL FileReader inputs data obtained from section 3.3.2 regarding mass flow of LH_2 required in the main engines. The LH_2 inlet temperature and pressure was -248.5 °C and 3 bar, respectively. In the first plate heat exchanger, LH_2 is evaporated absorbing heat from water at a temperature 12 °C. A PI controller was used in order to regulate the mass flow of water in order to achieve 7 °C, providing cooled water to the AHU's. The plate heat exchanger was designed to achieve a pinch of 1 K at maximum load, corresponding to an heat transfer area of 22.38 m^2. Further, engine cooling water was used in order to meet required hydrogen fuel injection criteria. The cooling water rejects heat to the hydrogen, where a PI controller adjust the required mass flow of cooling water

such that hydrogen achieved 80 °C.

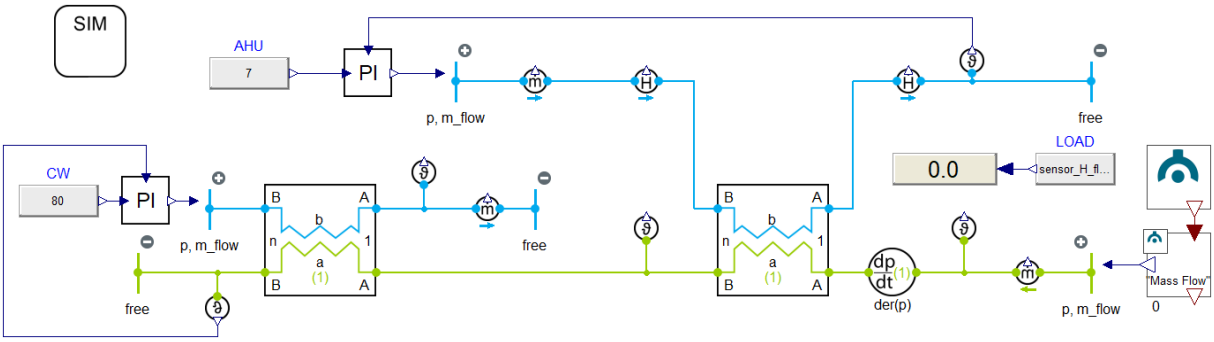

Figure 58: HVAC application simulation model

4.6 Cold thermal energy storage

The cold thermal energy storage tank was designed such that 32000 kg of ice could be melted providing at least 2928 kWh of cooling during port stay. The tank was designed as a double bundle tube in tank concept. Dymola simulation does not support this concept, therefore, two separate simulations has been created for charging and discharging. The tank requires a total volume of 57.1 m^3, in comparison to the theoretical volume of 34.31 m^3 calculated in section 3.9.1. This was due to the total volume of tubing for both charging and discharging. Copper material is used for tubing given the high thermal conductivity, advantageous for charging and discharging. Table 18 presents the characteristics of the CTES tank.

Characteristics	Value
Length [m]	3.85
Width [m]	3.85
Height [m]	3.85
Tank volume [m^3]	57.1
Total mass [kg]	45844.5
Material	Copper
PCM phase-change temperature [°C]	0
PCM mass [kg]	32000

Table 18: Thermal energy storage characteristics

Charging

Figure 59 presents the simulation model of CTES charging. The initial temperature of the PCM was set to 0.5 °C to ensure liquid PCM. The CTES system charges as a function of the main engine fuel consumption, starting after the 3-hour port stay in Stockholm. Once again, Til FileReader was therefore used to regulate the mass flow of LH_2 entering the CTES tank. The charging layout was then designed such that full charge was achieved before the 3-hour port stay with minimal subcooling of the PCM. The required tube layout and heat transfer area is provided in Table 19. After the CTES tank, cold gaseous hydrogen further provides cooling to the AHU's before finally being heated to engine injection criteria. The latter is the same concept as presented in Figure 58.

Characteristics	Value
Tube inner diameter [mm]	10
Tube wall thickness [mm]	1
Number of tubes	12 x 12
Tube volume [m^3]	0.036
Tube mass [kg]	142.2
Total heat transfer area outer tube [m^2]	17.3
Total heat transfer area inner tube [m^2]	14.4

Table 19: Tube layout charging the PCM

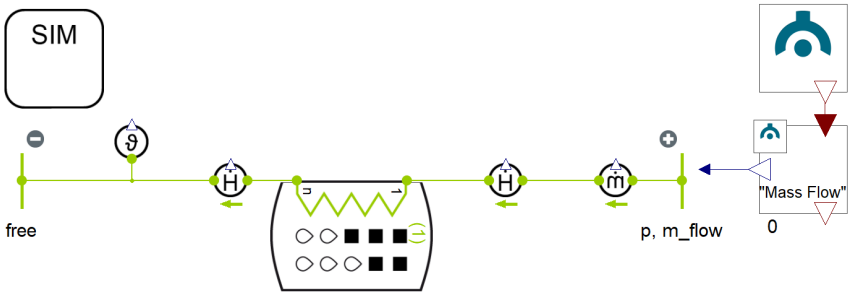

Figure 59: CTES charging simulation model

Discharging

Figure 60 presents the simulation model of CTES discharging. During port stay, the CTES system completes a full discharge. The initial temperature of the PCM was then set to 0 °C to ensure pure solid PCM. A PI controller was then used to regulate the mass flow of water entering the CTES system from the AHU's to ensure water at outlet temperature of 7 °C. The tube layout was designed such that full discharge was achieved within the 3-hour port stay. Providing 2928 kWh of cool water at 7 °C to the AHU's. The required tube layout characteristics is presented in Table 20.

Characteristics	Value
Tube inner diameter [mm]	43.5
Tube wall thickness [mm]	0.8
Number of tubes	60 x 60
Tube volume [m^3]	20.6
Tube mass [kg]	13826.6
Total heat transfer area outer tube [m^2]	1963.8
Total heat transfer area inner tube [m^2]	1894.1

Table 20: Tube layout discharging the PCM

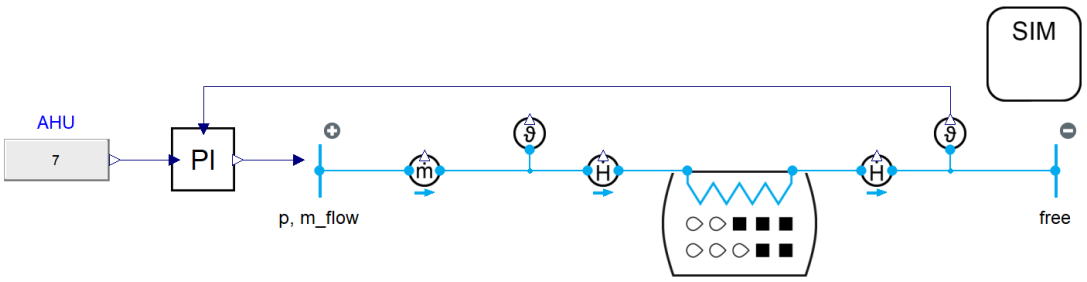

Figure 60: CTES discharging simulation model

5 Results

This section presents the results obtained from the thermal systems described in section 3 and 4.

5.1 Fuel storage

The mechanical energy requirement for propulsion was 54987 kWh and the electrical energy requirement was 41252 kWh, for a total of 96239 kWh obtained from Figure 38. This represents the total energy required from the main engines and auxiliary engines. The total required input energy was then calculated based on the thermal efficiency of the ICE's. Further, the total fuel storage volume and storage mass was calculated using the volumetric and gravimetric energy density of hydrogen and ammonia, presented in Table 21.

Fuel type	GH_2	LH_2	NH_3
Thermal efficiency [%]	35	35	40
Required input energy [kWh]	274968	274968	240597
Volumetric energy density [kWh/m^3]	1400	2360	4820
Total storage volume [m^3]	196.4	116.5	49.9
Gravimetric energy density [kWh/kg]	33.3	33.3	5.2
Total storage mass [kg]	8257	8257	46268

Table 21: Total fuel storage volume/mass to provide 96239 kWh

5.2 CO_2 refrigeration cycle

From the reference case, the refrigeration system had a COP 1.03, significantly lower than state of the art technology. The most common refrigerant for marine refrigeration systems is R134a. Simulations using Dymola found that a simple subcritical R134a refrigeration cycle achieved a COP of 3.258, providing a constant 1000 kW of cooling output. Showing great improvements in comparison to the reference case. However, with the large GWP of 1300, the refrigerant may contribute to global warming effects considering the refrigerant leakage reported in marine refrigeration units. The first CO_2 refrigeration system simulated was the simple transcritical cycle. The cycle had a specific cooling capacity of 84.1 kJ/kg and specific compressor work of 39.8 kJ/kg. The results show that a COP of 2.118 was achieved with a refrigerant mass flow of 11.88 kg/s. The simple transcritical CO_2 cycle performance is notably lower than the R134a cycle, yet operates with near zero emissions relative to R134a. Figure 61 shows the log(p)-h diagram of the simple CO_2 cycle.

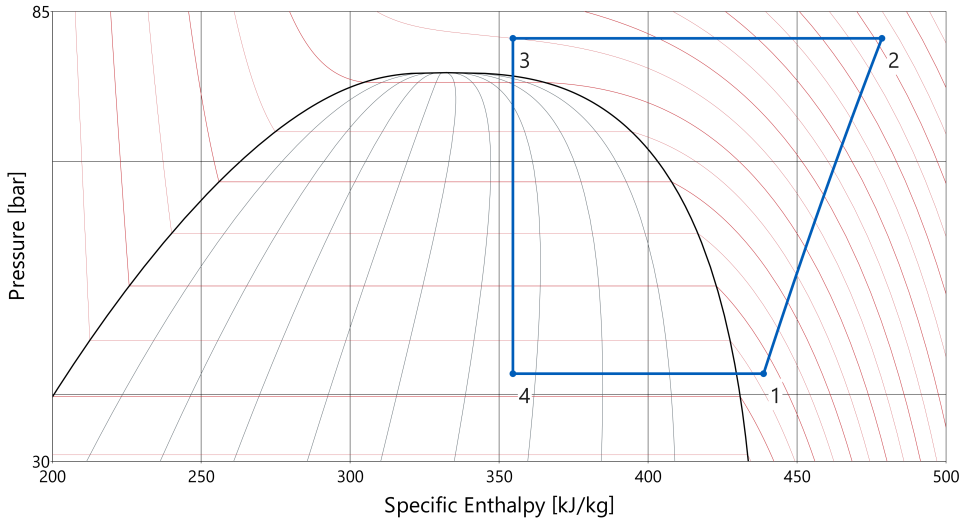

Figure 61: Log(p)-h diagram simple transcritical CO_2 cycle

The performance was greatly improved in the trancritical IHX cycle presented in the log(p)-h diagram of Figure 62. The integration of a internal heat exchanger significantly increased the specific cooling capacity to 157.9 kJ/kg and with a specific compressor work of 52.1 kJ/kg. The cycle then operated with a COP of 3.03 with a CO_2 mass flow of 6.335 kg/s for 43% increase in performance compared to the simple transcritical cycle.

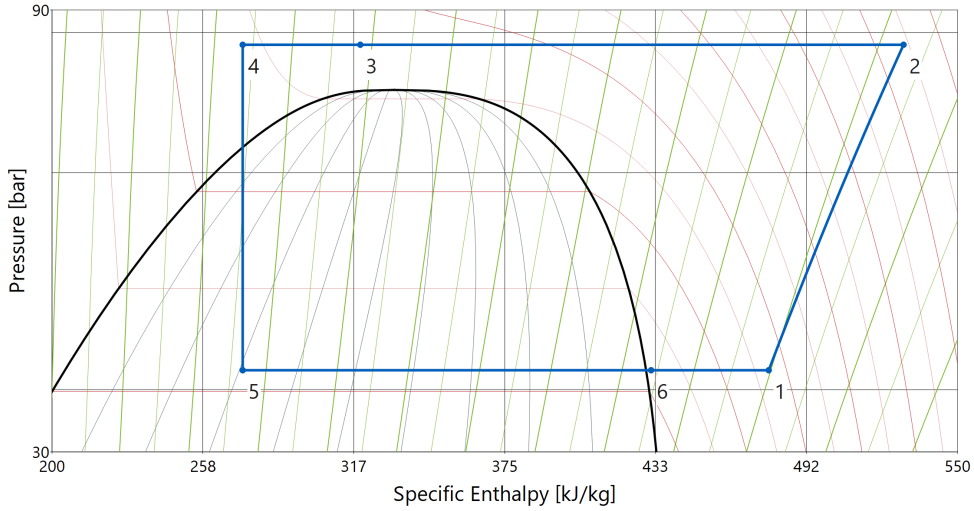

Figure 62: Log(p)-h diagram transcritical CO_2 IHX cycle

The greatest performance was achieved in the transcritical ejector cycle with a COP of 3.656, presented in the schematic of Figure 42. The issue with this cycle is that the configuration does not ensure superheat before the compressor. An IHX must therefore be integrated such that 5K superheat is achieved, as presented in Figure 53. The transcritical ejector cycle with internal heat exchange had a specific cooling capacity of 213.3 kJ/kg and specific compressor work of 34.2 kJ/kg as presented in the log(p)-h diagram of 63. With a mass flow of 8.159 kg/s, the unit operates with a COP of 3.588 where 0.574 of the mass flow fraction enters the evaporator. This resulted in a performance increase of 69.4% and 10.13% in comparison to the simple transcritical cycle and subcritical isobutane cycle, respectively.

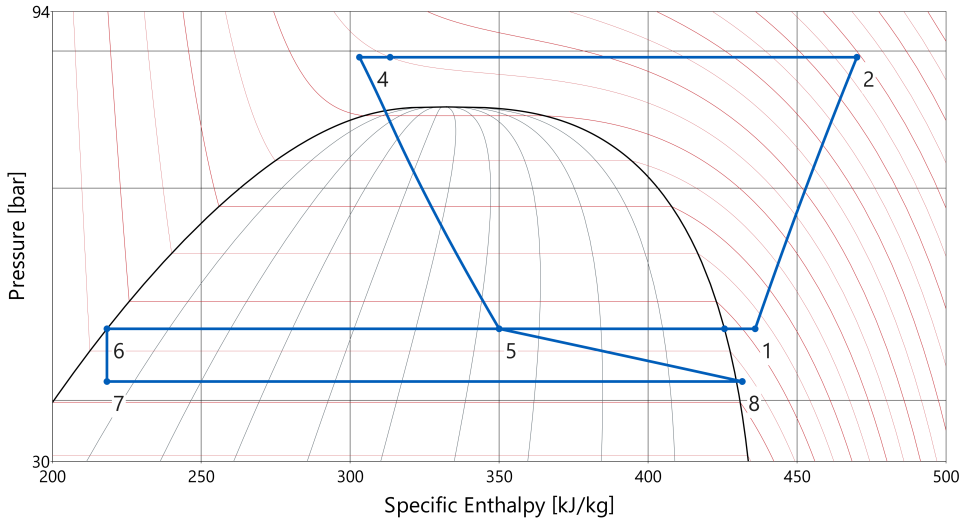

Figure 63: Log(p)-h diagram transcritical CO_2 ejector cycle

Finally, the result from the simulated refrigeration cycles are presented in Table 22. The ejector cycle was proven to be the best performing cycle out of the selection with a 10.13% performance increase to the subcritical R134a cycle.

Refrigeration cycle	COP
Simple subcritical R134a	3.258
Simple transcritical CO_2	2.118
Transcritical CO_2 with IHX	3.03
Transcritical CO_2 with ejector	3.588

Table 22: COP of simulated refrigeration cycles

5.3 Bottoming power cycle

5.3.1 Thermal efficiency

The maximum thermal efficiency of the power cycles was investigated in order to evaluate the performance and compare the power cycles. The subcritical isobutane cycle achieved a maximum thermal efficiency of 0.196. The thermal efficiency simulated applies for both design cases of hydrogen and ammonia exhaust waste heat throughout the cruise voyage. This thermal efficiency is in line with literature presented previously and represents the typical performance of subcritical ORC's. As previously stated, isobutane is highly flammable and experience thermal instability beyond 300 °C. CO_2 was therefore more applicable considering the non-flammable characteristic and exhaust waste heat of 400 °C.

Figure 64 presents the log(p)-h diagram of the simple transcritical RC for the hydrogen and ammonia design case. The maximum thermal efficiency was determined at the average exhaust mass flow rate for both design cases. With a pinch point of 25 K in the gas heater, the maximum thermal efficiency was 0.1524. With positive attributes such as non-flammable, thermal stability, and non-toxic operation, the cycle is a better alternative than isobutane but has significantly lower performance.

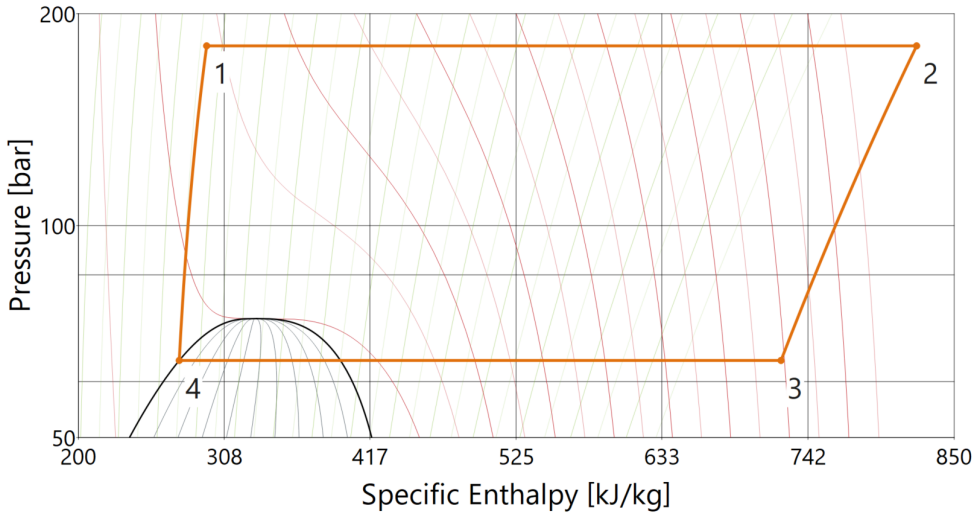

Figure 64: Log(p)-h diagram simple transcritical RC

The recuperative cycle showed a significant increase in thermal efficiency, surpassing the subcritical isobutane cycle. Figure 65 presents the log(p)-h for both the hydrogen and ammonia design case. The recuperator significantly reduced the heat output by pre-heating the CO_2 before the gas heater. With a recuperator effectiveness of 0.9, the hydrogen and ammonia design case achieved a maximum thermal efficiency of 0.271, 38.3% better than the isobutane cycle.

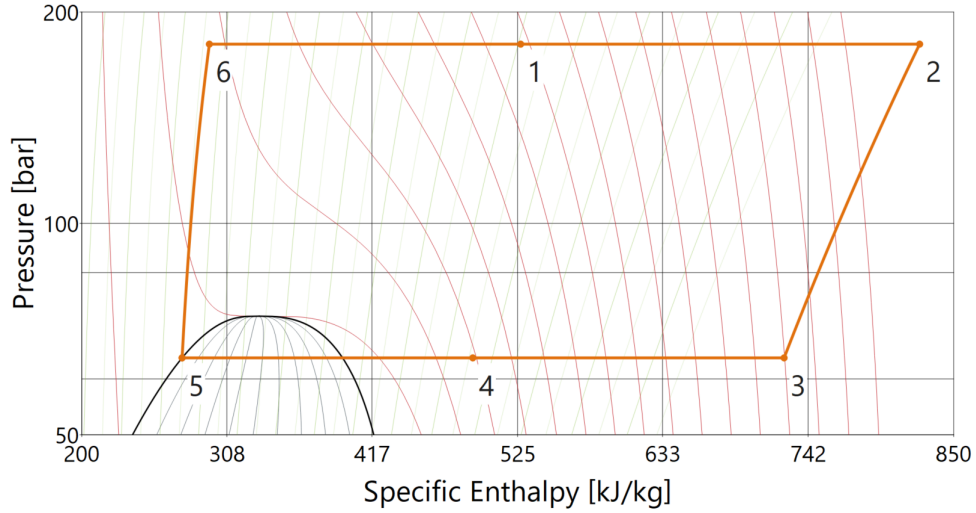

Figure 65: Log(p)-h diagram transcritical recuperative RC

5.4 Waste heat recovery

5.4.1 Electricity generation

Figure 66 presents the electricity generation of the transcritical recuperative RC of the hydrogen design case. For Scenario 1, the maximum and minimum electricity generation was 539 kW and 217 kW, respectively. The total electricity generation throughout the voyage amounts to 5973 kWh with an average thermal efficiency of 0.194. Scenario 2 generates a total of 3938.3 kWh at an average thermal efficiency of 0.262. The maximum and minimum net power output was then 282.3 kW and 235 kW, respectively.

Figure 67 presents the results from the ammonia design case. Scenario 1 generates a maximum

and minimum of 258 kW and 80 kW, respectively. The total electricity generation amounts to 2652 kWh with an average thermal efficiency of 0.18. For scenario 2 the electricity generation amounts to 0. Prioritizing heat recovery, all of the waste heat exhaust gas goes towards heat recovery, bypassing the power cycle. This was because the total potential heat energy of the waste exhaust gas does not cover the heating demand onboard. Therefore, all waste heat was recovered contributing only to the heating demand.

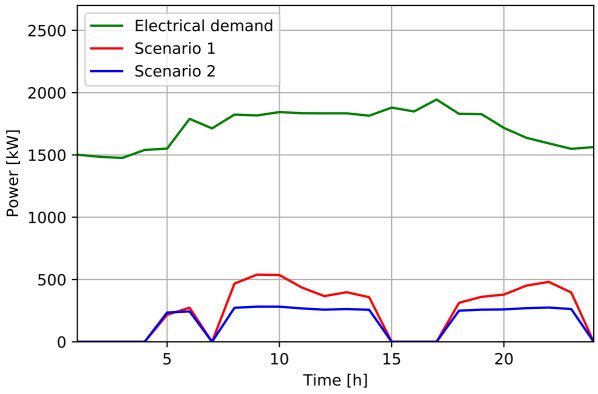

Figure 66: Hydrogen design case

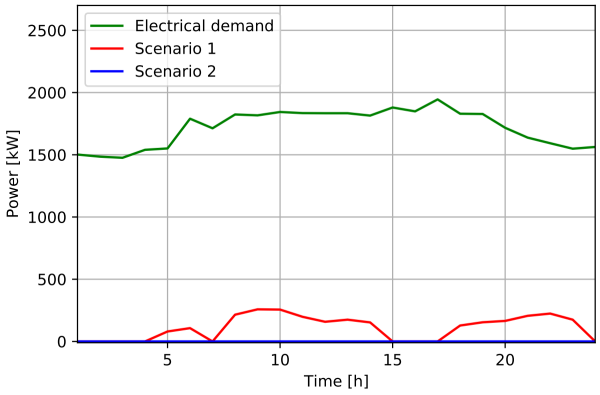

Figure 67: Ammonia design case

The hydrogen and ammonia auxiliary engines have a specific fuel consumption of 0.0833 kg/kWh and 0.474 kg/kWh, respectively. The total fuel saving from electricity generation was then calculated and presented in Table 23 in terms of kilograms fuel saved. The table also presents the fuel saving as a percentage out of the total fuel required for one voyage.

		Scenario 1	Scenario 2
Hydrogen design case	Electricity generation [kWh]	5973	3938.3
	% of total electrical demand	14.48%	9.54%
	Fuel saving [kg]	497.43	328
	% of total fuel	6.02%	3.97%
Ammonia design case	Electricity generation [kWh]	2652	0
	% of total electrical demand	6.42%	0
	Fuel saving [kg]	1256.2	0
	% of total fuel	2.71%	0

Table 23: Total electricity generation

The total electricity generation can further be presented in terms of emission reduction using the IMO tier III NO_x regulation of 3.4 g/kWh in the hydrogen and ammonia auxiliary engines. The total emission reduction as a result of generating electricity in the bottoming power cycle is presented in Table 24.

		Scenario 1	Scenario 2
Hydrogen design case	NO_x reduction [kg]	20.3	13.4
Ammonia design case	NO_x reduction [kg]	9	0

Table 24: Total NO_x reduction

5.4.2 Heat recovery

After electricity generation in the bottoming power cycle, waste heat exhaust gas was used for HTWH. Scenario 1 of the hydrogen design case recovered 22346 kWh of thermal energy, 61.9% of the total heating demand throughout the voyage. For scenario 2, heat recovery was prioritized and 100% of the heating demand was covered. Figure 68 and 69 presents heat recovery in comparison to the heating demand. Scenario 1 of the ammonia design case only contribute 17.74% of the heating demand, with no need for TES charging. In scenario 2, all waste heat exhaust gas was directed to the heat recovery unit with no electricity generation, yet only 56.13% of the heating demand was covered. Table 25 presents an overview of the total heat recovery.

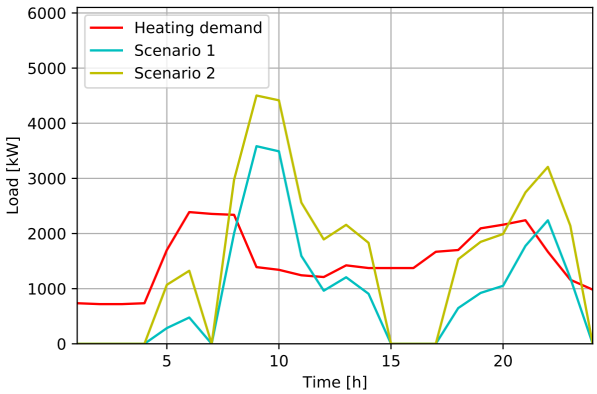

Figure 68: Hydrogen design case

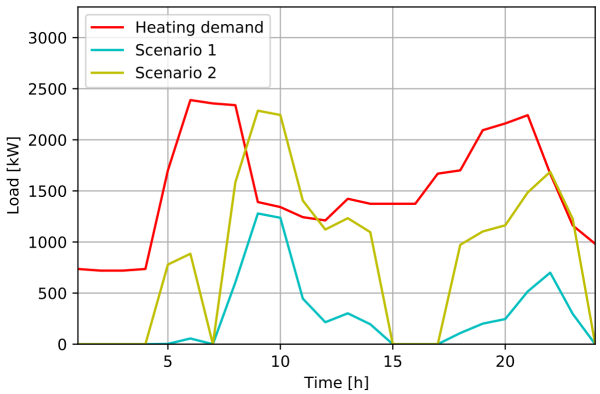

Figure 69: Ammonia design case

		Scenario 1	Scenario 2
Hydrogen design case	Heat recovery [kWh]	22346	36107
	% of total heating demand	61.9%	100%
Ammonia design case	Heat recovery [kWh]	6407	20270
	% of total heating demand	17.74%	56.13%

Table 25: Total heat recovery

The heat recovery is further presented in terms of emission reduction, providing thermal energy through heat recovery instead of combusting HFO in the boilers. Using the fuel-based emission factors provided in Table 15, the total emission reduction of CO_2, SO_x, and NO_x has been calculated and is presented in Table 26.

		Scenario 1	Scenario 2
Hydrogen design case	CO_2 [kg]	7693.4	12431.1
	NO_X [kg]	76.58	123.6
	SO_X [kg]	125.5	202.8
Ammonia design case	CO_2 [kg]	2205.83	6978.5
	NO_X [kg]	21.96	69.5
	SO_X [kg]	36	113.84

Table 26: Total emission reduction with heat recovery

5.4.3 TES

To provide 4417 kWh of heating during port stay, the TES discharging simulation model provided a constant 1472.33 kW per hour for 3 hours. This required thermal oil with a mass flow of 6.871

kg/s. The total quantity of thermal oil required to cover the heating demand during port stay was then 74206.8 kg. This validates the assumed quantity of thermal oil calculated in section 3.7.2, estimating that 74210.35 kg of thermal oil was required. Using equation 21 from section 3.7.2, the quantity of thermal oil stored was then estimated based on the excess heat surpassing the heating demand presented in Figure 68 and 69.

As presented in Table 27, the hydrogen design case is capable of covering the heating demand during port stay for both scenario 1 and 2. The remaining thermal oil was used to further contribute to heating demand. Assuming a thermal oil density of 723.2 kg/m^3, scenario 1 and 2 required a total storage volume of 123.08 and 303 m^3, respectively. Scenario 2 then covered 100% of the heating demand. For scenario 1 in the ammonia design case, no excess heat was stored. However, scenario 2 required a storage volume of 47.8 m^3, then only capable of covering 46.2% of the heating demand during port stay.

		Scenario 1	Scenario 2
Hydrogen design case	Thermal oil storage mass [kg]	88995.3	219102.82
	Thermal oil storage volume [m^3]	123.08	303
Ammonia design case	Thermal oil storage mass [kg]	0	34274.2
	Thermal oil storage volume [m^3]	0	47.8

Table 27: Total storage mass/volume for TES tank

To provide 4417 kWh of thermal energy during port stay the auxiliary boiler have to burn 488.4 kg of heavy fuel oil. Ones again, using the fuel-based emission factors provided in Table 15, the total saved emissions of CO_2, SO_x, and NO_x is presented in Table 28.

Emission type	Emission saved
CO_2	1520.87 kg
SO_x	24.81 kg
NO_x	15.14 kg

Table 28: Emission reduction during port stay

5.5 Cold recovery

Figure 70 presents the amount of cold energy recovered at various LH_2 mass flow rates. The maximum cold recovery was 503.8 kW at a LH_2 mass flow of 0.1394 kg/s and minimum of 167 kW at a mass flow of 0.0456 kg/s. With an average cooling demand of 1000 kW onboard the ship will this cold recovery contribute significantly. After regasification of LH_2 providing cool water to the AHU's, gaseous hydrogen of about 11 °C was further heated to 80 °C using engine cooling water at 90 °C. This engine cooling water was cooled down, contributing on average an additional 79.7 kW which may be used to cool down the main engines.

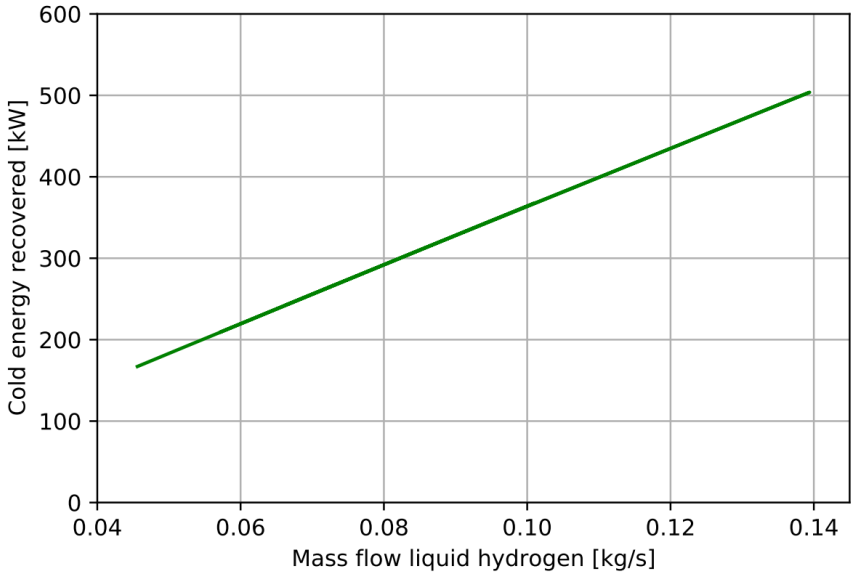

Figure 70: Cold recovery at various LH_2 mass flows

Figure 71 presents the cold recovery throughout the voyage. The plot demonstrates the cold recovery's contribution in terms of percent coverage of the hourly cooling demand. Cold recovery contributed 50.3% at maximum LH_2 mass flow rate and 16.7% at the lowest LH_2 mass flow rate. All together including engine standstill, the cumulative cold energy recovery throughout the whole voyage amounted to 4403.7 kWh, 17.22% of the total cooling demand.

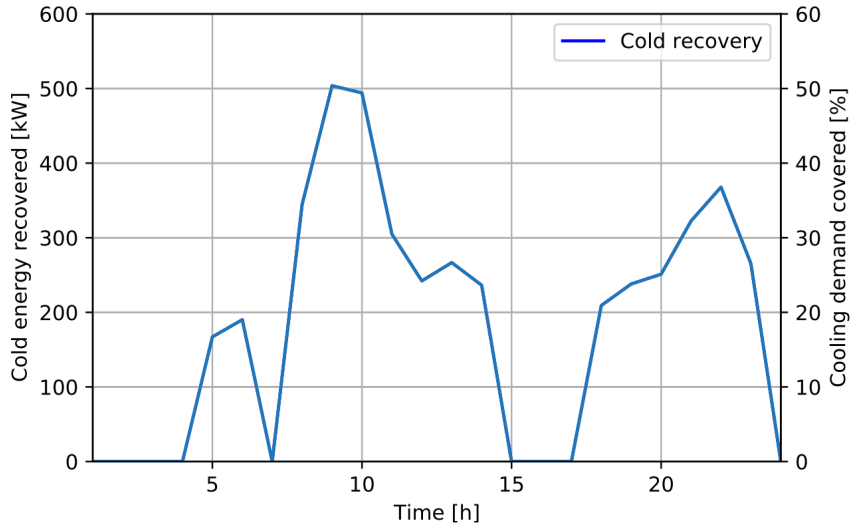

Figure 71: Cold recovery throughout voyage

Fuel saving

The quantity of cold recovery can further be measured in terms of fuel saving. The hydrogen auxiliary engines have a specific fuel consumption of 0.083 kg/kWh. With an average cold recovery of 293.58 kW, the fuel saving can be plotted in terms of COP of the refrigeration systems as presented in Figure 72. At lower COP, the recovered cold energy has the potential to save more fuel. This is because refrigeration systems of low COP require more electricity to provide the same cooling output as a system of high COP. Thus, requiring more fuel in the auxiliary engines generating electricity.

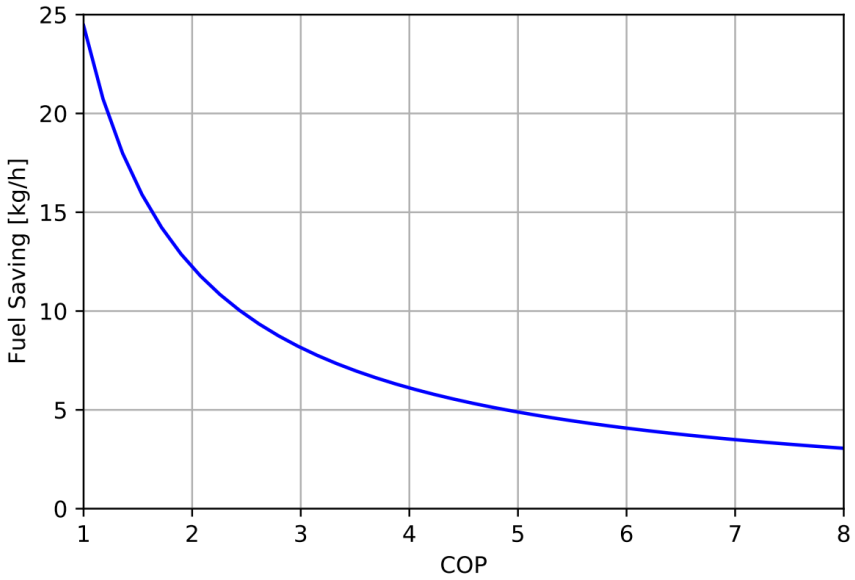

Figure 72: Average fuel saving for various COP

Considering a COP of 3.588 achieved in the transcritical ejector cycle and the total cold recovery throughout the voyage, will the total fuel saved amount to 102.22 kg. Figure 73 presents the hourly fuel saving throughout the voyage, with a maximum of 11.7 kg/h and minimum of 3.87 kg/h. This corresponds to 1.23% of the total fuel required to complete one voyage onboard the hydrogen driven cruise ship. This also amounts to a NO_x reduction of 4.17 kg, with respect to the IMO tier III NO_x regulation.

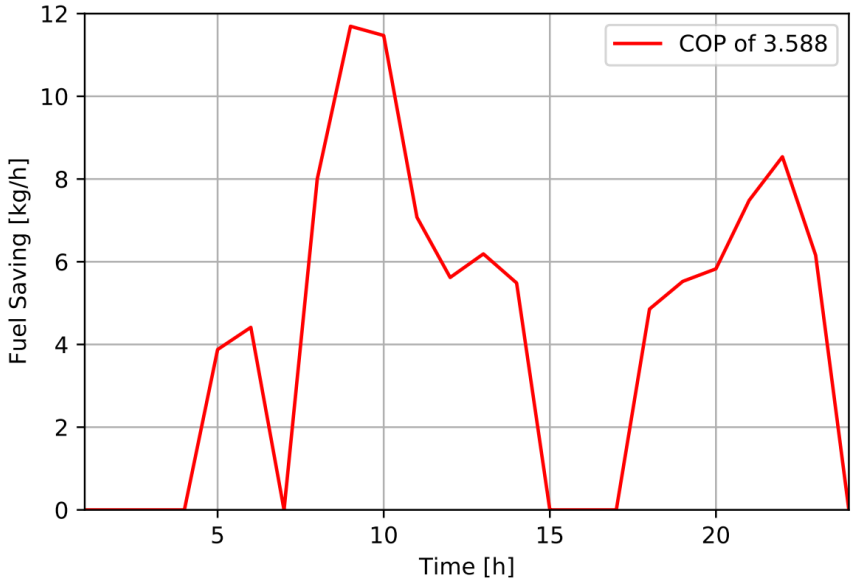

Figure 73: Cold recovery fuel saving design case

5.6 Cold thermal energy storage

The final design of the CTES tank had a total volume of 57.1 m^3. 34.94 m^3 of the volume was from phase-change material alone, corresponding to 32021 kg of ice, the remaining volume was tubing required for charging and discharging. The total CTES tank mass including PCM and piping then amounts to 45845 kg.

5.6.1 Charging

Figure 74 presents the complete charging of the ice thermal energy storage tank. The plot illustrates how water PCM freezes throughout the voyage by plotting the decrease in mass liquid PCM. The initial freezing in hour 0 represents start of charging after port stay in Stockholm. Complete charge is achieved after 20 hours and 41 minutes. The remaining 19 minutes before discharging, the ice was further subcooled to -3.25 °C.

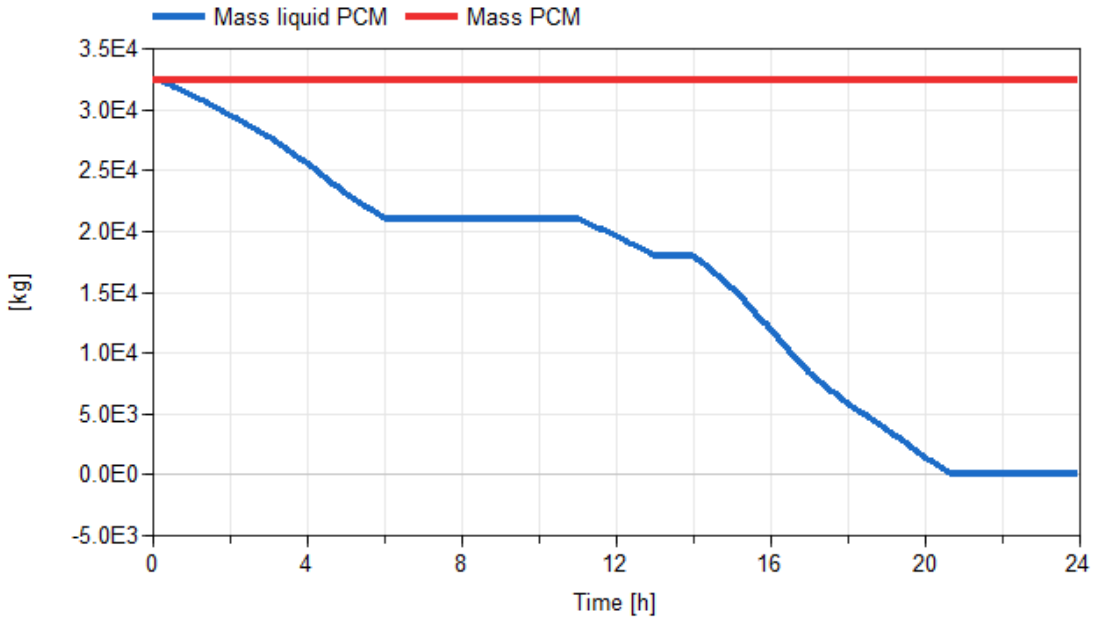

Figure 74: CTES charging

After charging the CTES tank, gaseous hydrogen had a temperature ranging from -37 to -87 °C which was further exploited using water from the AHU's for cold recovery. As presented in Figure 75, the cold recovery is significantly lower in comparison to cold recovery without CTES, covering only 1323.4 kWh or 5.2% of the total cooling demand. In terms of fuel saving will the concepts save about 30.7 kg of fuel or 0.371% of the total fuel onboard. Finally, an additional average 79.7 kW may be recovered heating the hydrogen using engine cooling water.

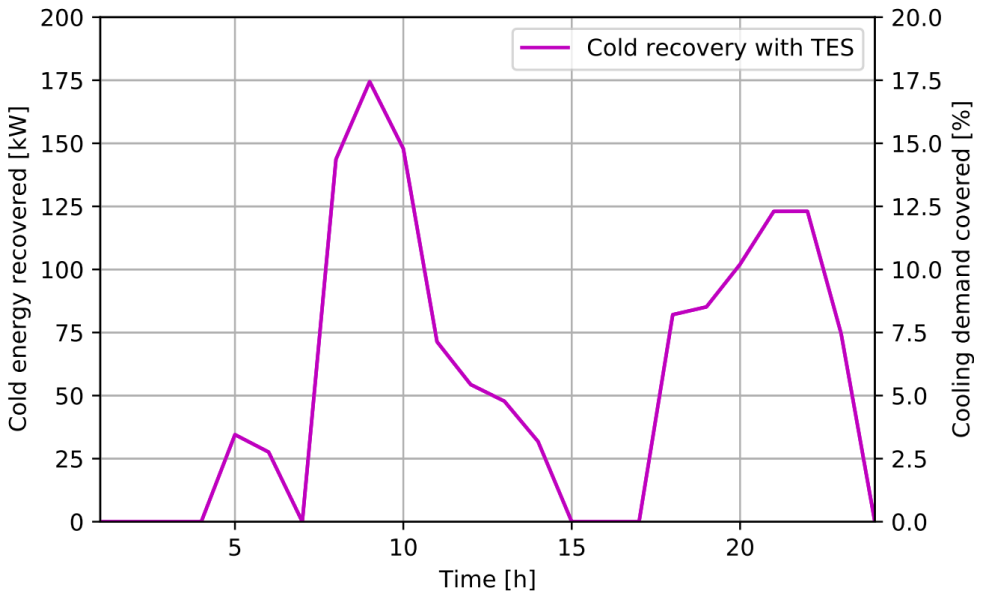

Figure 75: Cold recovery throughout voyage with TES

5.6.2 Discharging

Figure 76 presents the complete discharging of the CTES system. The plot illustrates how the mass of liquid PCM increased as ice melts. After 3 hours, 31716.8 kg of ice is melted providing 2928.8 kWh of cooling to the decentralized AHU's. Without CTES, this cold energy would otherwise be provided by the CO_2 refrigeration system. With a COP of 3.588, the refrigeration system consumes about 68 kg of hydrogen. With a energy-based NO_x emission of 3.4 g/kWh and a specific fuel consumption of 0.0833 kg/kWh, will the total emission saved amount to 2.774 kg during port stay.

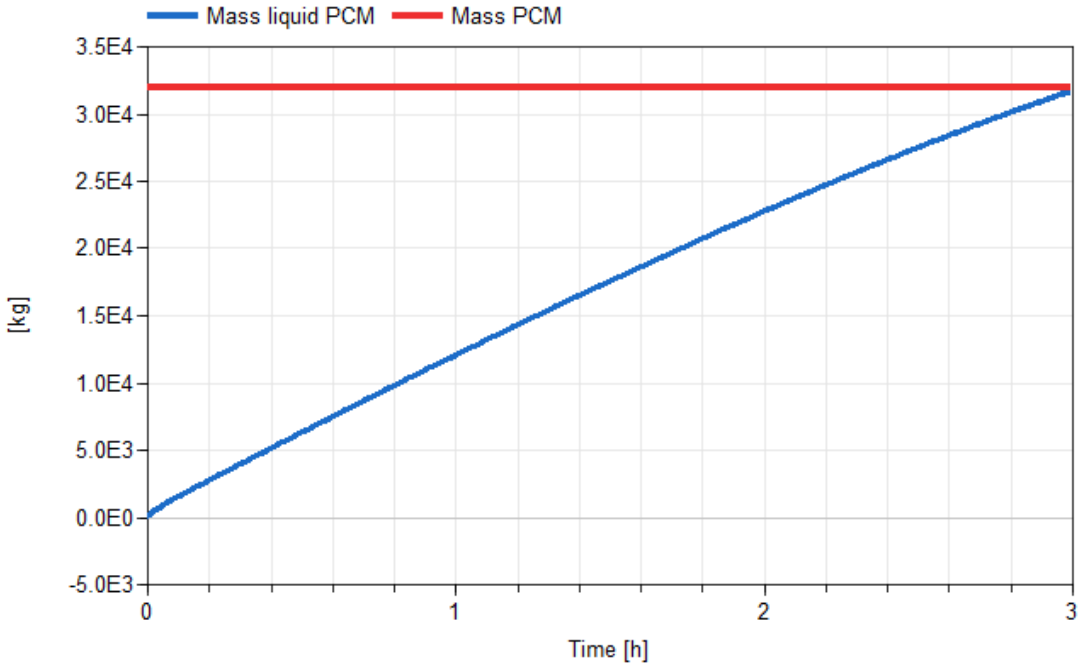

Figure 76: CTES discharging

During discharging, the maximum and minimum discharging power was 1132.7 kW and 728.3 kW, respectively. Due to the nature of the simulation model will the pump adjust the mass flow rate of water such than an exit temperature of 7 °C is achieved. As the ice melts, the mass flow rate of water decreases, as a result decreasing the discharging power as presented in Figure 77. This is further discussed in section 6.5.

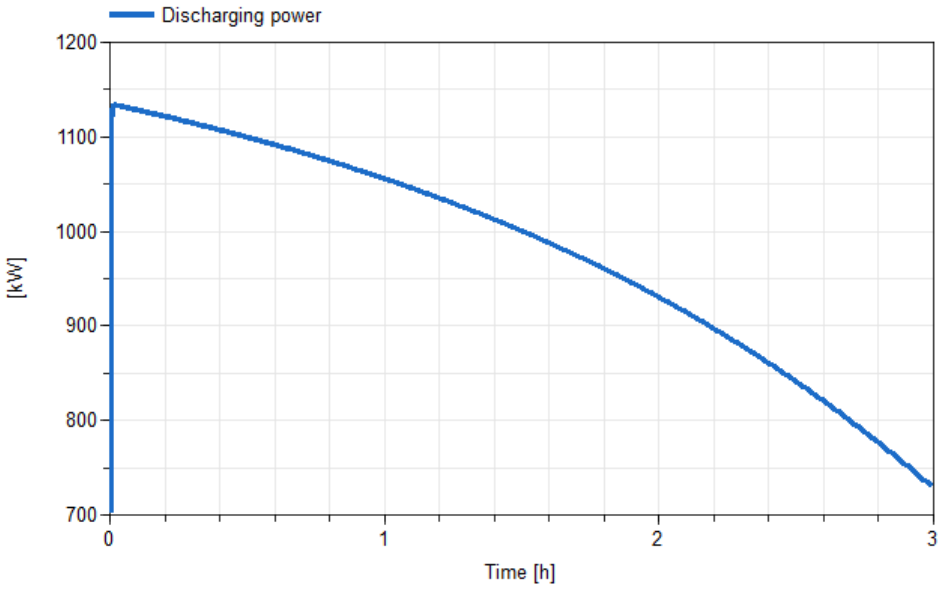

Figure 77: CTES discharging power

5.7 Key findings

Table 29 presents an overview of the total fuel savings from integrating the thermal systems. For the refrigeration system, the study only investigated the performance of CO_2 cycles in comparison to the reference case and subcritical R134a cycle. Fuel saving and emission reduction of the refrigeration systems was therefore not incorporated. Table 29 represents the total fuel saved from electricity generation in the power cycle and cold recovery through regasification of LH_2. 1.23% of the fuel saving comes from cold recovery for both scenario 1 and 2 of the hydrogen design case, the rest is from electricity generation. In the ammonia design case, fuel saving was only obtained in scenario 1 of electricity generation.

		Scenario 1	Scenario 2
Hydrogen design case	Fuel saving [kg]	599.7	430.2
	% of total fuel	7.26%	5.21%
Ammonia design case	Fuel saving [kg]	1256.2	0
	% of total fuel	2.71%	0

Table 29: Total fuel saving

Table 30 presents an overview of the total emission reduction from integrating the thermal systems. The reduced emission is then a result of electricity generation and heat recovery for both design cases. The hydrogen design case also achieved emission reduction through cold recovery of LH_2.

		Scenario 1	Scenario 2
Hydrogen design case	CO_2 [kg]	7693.4	12431.1
	NO_X [kg]	101.1	141.2
	SO_X [kg]	125.5	202.8
Ammonia design case	CO_2 [kg]	2205.83	6978.5
	NO_X [kg]	31	69.5
	SO_X [kg]	36	113.84

Table 30: Total reduction of emissions with TES/CTES integrated

6 Discussion

This section will discuss the results of section 5 and justify some of the choices made when modeling the thermal systems.

6.1 Hydrogen and ammonia operation

With a much higher volumetric energy density, ammonia required much smaller fuel storage volume than liquid hydrogen. At 2.33 times higher storage volume for liquid hydrogen fuel, the storage tank may significantly limit the amount of cabins onboard reducing passenger capacity. The cryogenic hydrogen fuel storage also require substantial amount of insulation just to minimize liquid hydrogen boil off. Ammonia has the great advantage of relatively simple fuel storage in comparison. Ammonia is therefore likely a much cheaper alternative in terms of storage, also considering the energy intensive process of hydrogen liquefaction as mentioned in section 2.3.2.

On the other hand, hydrogen has a much greater gravimetric energy density. As a result, the fuel storage of hydrogen was relatively light in comparison to ammonia design case. The heavy fuel storage may have significant effect of the cruise ship performance, considering the added weight. This may result in a larger fuel consumption than anticipated, but be in favor of the hydrogen design case.

From an environmental aspect will ammonia likely have a larger environmental impact compared to hydrogen considering that hydrogen is a major feedstock for producing ammonia. The environmental footprint of ammonia production will therefore be of greater impact. However, as renewable energy sources become more common will the carbon footprint of production of both fuels decline. As a result, more hydrogen and ammonia will be produced. Ammonia then has the advantage of a more developed infrastructure, considering the long history of ammonia use. This also explains the significantly lower price of ammonia in comparison to hydrogen. Ammonia may therefore be a more viable alternative in terms of marine applications in today's technological developments.

6.2 Optimization of refrigeration cycle

This section describe the results and discuss the performance of the refrigeration cycles investigated in this study.

Optimum high-side pressure

From the literature review provided in section 2.2.5, the R134a cycle showed about 21% higher COP compared to the simple transcritical CO_2 cycle. The simulated models of this study show 53.8% higher COP in the R134a cycle compared to the simple CO_2 cycle. This large difference can be explained by the lack of optimum high-side pressure in the CO_2 cycle.

Figure 61 presents the log(p)-h diagram of the simple transcritical CO_2 cycle. The low performance is justified by the low high-side pressure. With a constant gas cooler outlet temperature of 35 °C, statepoint 3 follows the 35 °C isothermal line as high-side pressure is increased. With the current high-side pressure of 79.87 bar, the expansion valve throttles down to a high steam mass fraction of 0.66 resulting in a low specific cooling capacity.

The COP of the refrigeration system is defined as the ratio of cooling capacity and compressor work. By slightly increasing the high-side pressure, the specific cooling capacity is significantly

increased due to the nature of the isothermal line near critical point as demonstrated in Figure 78. The change in specific cooling capacity increases more than the change in specific compressor work, resulting in an increase in COP. According to a refrigeration software developed by IPU, the optimum high-side pressure is 89 bar for this configuration with a gas cooler outlet temperature of 35 °C, achieving a COP of 2.97.[115] As the high-side pressure is increased beyond the optimum high-side pressure, specific compressor work increases more than the specific cooling capacity, thus lowering COP. Comparing the COP of 2.97 to that of the R134a cycle of the literature study, 9.7% higher COP is achieved in the R134a cycle.

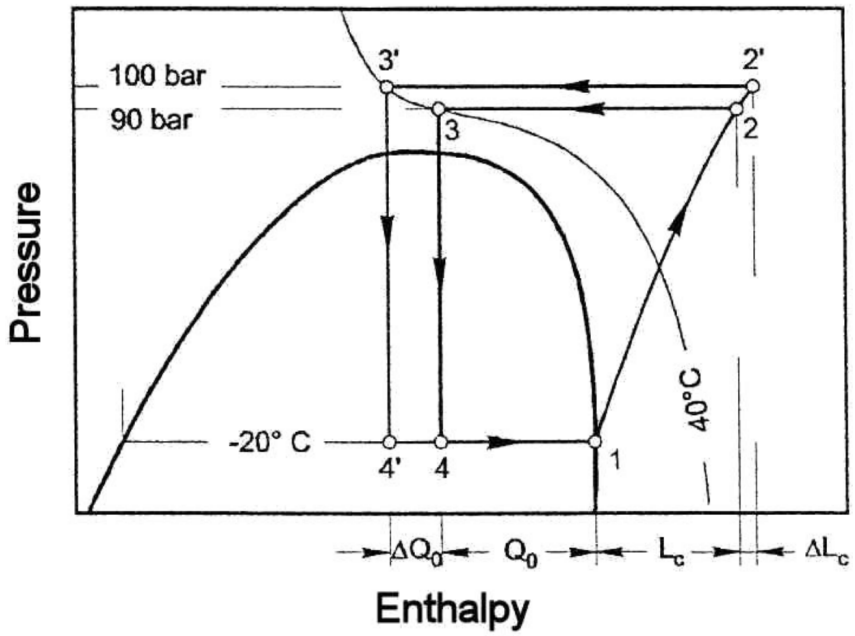

Figure 78: High-side pressure optimization [116]

The integration of an internal heat exchanger significantly improves the COP of the refrigeration unit. The IHX pre-cools the refrigerant before the expansion valve, increasing the cooling capacity. Providing a constant cooling output of 1000 kW, the mass flow of CO_2 may be reduced as a result of this increased cooling capacity, hence, reducing the optimal high-side pressure due to subcooling in the IHX. The optimum high-side pressure is then reduced from 89 to 85 bar, achieving a maximum COP of 3.05 according to the refrigeration software developed by IPU. The literature review found a performance enhancement of 15% when integrating the IHX. Once again, the results of the simulation models deviate significantly from these values of the literature study, with a 43% increases in COP. This illustrates the importance of optimum high-side pressure. Yet, comparing the optimum COP of 2.97 of the IPU refrigeration software, the simulated IHX cycle achieves a 2% higher COP compared to the IPU simple cycle.

The optimum high-side pressure of the ejector cycle is 85 bar according to the IPU refrigeration software. The cycle then achieves a COP of 3.42 whereas the simulation model of this study achieves a COP of 3.588. Assuming a COP of 2.97 for the simple transcritical cycle, will the ejector cycle be in line with literature study with a performance increase of 20.8%.

Effects of superheating

The specific cooling capacity may also be increased by further superheating the working fluid in the evaporator. In the case of the simple transcritical CO_2 cycle, further superheating actually increases the COP. Below the optimum high-side pressure of 89, the superheating result in a greater increase in the specific cooling capacity compared to specific work in the compressor.

The simple CO_2 cycle therefore experience a COP increase of 15% with 20 K superheat, in comparison to 5 K. However, with a 20 K superheat the evaporator outlet temperature is 22 °C and that in not possible with countercurrent flow heated by circulating water of 12 °C from the AHU's. Above or near optimum high-side pressure superheating reduces the COP, but is necessary to avoid damage to the compressor.

Controlling high-side pressure

In a traditional subcritical cycle, the high-side pressure is dependent on the heat transfer characteristics of the condenser defining the condensation pressure. The heat transfer area of the condenser can then be adjusted in order to achieve an optimum high-side pressure for maximum COP. A thermostatic valve is then common, regulating the mass flow of working fluid to ensure certain amount of superheat after the evaporator prior to the compressor. However, in a transcritical cycle the high-side pressure is adjusted based on the compressor capacity and its balance to the resistance of an expansion device. As presented in Figure 78, when the gas cooler outlet temperature is constant the COP of the system is highly dependent of the high-side pressure. A back pressure valve is then common ensuring optimum high-side pressure for maximum COP. Yet, this method does not ensure superheat prior to compressor. A solution is then to use both a back pressure valve and a thermostatic valve with an intermediate pressure stage in a liquid receiver. The thermostatic valve then feeds the evaporator a sufficient mass flow of working fluid to ensure dry expnasion, while the back pressure valve ensures optimum high-side pressure. Due to the nature of the simulation model will this method not be possible to simulate. Only a thermostatic valve has been used in this simulation and optimum high-side pressure is therefore difficult to attain. As a result the high-side pressure may vary unpredictably and optimum COP is difficult to achieve.

IHX effectiveness

The IHX increases the cooling capacity, on the other hand, the refrigerant is superheated before the compressor. This superheating pushes statepoint 1 further right in the log(p)-h diagram of Figure 62. With a constant isentropic efficiency of 0.8 in the compressor, the specific compressor work increases as the working fluid is superheated by the IHX. This is due to the fact that the gradient of the entropy lines decrease moving along the positive x-axis, increasing specific compressor work. The increase in specific cooling capacity and specific compressor work is plotted as a function of IHX effectiveness in Figure 79. The plot clearly demonstrates how the gradient of the specific cooling capacity is larger than the gradient of specific compressor work. Thus, the COP increases with increasing IHX effectiveness. The IHX effectiveness of the IHX cycle was therefore set to 0.9, maximizing COP at minimal increase in total heat transfer area.

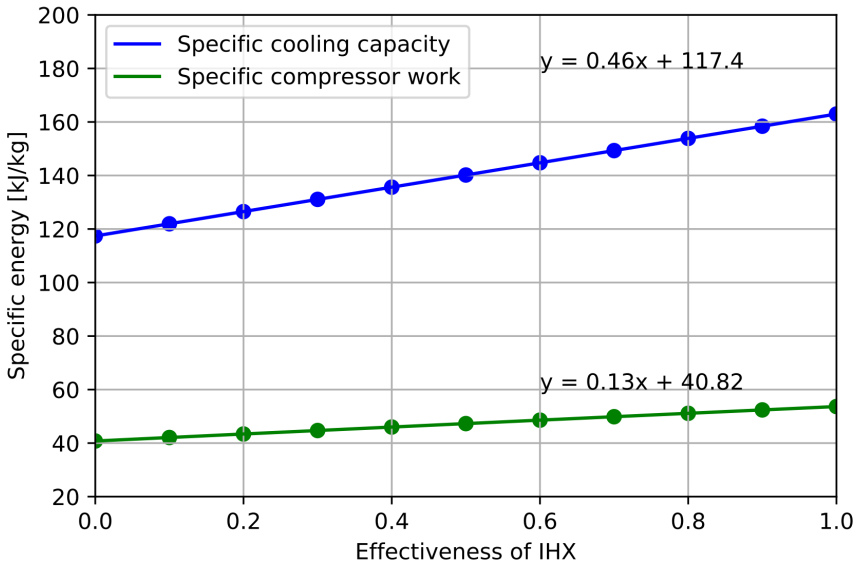

Figure 79: Change in specific energy as a function of IHX effectiveness

Unlike the simple transcritical cycle, will integration of an IHX not be advantageous for the transcritical ejector cycle. Figure 80 illustrates the change in COP as a function of the high-side pressure for various values of IHX effectiveness. At high-side pressures above 80 bar, the IHX penalize the performance of the refrigeration cycle. However, the IHX is essential to ensure superheat prior to the compressor. The IHX effectiveness of the simulation cycle was therefore set to 0.178, the minimum effectiveness still providing 5 K superheat prior to the compressor.

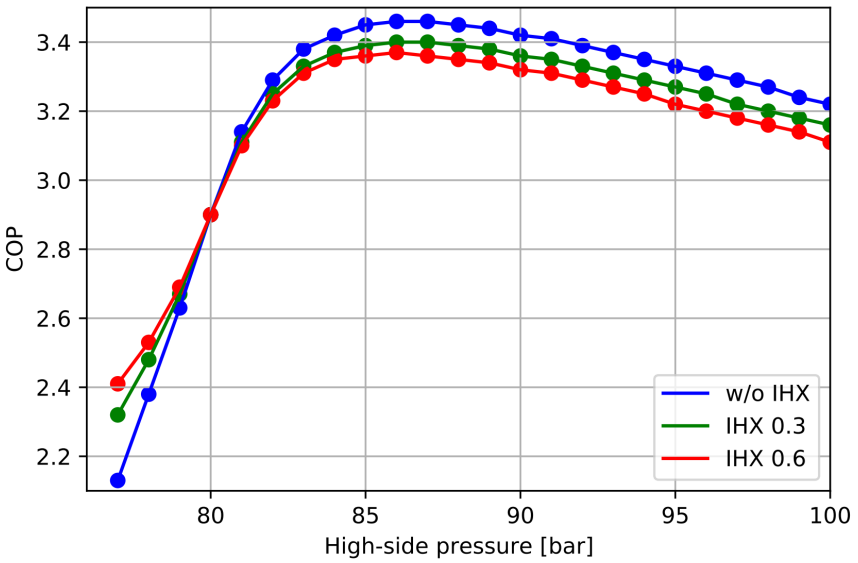

Figure 80: COP of ejector cycle at various IHX effectiveness

Heat recovery high-side

As the gas cooler outlet temperature increases as a result of higher ambient temperatures, will the optimum high-side pressure of the transcritical CO_2 refrigeration system increase. With higher high-side pressure comes a higher heat rejection temperature. To further increase the energy efficiency of the refrigeration system can heat recovery be integrated. The refrigeration system thus provides cooling output and heating output. This is achieved by integrating a desuperheater recovering heat prior to the gas cooler.

The refrigeration systems presented in this study have a gas cooler inlet temperatures in the range of 69-72 °C. This heat is rejected to seawater as wasted thermal energy. Cooling output is priority, however, there is a considerable amount of thermal energy that could be recovered and utilized onboard the cruise ship. This concept of integrated cooling and heating system is explained further in the master's thesis (Development of CO_2 refrigeration systems and thermal energy storage for cruise ships) by Henrik Andersen, a fellow student.

6.3 Waste heat recovery

This study investigates the potentials of recovering waste heat exhaust gas by generating electricity and heating water contributing to heating onboard the cruise ship. Considering two design cases of hydrogen or ammonia operation, the study examines two scenarios of waste heat recovery. Scenario 1, maximizing electricity generation, and scenario 2, prioritizing heat recovery. Assuming one stream of waste heat exhaust gas, the study considers first generating electricity with a bottoming power cycle, then heating thermal oil to a temperature of 120 °C for HTWH. The two scenarios considered thus make it possible to evaluate what concept makes for a better alternative in terms of energy efficiency, fuel saving and emission reduction.

6.3.1 Optimization of power cycles

High-side pressure

The high-side pressure of the bottoming power was investigated for optimal performance. The pressure optimization of the simulation models was performed by adjusting the high-side pressure in 5 bar increments. The mass flow of the working fluid and heat source remained constant. As the pressure is increasing, the pump outlet temperature increases reducing the approach temperature in the gas heater, thus reducing the heat input. On the other hand, as pressure increases will the expansion in the turbine experience larger enthalpy differences, resulting in a lower turbine outlet temperature. The reduction in heat output is larger than the reduction in heat input which increases the thermal efficiency of the cycle. Maximum high-side pressure is therefore desirable, however, was limited to 180 bar in this study in regards to the maximum working pressure of the components. Figure 81 demonstrates how the thermal efficiency of the power cycle increases with increasing high-side pressure. Higher thermal efficiency is desirable as the net power output can be increased with the same heat input from the exhaust gas.

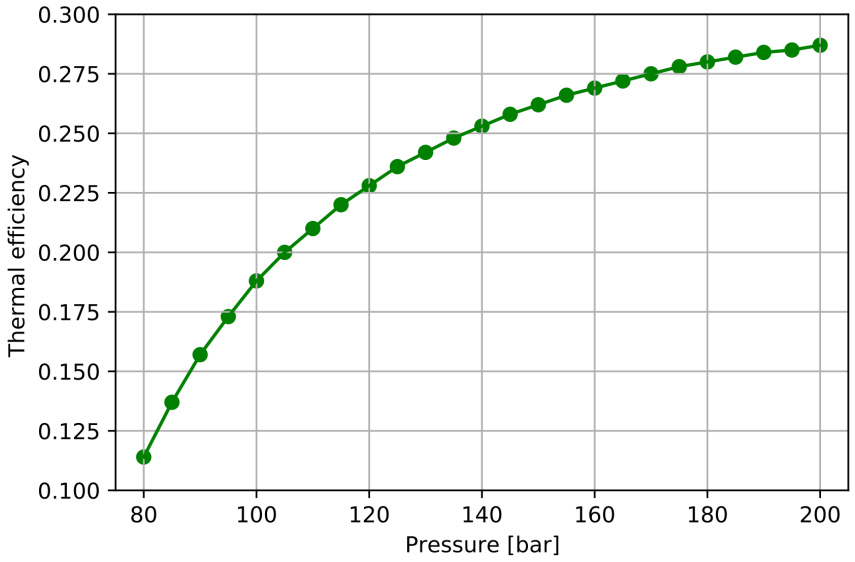

Figure 81: High-side pressure optimization

Recuperator effectiveness

Further optimization was performed in the recuperator of the recuperative bottoming power cycle. Referring back to the thermodynamic energy balance of a rankine cycle explained in section 2.6.3, the thermal efficiency is denoted as the ratio of net power output and heat input from the exhaust gas. As the recuperator effectiveness is increased, the CO_2 working fluid is further pre-heated by the high temperature working fluid exiting the turbine. The amount of heat input from the exhaust gas is then decreased providing the same amount of net power output at the same working fluid mass flow rate, thus increasing the thermal efficiency of the power cycle. Alternatively, the power cycle can increase the net power output by increasing the working fluid mass flow rate at the same exhaust heat input. Yet again increasing thermal efficiency. This is illustrated in Figure 82, where the thermal efficiency is increased as a function of the recuperator effectiveness.

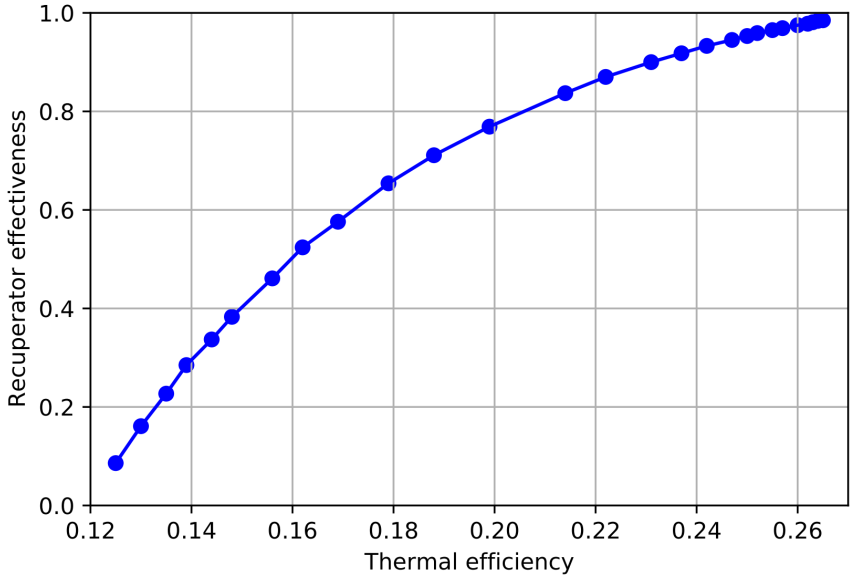

Figure 82: Thermal efficiency with increasing recuperator effectiveness

In order to maximize the thermal efficiency of the power cycle, the ideal recuperator effectiveness was near 1 as presented in Figure 82. This was discovered by performing a manual iterative process increasing the recuperator area. As the recuperator area increases will the recuperator effectiveness also increase. This is because the ratio of actual heat transfer to potential heat transfer in the recuperator increases as defined in equation 18. However, illustrated in figure 83, the recuperator area increases exponentially when surpassing a recuperator effectiveness of 0.9. A recuperator effectiveness beyond 0.9 will significantly increase capital costs with minimal performance enhancement. Naturally, the optimal recuperator effectiveness is then found at the point of largest thermal efficiency and lowest increase in total heat transfer area. Therefore, set to 0.9 for this study.

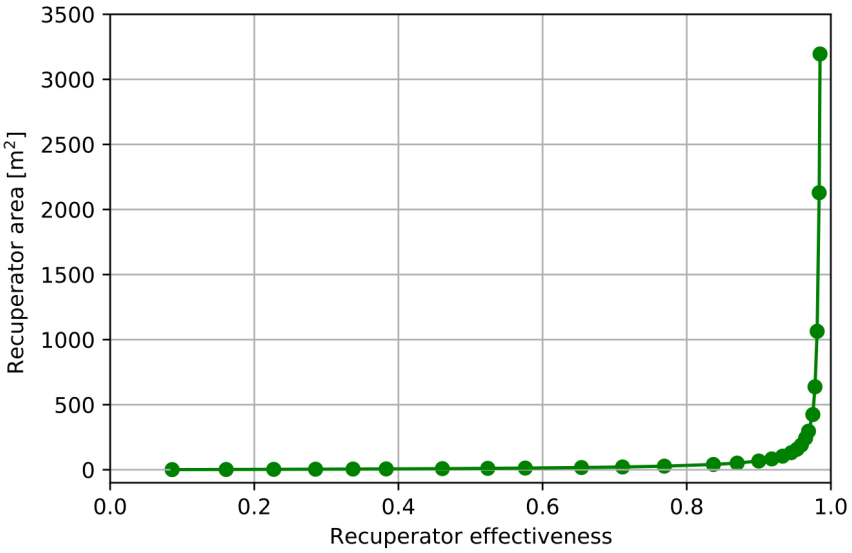

Figure 83: Recuperator area with increasing recuperator effectiveness

6.3.2 Optimization of electricity generation

The thermal efficiency of a power cycle defines the fraction of heat input which is converted to work. Maximum thermal efficiency is desired considering the fact that waste heat is to be recovered after the power cycle. However, maximum thermal efficiency is not directly correlated to maximum net power output. For this study, the maximum thermal efficiency is obtained at design conditions, where the gas heater achieves a pinch of 25 K. As the mass flow of the working fluid is increased, the pinch point and net power output increases but thermal efficiency decrease. Therefore, there exists an optimum mass flow for maximum net power output. This is demonstrated in Figure 84.

At low working fluid mass flow rates, CO_2 achieves a high temperature being heated in the gas heater. The statepoint of CO_2 in a log(p)-h diagram will therefore be far right in the diagram before the turbine where the entropy lines are less steep. Thus, resulting in a large specific work in the turbine. However, because of the low mass flow rate, the net power output is relatively low and the thermal efficiency is high. By increasing the working fluid mass flow rate, the net power output is increased but the specific work in the turbine decreases as a result of lower gas cooler outlet temperature. An optimum mass flow rate will therefore exist.

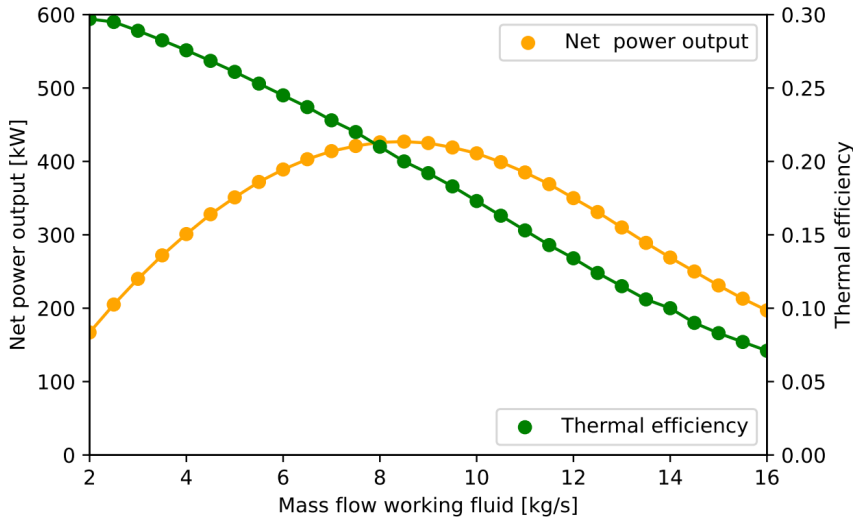

Figure 84: Optimum CO_2 mass flow for maximum net power output

As a dynamic simulation will the optimal mass flow of the working fluid also vary depending on the exhaust mass flow. In the case of scenario 1, will the optimal mass flow of the working fluid be when maximum electricity generation is achieved throughout the voyage in the power cycle. Net power output can then be plotted as a function of the working fluid mass flow for various exhaust mass flow rates to determine the optimum conditions in Figure 85. The minimum, average, and maximum exhaust mass flow for the hydrogen design case was plotted to demonstrate these effects. With an average exhaust mass flow of 11.3 kg/s will a working fluid mass flow rate of 8.5 kg/s be the optimum for the hydrogen design case. 4 kg/s was then the optimum for the ammonia design case where the average exhaust mass flow rate was 4.34 kg/s.

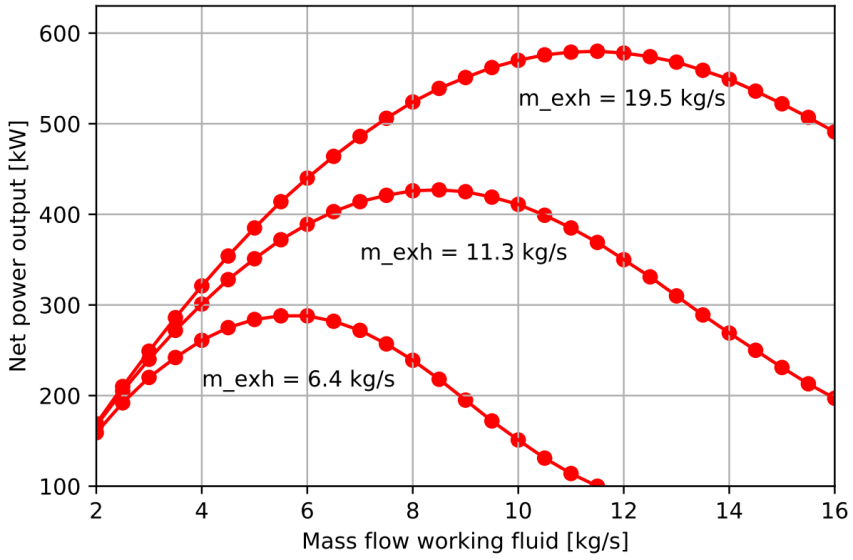

Figure 85: Optimum CO_2 mass flow rate for maximum electricity generation

To further improve the system in terms of maximum electricity generation, the system should vary the mass flow rate of the CO_2 working fluid depending on the exhaust mass flow rate. This will significantly increase net power output in the low range and high range of exhaust mass flow rate, more so in the low range. With a constant mass flow of 8.5 kg/s, the power cycle generates about 195 kW when the exhaust mass flow is 6.4 kg/s. By shifting the working fluid mass flow to 6 kg/s, the net power output increases to 288 kW.

Another complication with a constant working fluid mass flow rate in the power cycle is that at low exhaust flow rates, the lower temperature boundary of 120 °C may be exceeded limiting electricity generation. In scenario 1 of the ammonia design case, the lowest exhaust gas heater outlet temperature in the power cycle was 120.5 °C. This occurred during the minimum exhaust mass flow rate. By reducing the working fluid mass flow rate, net power output increases, available heat for heat recovery increases, and the lower temperature boundary of 120 °C may be avoided.

6.3.3 TES

The thermal oil charging and discharging quantity was calculated based on the amount of thermal energy exceeding the heating demand when recovering heat in Figure 68 and 69. Equation 21 was then used to calculate the quantity of oil charged assuming a pinch point of 2 K in the HTWH plate heat exchanger. In other word, assuming a ΔT of 93 K. The results was validated by comparing the calculated quantity of thermal oil with the simulated quantity of thermal oil required during discharging. Further validating the assumed specific heat capacity and density of the thermal oil.

The simulated TES discharging model was designed to provide 1472.33 kWh of high temperature water with a pinch point of 2 K. Discharging for 3 hours providing the thermal demand of 4417 kWh during port stay. However, as the heating demand varies from the design conditions will the pinch point vary. For instance during a heating demand of 2356 kWh, of hour 7, the mass flow of thermal oil is much larger than the case of 1472.33 kWh. The pinch of 2 K will then no longer be valid and a much larger quantity of thermal oil is required to meet the thermal demand. The estimated quantity of thermal oil for TES may therefore be inaccurate. However, the average heating demand throughout the voyage is 1504 kWh. The design condition of 1472.33 will therefore represent a good estimation of necessary TES quantity and volume.

6.3.4 Scenario 1 versus scenario 2

For both design cases scenario 1 is likely the better alternative from an economic perspective, as prioritizing electricity generation results in a greater hydrogen and ammonia fuel saving. From an environmental perspective, scenario 2 is more attractive. One of the reasons lies in the location of emitted emissions.

One of the main environmental restrictions regarding passenger ships concerns emission amongst EU ports and harbours. Reducing emissions during port stay may therefore be more favourable. Scenario 1 reduces emissions by a considerable amount, as presented in Table 30, but majority is during seagoing. Emission during seagoing is not desirable, nonetheless, but does not have a direct effect on human health in the same degree as emission in harbours.[117]

The second reason is that HFO emitt larger levels of pollutants than hydrogen and ammonia during combustion as demonstrated in Table 28. Preferably, all combustion of HFO is avoided. As transcritical CO_2 heat pumps become more common for marine applications such as cruise ships will emissions from thermal supply will be reduced significantly. With the gliding temperature of transcritical CO_2, heat pumps are superior for heat pumping processes such as HTWH at 90 °C. These heat pumps require electricity to supply thermal energy. Using the electricity generated from waste heat to supply thermal energy using heat pumps result in a double penalties, in terms of energy efficiency. Therefore, heat recovery of exhaust gas for HTWH will likely be the better alternative either way.

The downside of scenario 2 is the large storage volumes of the TES tanks. Again, making scenario 1 a better alternative from an economic perspective. The hydrogen design case required

a storage volume of 303 m^3. The design case covered 100% of the heating demand, but may significantly reduce the passenger capacity and require large capital costs. The TES tank may then be split into multiple tanks running in parallel, making better use of the tank volume. Alternatively, this study could investigate two separate streams of waste heat exhaust gas, both with a temperature of 400 °C. The split ratio between the streams of electricity generation and heat recovery would then be adjusted based on electrical and thermal demand throughout the voyage for more reliable controllability. The benefits lie in the thermal oil of higher temperature, reducing necessary TES storage volume. As an example, by increasing the temperature of the thermal oil from 120 to 150 °C, the total storage volume is reduced by nearly 25%.

6.4 Cold recovery

The cold recovery from regasification of LH_2 show promising results. The proposed concept makes sense from an economic perspective, with a daily fuel saving of 102.22 kg of LH_2 and a 17.22% coverage of the cooling demand, with the possibility of significantly reducing the required cooling output of the refrigeration system. Yet, there are many aspects to be considered when evaluating the attractiveness of this concept. From a pure technical aspect, the concept is promising. With relatively little components, the concept is expected to have a reasonable capital cost and low maintenance. However, some modifications should be considered. The design case uses water as the heat source for regasification of LH_2. Glycol-water is likely a better alternative, avoiding potential freezing of water in the plate heat exchanger. The design case also assumed that engine cooling water is accessible at all times at a temperature of 90 °C. During startup after port stay as the main engines are cold, external heat may be necessary in order heat gaseous hydrogen to 80 °C.

The sailing conditions also have a large impact on the feasibility of cold recovery. First of all, the concept depends on a cooling requirement onboard the cruise ship. During winter the cooling demand is likely small in comparison to summer conditions, an alternative utilization of the recovered cold energy may than be more attractive. Cold energy may than be used to improve performance of on-board rankine cycles generating electricity, as investigated by Baldasso et al. in section 2.7. This alternative concept would not be affected in the same manner considering the change in ambient conditions, as the electrical demand is not seasonal based. Cold energy may also be used for preservation of food onboard, again not dependent ambient conditions in the same degree.

The ambient conditions also have a large impact on the performance of the CO_2 refrigeration system. The design case considered a rather warm condition where the gas cooler outlet temperature was 35 °C. As ambient temperatures drop and seawater temperature drop, will the COP of the refrigeration system significantly improve. Thus, saving less fuel in terms of cold energy recovered because the auxiliary engines have to generate less electricity to the refrigeration system. The study also computed the amount of fuel saving based on a constant COP of 3.588, however, this may vary throughout the voyage. To minimize this variation in COP, multiple smaller refrigeration systems should be run in parallel. Regardless of cooling demand, this ensures near peak performance of the refrigeration systems. The calculated fuel saving of cold recovery should therefore not be far off a realistic value.

6.5 Cold thermal energy storage

The objective of the CTES system was to recover cold energy from regasification of LH_2 such that the cooling demand could be covered during port stay with zero emissions. Within the 3 hour port stay, 2928.8 kWh of cooling was successfully provided by circulating water from decentralized AHU's onboard the cruise ship. The charging was designed such that a full charge

was achieved just prior to the 3 hour port stay in Stockholm. Considering the long time period of charging and the large heat transfer driving forces, could a full charge be achieved with relatively small heat transfer area.

CTES charging

With tubing amounting to only 17.3 m^2 of heat transfer area distributed evenly in a tank of 57.1 m^3, it is reason to believe that complications will arise. As the PCM is charging, the thermal conductivity of the tubing play a big role in the charging rate. As ice starts to freeze around the tubing, the thermal conductivity of ice play a bigger role and thus reduce the charging rate. Ice surrounding the tubing will likely also experience extreme degrees of subcooling, which is undesirable. Reducing the spacing between heat transfer tubing may solve these potential complications, as the ice thermal barrier between liquid PCM and LH_2 is reduced. A potential solution is then to operate smaller CTES tanks in parallel, with the possibility of minimizing dead water zones not exposed to the same rate of freezing. Other modification include tube fins, increasing the thermal conductivity.

Effects of subcooling

After complete charge of the ice CTES tank, the PCM is slightly subcooled to -3.25 °C. The PCM is completely solid and is further cooled through sensible heat storage. As discovered in the literature review of section 2.8, latent heat storage has a greater energy density in comparison to sensible heat storage. The subcooling should therefore be avoided as the cold energy could be utilized more efficiently. The initial temperature during CTES discharging was set to 0 °C, neglecting the -3.25 °C subcooling of ice. As a result, 55.85 kWh of cold thermal energy was neglected. The amount does not account for a large portion of the total system energy storage, but should be considered during latent CTES design.

Subcooling of the CTES indicates that the equipped heat transfer area for charging is over-sized, and capital costs may therefore be reduced. However, the total heat transfer area for charging is only a small fraction of the total heat transfer area for discharging. The finding will therefore not account for a larger capital cost saving, but is still noteworthy.

CTES discharging

Discharging the CTES tank is much more demanding considering the little time frame of 3 hours in comparison to 21 hours for charging. This explains the significant difference in heat transfer area. Figure 77 illustrates the CTES discharging power throughout the 3 hour port stay. The maximum discharging power is achieved in the start and decreases throughout the 3 hour time frame. The simulation model adjust the mass flow of water entering the CTES system based on the water outlet temperature. As the discharging power decreases, so does the mass flow rate of water. This is justified by the change in heat transfer characteristics. During discharging, the ice around the tubes melt from the inside out as presented in Figure 86, thus enabling both natural convection and conductive heat transfer. Natural convection occurs as a result of change in PCM density through phase-change. However, the simulation model may not consider this phenomena making conduction more dominant. Water has a thermal conductivity 0.55 W/mK and ice has a thermal conductivity of 2.22 W/mK.[14]

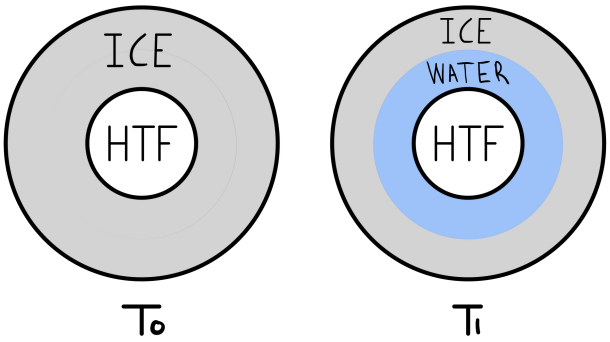

Figure 86: PCM phase-change during CTES discharging

As the CTES discharges, the cooling load is reduced due to the additional thermal barrier of water, causing a reduction in thermal conductivity. As for charging, multiple CTES tanks in parallel may solve this issue. This also allows for more efficiency relocation of the CTES tank volume, considering the 57.1 m^3 required excluding insulation. Further modification include adding fins to the tubing, increasing heat transfer area and thermal conductivity.

The thermal conductivity of the heat transfer material also have a significant effect on the discharging rate. Copper was chosen as heat transfer material given the high thermal conductivity. Using stainless steel on both tank housing and tubing, the discharging time increases from 3 hours to 43 hours. Aluminum is a much better alternative than stainless steel, achieving a complete discharge in 3 hours and 52 minutes with the same heat transfer area. Aluminum will also be a better alternative with respect to capital costs, considering the near 14 tonnes of material required to build the CTES tank.

When configuring the tubing layout, the change in PCM density must be considered. Assuming one large PCM tank, as investigated in this study, the PCM density increase from 917 kg/m^3 to about 1000 kg/m^3 when melting during discharging. Tubing near the ceiling of the CTES tank may therefore not be in contact with the PCM as the PCM level is dropping during discharging. This may significantly reduce the discharging rate. Ones again, a potential solution is to operate smaller CTES tanks in parallel. Either way, an optimal tubing configuration must be further investigated.

Emission

The amount of emission avoided through discharging the CTES during port stay is not significant at 2.774 kg NO_x. However, the concept realize the objective of providing the cooling demand during port stay with zero emission. New regulations proposed by the EU state that ships docked in harbours of a duration longer that 2 hours should connect to shore-side electricity.[118] Electricity may then be used from shore to operate the refrigeration systems. However, during port stay of 2 hours or shorter, the concept of CTES is a promising alternative ensuring zero-emission cooling demand.

7 Conclusion

The objective of this master's thesis was to design and simulate different thermal systems of hydrogen and ammonia driven cruise ships for increased energy efficiency and low emissions. A reference case by Baldi et al. was used to gather energy loads of a cruise ship travelling the Baltic Sea. Two design cases of hydrogen and ammonia operation was created to analyze and discuss the thermal systems developed.

The reference case required an average cooling demand of about 1000 kW throughout the voyage. This master's thesis then investigated different configurations of CO_2 refrigeration systems providing a constant 1000 kW of cooling output to decentralized AHU's onboard the cruise ship. The refrigeration cycles were then analyzed and compared to a traditional subcritical R134a cycle. Simulations using Dymola found that a simple subcritical R134a refrigeration cycle achieved a COP of 3.258, providing a constant 1000 kW of cooling output. The simple transcritical CO_2 cycle performanced notebly lower with a COP of 2.118. This was justified by the low high-side pressure in section 6.2. The transcritical CO_2 cycle with an IHX performed significantly better with a COP of 3.03, however not surpassing the R134a cycle. The greatest performance was achieved in the transcritical ejector cycle with a COP of 3.656. However, as superheat was not sufficient an IHX must be integrated decreasing the COP to 3.588. The final configuration resulted in a performance increase of 10.13% in comparison to the R134a cycle.

Further, the thesis investigated waste heat recovery of the main engine exhaust gas. Two scenarios were defined for both design cases of hydrogen and ammonia. Scenario 1 for maximum electricity generation and scenario 2 for 100% coverage of the heating demand. Prior, the bottoming power cycles were optimized for maximum thermal efficiency. In comparison to a simulated subcritical isobutane ORC with a thermal efficiency of 0.196, a simple transcritical CO_2 rankine cycle achieved a thermal efficiency of 0.1524. This was further improved to 0.271 when integrating a recuperator. This increased the thermal efficiency by 38.3% over the isobutane cycle.

The hydrogen design case experienced the largest potential for waste heat recovery, considering the much larger exhaust mass flow rate. The hydrogen design case achieved an electricity generation covering 14.48% and 9.54% of the total electrical demand for scenario 1 and 2, respectively. The waste heat exhaust gas further contributed to 61.9% and 100% of the heating demand in the heat recovery unit for scenario 1 and 2, respectively. The ammonia design case achieved an electricity generation of 6.42% of the electrical demand for scenario 1 but did not generate electricity in scenario 2. Scenario 1 only contributed 17.74% of the heating demand whereas 56.13% was contributed in scenario 2, bypassing electricity generation.

Due to the mismatch of heat recovery and heating demand was a TES tank designed to store thermal oil when the heat recovery surpassed the heating demand in order to provide the total heat recovered. The hydrogen design case then required a tank with a volume of 123.08 m^3 and 303 m^3 storing thermal oil for scenario 1 and 2, respectively. Scenario 1 of the ammonia design case did not require a TES tank due to the low heat recovery. Scenario 2 required a tank volume of 47.8 m^3. To ensure zero emission heating demand during port stay, the study found that the hydrogen design case could provide heating during port stay for both scenarios. Ammonia was only able to cover 46.2% of the heating demand during port stay.

The two scenarios of waste heat recovery could then be compared in terms of fuel consumption reduction and emission reduction. From section 5.7 it is clear that scenario 1 is more favourable in terms of reduced fuel consumption, saving 7.26% and 2.71% of total fuel required onboard the cruise ship for the hydrogen and ammonia design case, respectively. Scenario 2 is more favourable in terms of emission reduction with a significant difference of CO_2, NO_x, and SO_x emission. This includes emission reduction during port stay, one key objective of the IMO

environmental regulations. Scenario 2 was therefore found more attractive for the design cases examined.

The thesis also investigated cold recovery of liquid hydrogen. Through regasification of liquid hydrogen, 17.22% of the cooling demand could be covered providing cooled water to decentralized AHU's. This resulted in a fuel saving 1.23% of the total fuel required onboard assuming a COP of 3.588 in the refrigeration system. This corresponds to 4.17 kg of NO_x reduction. Alternatively, by integrating CTES the emission reduction could be shifted from seagoing to port stay. With a CTES tank containing ice with a total volume of 57.1 m^3, 2928 kWh of cooling could be provided during port stay. This resulted in a NO_x emission reduction 2.774 kg amongst the harbour.

8 Further Work

This section presents suggestions for further work either improving the proposed thermal systems or for further research.

- Examine hydrogen and ammonia storage in terms capital costs and feasibility.
- Validate engine characteristics of the hydrogen and ammonia ICE's.
- Evaluate possibilities of waste heat recovery of multiple heat sources to improve energy efficiency.
- Investigate combined power cycles of both turbo-compounding and bottoming power cycles.
- Investigate nitric acid formation and its effect on waste heat recovery of hydrogen and ammonia ICE's.
- Further investigation of other applications of liquid hydrogen cold recovery. Such as, integration of cold recovery with bottoming power cycles for improved thermal efficiency, cold recovery for provision cooling, potentials of reducing refrigeration capacity saving capital costs.
- Investigate CO_2 heat pumps for replacing HFO thermal boilers.
- Examine possibilities of using a different PCM of lower phase-change temperature in CTES.
- Examine possibilities of storing thermal oil of higher temperatures and potential applications of high temperature oil for emission reduction.
- Optimized tubing layout for optimal CTES charging and discharging.

References

1. SINTEF. CruiZE - Cruising towards Zero Emissions. Available from: https://www.sintef.no/en/projects/2020/cruize-cruising-towards-zero-emissions/ [Accessed on: 2021 Dec 16]
2. al JF et. Fourth IMO GHG Study 2020. Tech. rep. London, 2021
3. Ancona MA, Baldi F, Bianchi M, Branchini L, Melino F, Peretto A and Rosati J. Efficiency improvement on a cruise ship: Load allocation optimization. Energy Conversion and Management 2018; 164:42–58
4. McKinlay CJ, Turnock S and Hudson D. A Comparison of hydrogen and ammonia for future long distance shipping fuels. 2020
5. Jakhrani AQ, Rigit ARH, Othman AK, Samo SR and Kamboh SA. Estimation of carbon footprints from diesel generator emissions. *2012 International Conference on Green and Ubiquitous Technology*. IEEE. 2012 :78–81
6. Manzan M, Pezzi A, Zorzi EZ de, Freni A, Frazzica A, Vaglieco BM, Lucio Z and Claudio D. Potential of thermal storage for hot potable water distribution in cruise ships. Energy Procedia 2018; 148:1105–12
7. Baldi F, Ahlgren F, Nguyen TV, Thern M and Andersson K. Energy and exergy analysis of a cruise ship. Energies 2018; 11:2508
8. Baldasso E, Mondejar ME, Mazzoni S, Romagnoli A and Haglind F. Potential of liquefied natural gas cold energy recovery on board ships. Journal of Cleaner Production 2020; 271:122519
9. Baldi F, Ahlgren F, Melino F, Gabrielii C and Andersson K. Optimal load allocation of complex ship power plants. Energy Conversion and Management 2016; 124:344–56
10. Briley GC. A History of Refrigeration. ASHRAE 2004 :S31–S34
11. Sandvik Group. The History of The Refrigerator. Available from: https://www.materials.sandvik/en/campaigns/fridge-of-the-future/the-history-of-the-refrigerator/ [Accessed on: 2021 Oct 6]
12. NTNU, Department of Marine Technology. Discovery of Ozone Hole announced. Available from: https://www.history.com/this-day-in-history/discovery-of-antarctic-ozone-hole-announced [Accessed on: 2021 Oct 6]
13. G.F.C Rogers YM. Work and Heat Transfer. Pearson Education Limited, 1992
14. Moran MJ, Shapiro HN, Boettner DD and Bailey MB. Fundamentals of engineering thermodynamics. John Wiley & Sons, 2010
15. Bahrami M. refrigeration Cycle. Available at http:https://www.sfu.ca/~mbahrami/ENSC%20461/Notes/Refrigeration%20Cycle.pdf (2005/06/12)
16. Kim MH, Pettersen J and Bullard CW. Fundamental process and system design issues in CO2 vapor compression systems. Progress in energy and combustion science 2004; 30:119–74
17. Dincer I. Refrigeration systems and applications. John Wiley & Sons, 2017
18. Protocol M. Montreal protocol on substances that deplete the ozone layer. Washington, DC: US Government Printing Office 1987; 26:128–36
19. Nekså P, Walnum HT and Hafner A. CO2-a refrigerant from the past with prospects of being one of the main refrigerants in the future. *9th IIR Gustav Lorentzen conference*. Citeseer. 2010 :2–14
20. Purohit P and Höglund-Isaksson L. Global emissions of fluorinated greenhouse gases 2005–2050 with abatement potentials and costs. Atmospheric Chemistry and Physics 2017; 17:2795–816

21. Agency USEP. Understanding Global Warming Potentials. Available at https://www.epa.gov/ghgemissions/understanding-global-warming-potentials (2021/10/23)

22. Hafner IA, Gabrielii C and Widell K. Refrigeration units in marine vessels: Alternatives to HCFCs and high GWP HFCs. Nordic Council of Ministers, 2019

23. Pigani L, Boscolo M and Pagan N. Marine refrigeration plants for passenger ships: Low-GWP refrigerants and strategies to reduce environmental impact. International journal of refrigeration 2016; 64:80–92

24. Bellos E and Tzivanidis C. A comparative study of CO2 refrigeration systems. Energy Conversion and Management: X 2019; 1:100002

25. Giljarhus KET, Munkejord ST and Skaugen G. Solution of the Span–Wagner equation of state using a density–energy state function for fluid-dynamic simulation of carbon dioxide. Industrial & Engineering Chemistry Research 2012; 51:1006–14

26. Yu B, Yang J, Wang D, Shi J and Chen J. An updated review of recent advances on modified technologies in transcritical CO2 refrigeration cycle. Energy 2019; 189:116147

27. Santini L, Accornero C and Cioncolini A. On the adoption of carbon dioxide thermodynamic cycles for nuclear power conversion: A case study applied to Mochovce 3 Nuclear Power Plant. Applied Energy 2016; 181:446–63

28. Brown JS, Yana-Motta SF and Domanski PA. Comparitive analysis of an automotive air conditioning systems operating with CO2 and R134a. International Journal of refrigeration 2002; 25:19–32

29. Koegelenberg I. World Guide to Transcritical CO2 Refrigeration. Shecco: Brussels, Belgium 2020

30. Koling K. Development and demonstration of a prototype transcritical CO2 refrigeration system. Tech. rep. Koge, Denmark, 2008

31. Gullo P, Tsamos K, Hafner A, Ge Y and Tassou SA. State-of-the-art technologies for transcritical R744 refrigeration systems–a theoretical assessment of energy advantages for European food retail industry. Energy Procedia 2017; 123:46–53

32. Van Hoecke L, Laffineur L, Campe R, Perreault P, Verbruggen SW and Lenaerts S. Challenges in the use of hydrogen for maritime applications. Energy & Environmental Science 2021; 14:815–43

33. Dimitriou P and Javaid R. A review of ammonia as a compression ignition engine fuel. International Journal of Hydrogen Energy 2020; 45:7098–118

34. Li HW and Onoue K. Compressed Hydrogen: High-Pressure Hydrogen Tanks. *Hydrogen Energy Engineering*. Springer, 2016 :273–8

35. Wang X, Wang R, Bian X, Cai J, Tian H, Shu G, Li X and Qin Z. Review of dynamic performance and control strategy of supercritical CO2 Brayton cycle. Energy and AI 2021 :100078

36. Al Ghafri SZ, Swanger A, Jusko V, Siahvashi A, Perez F, Johns ML and May EF. Modelling of Liquid Hydrogen Boil-Off. Energies 2022; 15:1149

37. Krasae-in S, Stang JH and Neksa P. Development of large-scale hydrogen liquefaction processes from 1898 to 2009. International journal of hydrogen energy 2010; 35:4524–33

38. Aasadnia M and Mehrpooya M. Large-scale liquid hydrogen production methods and approaches: A review. Applied Energy 2018; 212:57–83

39. Ni M. An overview of hydrogen storage technologies. Energy exploration & exploitation 2006; 24:197–209

40. Heywood JB. Internal combustion engine fundamentals. McGraw-Hill Education, 2018

41. Naber JD and Johnson JE. Internal combustion engine cycles and concepts. *Alternative Fuels and Advanced Vehicle Technologies for Improved Environmental Performance*. Elsevier, 2014 :197–224

42. Heck RM, Farrauto R and Gulati S. "Catalytic Air Pollution Control: Commercial Technology". Platinum Metals Rev 2010; 54:180–3

43. Noor CM, Noor M and Mamat R. Biodiesel as alternative fuel for marine diesel engine applications: A review. renewable and sustainable energy reviews 2018; 94:127–42

44. Ni P, Wang X and Li H. A review on regulations, current status, effects and reduction strategies of emissions for marine diesel engines. Fuel 2020; 279:118477

45. Jayaram V, Nigam A, Welch WA, Miller JW and Cocker III DR. Effectiveness of emission control technologies for auxiliary engines on ocean-going vessels. Journal of the Air & Waste Management Association 2011; 61:14–21

46. MAN Energy Solutions. Exhaust after-treatment systems. Available from: https://www.man-es.com/marine/solutions/exhaust_gas_after_treatment_systems [Accessed on: 2022 Feb 16]

47. Smith T, Jalkanen J, Anderson B, Corbett J, Faber J, Hanayama S, O'keeffe E, Parker S, Johansson L, Aldous L et al. Third IMO greenhouse gas study 2014. 2015

48. Zhu Y, Xia C, Shreka M, Wang Z, Yuan L, Zhou S, Feng Y, Hou Q and Ahmed SA. Combustion and emission characteristics for a marine low-speed diesel engine with high-pressure SCR system. Environmental Science and Pollution Research 2020; 27:12851–65

49. Kumar V, Gupta D and Kumar N. Hydrogen use in internal combustion engine: A review. International Journal of Advanced Culture Technology 2015; 3:87–99

50. Karim GA. Hydrogen as a spark ignition engine fuel. International Journal of Hydrogen Energy 2003; 28:569–77

51. Seddiek IS, Elgohary MM and Ammar NR. The hydrogen-fuelled internal combustion engines for marine applications with a case study. Brodogradnja: Teorija i praksa brodogradnje i pomorske tehnike 2015; 66:23–38

52. Ammar NR. Energy efficiency and environmental analysis of the green-hydrogen fueled slow speed marine diesel engine. Int. J. Multi. Curr. Res 2018; 6:1–10

53. Radica G, Mrakovčić T, Račić N, Jelić M, Lalić B, Pelić V, Bratić K, Kozina A and Bulat D. Marine engines running on hydrogen additive in diesel fuel for emission reduction. *2021 6th International Conference on Smart and Sustainable Technologies (SpliTech)*. IEEE. 2021 :1–3

54. El-Gohary MM. Design of marine hydrogen internal combustion engine. Alexandria Engineering Journal 2008; 47:57–65

55. Oh D and Plante JS. A Hydrogen-Fueled, Direct-Injected, Two-Stroke, Small-Displacement Engine for Recreational Marine Applications With High Efficiency and Low Emissions. *Internal Combustion Engine Division Fall Technical Conference*. Vol. 55096. American Society of Mechanical Engineers. 2012 :859–68

56. Cornelius W, Huellmantel LW and Mitchell HR. Ammonia as an engine fuel. SAE Transactions 1966 :300–26

57. Starkman ES, Newhall H, Sutton R, Maguire T and Farbar L. Ammonia as a spark ignition engine fuel: theory and application. Sae Transactions 1967 :765–84

58. Yapicioglu A and Dincer I. Experimental investigation and evaluation of using ammonia and gasoline fuel blends for power generators. Applied Thermal Engineering 2019; 154:1–8

59. Comotti M and Frigo S. Hydrogen generation system for ammoniaehydrogen fuelled internal combustion engines. international journal of hydrogen energy 2015; 40:e10686

60. Kurien C and Mittal M. Review on the production and utilization of green ammonia as an alternate fuel in dual-fuel compression ignition engines. Energy Conversion and Management 2022; 251:114990

61. Liu L, Wu Y and Wang Y. Numerical investigation on the combustion and emission characteristics of ammonia in a low-speed two-stroke marine engine. Fuel 2022; 314:122727

62. Cardoso JS, Silva V, Rocha RC, Hall MJ, Costa M and Eusébio D. Ammonia as an energy vector: Current and future prospects for low-carbon fuel applications in internal combustion engines. Journal of Cleaner Production 2021; 296:126562

63. Guo B, Ichiyanagi M, Kajiki K, Aratake N, Zheng Q, Kodaka M and Suzuki T. Combustion Analysis of Ammonia Fueled High Compression Ratio SI Engine with Glow Plug and Sub-Chamber-Effects of Ammonia Content under Condition of Co-combustion with Gasoline/Ammonia/Air. International Journal of Automotive Engineering 2022; 13:1–8

64. Guangrong Z. Ship energy efficiency technologies-now and the future. 2017

65. Shu G, Liang Y, Wei H, Tian H, Zhao J and Liu L. A review of waste heat recovery on two-stroke IC engine aboard ships. Renewable and Sustainable Energy Reviews 2013; 19:385–401

66. Singh DV and Pedersen E. A review of waste heat recovery technologies for maritime applications. Energy conversion and management 2016; 111:315–28

67. Johnson I, Choate WT and Davidson A. Waste heat recovery. Technology and opportunities in US industry. Tech. rep. BCS, Inc., Laurel, MD (United States), 2008

68. Soffiato M, Frangopoulos CA, Manente G, Rech S and Lazzaretto A. Design optimization of ORC systems for waste heat recovery on board a LNG carrier. Energy Conversion and Management 2015; 92:523–34

69. Mondejar M, Andreasen J, Pierobon L, Larsen U, Thern M and Haglind F. A review of the use of organic Rankine cycle power systems for maritime applications. Renewable and Sustainable Energy Reviews 2018; 91:126–51

70. Zhu S, Zhang K and Deng K. A review of waste heat recovery from the marine engine with highly efficient bottoming power cycles. Renewable and Sustainable Energy Reviews 2020; 120:109611

71. He W, Zhang G, Zhang X, Ji J, Li G and Zhao X. Recent development and application of thermoelectric generator and cooler. Applied Energy 2015; 143:1–25

72. Teo A, Chiong M, Yang M, Romagnoli A, Martinez-Botas R and Rajoo S. Performance evaluation of low-pressure turbine, turbo-compounding and air-Brayton cycle as engine waste heat recovery method. Energy 2019; 166:895–907

73. Paanu T, Niemi S and Rantanen P. Waste heat recovery: bottoming cycle alternatives. 2012

74. Larjola J. Electricity from industrial waste heat using high-speed organic Rankine cycle (ORC). International journal of production economics 1995; 41:227–35

75. Zhang X, He M and Zhang Y. A review of research on the Kalina cycle. Renewable and sustainable energy reviews 2012; 16:5309–18

76. Li X, Huang H and Zhao W. A supercritical or transcritical Rankine cycle with ejector using low-grade heat. Energy conversion and management 2014; 78:551–8

77. Baldi F, Johnson H, Gabrielii C and Andersson K. Energy and exergy analysis of ship energy systems–the case study of a chemical tanker. International Journal of Thermodynamics 2015; 18:82–93

78. Tian H, Liu P and Shu G. Challenges and opportunities of Rankine cycle for waste heat recovery from internal combustion engine. Progress in Energy and Combustion Science 2021; 84:100906

79. Chintala V, Kumar S and Pandey JK. A technical review on waste heat recovery from compression ignition engines using organic Rankine cycle. Renewable and Sustainable Energy Reviews 2018; 81:493–509

80. Başaran A and Yurddaş A. Thermal modeling and designing of microchannel condenser for refrigeration applications operating with isobutane (R600a). Applied Thermal Engineering 2021; 198:117446

81. Nawaz K, Shen B, Elatar A, Baxter V and Abdelaziz O. R290 (propane) and R600a (isobutane) as natural refrigerants for residential heat pump water heaters. Applied Thermal Engineering 2017; 127:870–83

82. Darvish K, Ehyaei MA, Atabi F and Rosen MA. Selection of optimum working fluid for organic Rankine cycles by exergy and exergy-economic analyses. Sustainability 2015; 7:15362–83

83. Raghulnath D, Saravanan K, Mahendran J, Lakshmanan P et al. Analysis and optimization of organic Rankine cycle for IC engine waste heat recovery system. Materials Today: Proceedings 2020; 21:30–5

84. Javanshir A and Sarunac N. Thermodynamic analysis of a simple Organic Rankine Cycle. Energy 2017; 118:85–96

85. Astolfi M, Alfani D, Lasala S and Macchi E. Comparison between ORC and CO2 power systems for the exploitation of low-medium temperature heat sources. Energy 2018; 161:1250–61

86. Motai T and Kobayashi N. Exhaust gas boiler. US Patent 5,660,799. 1997 Aug

87. Zheng X, Luo X, Luo J, Chen J, Liang Y, Yang Z, Chen Y and Wang H. Experimental investigation of operation behavior of plate heat exchangers and their influences on organic Rankine cycle performance. Energy Conversion and Management 2020; 207:112528

88. Xu B, Rathod D, Yebi A, Filipi Z, Onori S and Hoffman M. A comprehensive review of organic rankine cycle waste heat recovery systems in heavy-duty diesel engine applications. Renewable and Sustainable Energy Reviews 2019; 107:145–70

89. Bergman TL, Incropera FP, DeWitt DP and Lavine AS. Fundamentals of heat and mass transfer. John Wiley & Sons, 2011

90. Erling Næss AA. Varmevekslere. 2022 Mar

91. Mavridou S, Mavropoulos G, Bouris D, Hountalas D and Bergeles G. Comparative design study of a diesel exhaust gas heat exchanger for truck applications with conventional and state of the art heat transfer enhancements. Applied Thermal Engineering 2010; 30:935–47

92. Zehnder M. Efficient air-water heat pumps for high temperature lift residential heating, including oil migration aspects. Tech. rep. EPFL, 2004

93. Borsukiewicz-Gozdur A. Pumping work in the organic Rankine cycle. Applied Thermal Engineering 2013; 51:781–6

94. Sarkar J. Review and future trends of supercritical CO2 Rankine cycle for low-grade heat conversion. Renewable and Sustainable Energy Reviews 2015; 48:434–51

95. Garg P, Srinivasan K, Dutta P and Kumar P. Comparison of CO2 and steam in transcritical Rankine cycles for concentrated solar power. Energy procedia 2014; 49:1138–46

96. Zhang Q, Luo Z, Zhao Y and Pavel S. Thermodynamic analysis and multi-objective optimization of a transcritical CO2 waste heat recovery system for cruise ship application. Energy Conversion and Management 2021; 227:113612

97. Carnival Corporation plc. Carnival Corporatio's AIDAnova First Ship to be Supplied with LNG in Mediterranean. Available from: https://https://www.carnivalcorp.com/news-releases/news-release-details/carnival-corporations-aidanova-first-ship-be-supplied-lng [Accessed on: 2021 Nov 14]

98. Khor J, Dal Magro F, Gundersen T, Sze J and Romagnoli A. Recovery of cold energy from liquefied natural gas regasification: Applications beyond power cycles. Energy Conversion and Management 2018; 174:336–55

99. Yamamoto T, Fujiwara Y and Kitagaki S. Challenges of advanced utilization of LNG cold in osaka gas senboku LNG terminals. *Design for Innovative Value Towards a Sustainable Society*. Springer, 2012 :148–53

100. Xia G, Sun Q, Cao X, Wang J, Yu Y and Wang L. Thermodynamic analysis and optimization of a solar-powered transcritical CO2 (carbon dioxide) power cycle for reverse osmosis desalination based on the recovery of cryogenic energy of LNG (liquefied natural gas). Energy 2014; 66:643–53

101. Wang J, Wang J, Dai Y and Zhao P. Thermodynamic analysis and optimization of a transcritical CO2 geothermal power generation system based on the cold energy utilization of LNG. Applied Thermal Engineering 2014; 70:531–40

102. Dincer I and Rosen MA. Thermal energy storage systems and applications. John Wiley & Sons, 2021

103. SOCACIU LG. Seasonal thermal energy storage concepts. ACTA TECHNICA NAPOCENSIS-Series: APPLIED MATHEMATICS, MECHANICS, and ENGINEERING 2012; 55

104. Kouvo J. Technical review of thermal energy storage technologies for waste heat recovery and related applications. 2021

105. Skovajsa J, Koláček M and Zálešák M. Phase change material based accumulation panels in combination with renewable energy sources and thermoelectric cooling. Energies 2017; 10:152

106. Sarbu I and Sebarchievici C. A comprehensive review of thermal energy storage. Sustainability 2018; 10:191

107. Cabeza LF, Martorell I, Miró L, Fernández AI and Barreneche C. Introduction to thermal energy storage systems. *Advances in Thermal Energy Storage Systems*. Elsevier, 2021 :1–33

108. Caprara G, Armas V, Mesquita Sousa D de, Kermani M and Martirano L. An Energy Storage System to support Cruise Ships Cold Ironing in the Port of Civitavecchia. *2021 IEEE International Conference on Environment and Electrical Engineering and 2021 IEEE Industrial and Commercial Power Systems Europe (EEEIC/I&CPS Europe)*. IEEE. 2021 :1–5

109. Baldi F, Gabrielii C, Melino F and Bianchi M. A preliminary study on the application of thermal storage to merchant ships. Energy Procedia 2015; 75:2169–74

110. Baldasso E, Gilormini TJA, Mondejar ME, Andreasen JG, Larsen LK, Fan J and Haglind F. Organic Rankine cycle-based waste heat recovery system combined with thermal energy storage for emission-free power generation on ships during harbor stays. Journal of Cleaner Production 2020; 271:122394

111. Tan H, Li Y, Tuo H, Zhou M and Tian B. Experimental study on liquid/solid phase change for cold energy storage of Liquefied Natural Gas (LNG) refrigerated vehicle. Energy 2010; 35:1927–35

112. Saeed MZ, Widell KN, Hafner A, Nordtvedt TS and Svendsen ES. Cryogenic cold utilization and system integration possibilities for LNG-driven fishing vessels. *6th IIR Conference on Sustainability and the Cold Chain-Proceedings*. International Institute of Refrigeration. 2020

113. Xu X, Liu E, Zhu N, Liu F and Qian F. Review of the Current Status of Ammonia-Blended Hydrogen Fuel Engine Development. Energies 2022; 15:1023

114. Klüssmann JN, Ekknud L, Ivarsson A and Schramm J. Ammonia application in CI engines. Special report, a report from the advanced motor fuels technology collaboration programme 2020

115. IPU. Simple one-stage CO2. Available from: https://www.ipu.dk/products/simple-one-stage-co2/ [Accessed on: 2022 Jun 5]

116. Reulens W. Natural refrigerant CO 2. KHLim vzw, 2009

117. Mondejar ME, Ahlgren F, Thern M and Genrup M. Quasi-steady state simulation of an organic Rankine cycle for waste heat recovery in a passenger vessel. Applied Energy 2017; 185:1324–35

118. Mustafa Mirza. The European Union's Proposal on Alternative Fuels and its Impact on Shore Power Adoption. Available from: https://powertechresearch.com/the-europeanunions-proposal-on-alternative-fuels-and-its-impact-on-shore-power-adoption/?fbclid=IwAR2mjcFJvh5kB1fm1MTbVUK6jn2LqPbx_BNT5dq2bz6OKoI3flDLO3_7Mwg [Accessed on: 2022 Jun 5]

Appendix - Draft version of scientific paper

Integrated thermal system for hydrogen and ammonia driven cruise ship

Magnus Egerdahl

Norwegian University of Science and Technology
Trondheim, 7030, Norway, magnuege@ntnu.no

ABSTRACT

The cruise ship industry is facing emission regulations due to climate change and global warming. Traditional fossil fuels consumed for propulsion and energy demands onboard cruise ships result in a high carbon footprint. The IMO has therefore circulated guidance and proposed environmental restrictions to reduce emissions from cruise ships. The objective of this article is to design and simulate different thermal systems to increase energy efficiency and reduce emissions of hydrogen and ammonia driven cruise ships. The article investigates CO_2 refrigeration systems for energy efficient and environmentally friendly cooling. Furthermore, waste heat recovery for electricity generation and heat recovery for onboard heating demand with the integration of TES. Finally, cold recovery of LH_2 for cooling contribution with the possibility of providing cooling during port stay with zero emissions integrating CTES.

Keywords: CO_2 refrigeration, Waste heat recovery, TES, CTES, PCM, Cruise ship

1. INTRODUCTION

Summer of 2019, the cruise ship industry was thriving in a growing market. As the Covid-19 pandemic struck the world, the cruise ship industry met a standstill. This led to a great opportunity for the cruise ship industry to take charge of the environmental footprint of the industry. Traditionally, the large energy demand onboard the cruise ships is met through combustion of fossil fuels. This results in a high carbon footprint in the cruise ship industry.[1] The IMO has therefore proposed environmental restrictions to reduce emissions from cruise ships. One of these regulations include the reduction of greenhouse gas emissions by 50% by 2050, compared to emissions of 2008. Other restrictions include zero emission from cruise ships along EU harbour and ports by 2030.[2] Hydrogen and ammonia are therefore investigated as possible fuels for environmentally friendly cruise ships. Along with eco-friendly and energy-efficient propulsion systems will effort towards thermal systems onboard have a significant impact on cruise ship emissions and energy efficiency. The refrigeration systems account for a large degree of emissions due to refrigerants of high global warming potential (GWP) and refrigerant leakage. One example is R134a, a common refrigerant of marine refrigeration systems. However, has a GWP of 1300. CO_2 is therefore an attractive refrigerant due to excellent thermophysical properties and negligible GWP. High temperature exhaust gas from cruise ships is wasted into the atmosphere with a large potential for thermal energy recovery. Waste heat recovery must therefore be investigated for the possibilities of generating electricity in a bottoming power cycle or recovering heat for thermal demands onboard. Thermal boilers and auxiliary engines emit large quantities of pollutants during port stay. Thermal energy storage may solve these issues through storing thermal heat from waste heat exhaust gas or recovering cold thermal energy from regasification of liquid hydrogen, providing thermal demands with zero emissions during port stay. Cold recovery of liquid hydrogen is also attractive, with potentials of reducing refrigeration system capacity.

2. SYSTEM DESIGN AND SIMULATIONS

2.1. Reference case

For this article a case study created by Baldi et al. was used as a reference case to evaluate the potentials of increasing energy efficiency and emissions onboard a cruise ship travelling in the Baltic Sea.[3][4] The case study provides the energy demands of mechanical, electrical, heating and cooling throughout the voyage.

The energy demands are presented in Figure 1. The reference case represents operational conditions during the summer. The ambient and seawater temperature was therefore 25 ℃ and 20 ℃, respectively

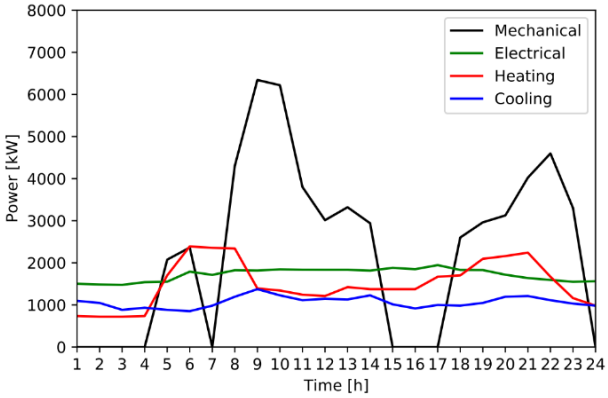

Figure 1. Energy loads

2.2. Design case

The aim of this article was to investigate possibilities of increasing energy efficiency and reducing emissions of cruise ships simulating in the simulation software Dymola. Two design cases have been considered in this study, operating with hydrogen and ammonia. The objectives were to investigate CO_2 refrigeration systems, waste heat recovery of exhaust gas, cold recovery of LH_2 and integration of TES. The fuel consumption of the main engines was then calculated based on the mechanical demand of Figure 1 and assuming a thermal efficiency of 35% and 40% and a lower heating value of 130 MJ/kg and 20 MJ/kg for the hydrogen and ammonia ICE, respectively. Furthermore, assuming an air-fuel ratio (AF) and excess air factor (λ) for both engines, the total exhaust mass flow could be calculated. For simplifications, the exhaust temperature was assumed to be a constant 400 ℃. Hydrogen ICE operates with an AF of 34.78 and λ of 4 while the ammonia ICE operates with an AF of 6.05 and λ of 1.4.[5][6] The results are plotted in Figure 2. The data was further used during simulating the thermal systems.

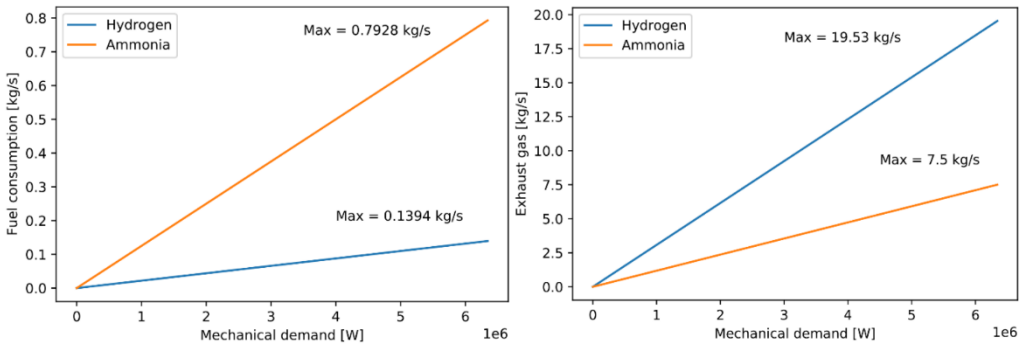

Figure 2. ICE fuel consumption and exhaust mass flow rate

To estimate the emission reduction of the proposed thermal systems, the IMO tier III NO_X regulation was used regarding emissions from the hydrogen and ammonia engines. The regulation limits NO_X emissions to 3.4 g/kWh. To provide heat from the thermal boilers, heavy fuel oil is combusted. As a result, CO_2, NO_X, and SO_X is emitted. The total emission can then be calculated based on the following fuel-based emission factors of Table 1.[2]

Table 1. Fuel-based emission factors of heavy fuel oil [2]

Emission type	Emission factor
CO_2	3.114 [kg/kg fuel]
SO_x	0.0508 [kg/kg fuel]
NO_x	0.031 [kg/kg fuel]

2.3. CO_2 refrigeration system

The reference case presents an average cooling demand of 1000 kW provided by a refrigeration unit with an EER of 3.5, equivalent to a COP of 1.03. The equipped unit performs significantly worse than state of the art refrigeration units. With the current operational conditions, a subcritical R134a cycle achieves a COP of 3.258. However, has a GWP of 1300 which contributes to global warming in the case of refrigerant leakage. A simple transcritical CO_2, transcritical CO_2 with IHX, and Transcritical CO_2 ejector cycle was therefore simulated and compared to the R134a cycle in terms of COP, the ratio of cooling output and power input. Figure 3 presents the schematic and log(p)-h diagram of the CO_2 transcritical ejector cycle. For simplifications, the cooling demand is assumed constant throughout the voyage given the low fluctuations in cooling demand as seen in Figure 1. The system was designed to operate as an indirect system. The refrigeration unit then cools water which circulates in decentralized AHU's. Water is cooled to a temperature of 7 ℃, which can be utilized to provide cool air in the cruise ship. Assuming a pinch point of 5 K and 15 K in the evaporator and gas cooler, respectively, the saturation temperature is set to 2 ℃ and the gas cooler outlet temperature is 35 ℃. The simulation models assume an isentropic efficiency of 0.8 in the compressor and an ejector efficiency 0.3.

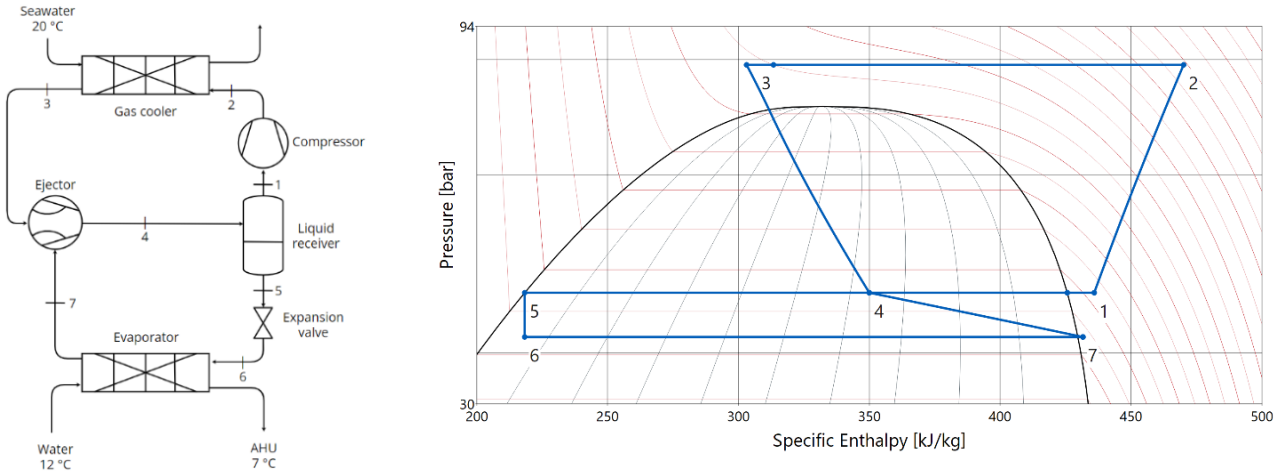

Figure 3. Transcritical ejector cycle

2.4. Waste heat recovery

The exhaust gas has great potential for waste heat recovery with a relatively large mass flow rate and heat quality of 400 ℃. This article has examined the feasibility of first recovering waste exhaust gas through electricity generation of a bottoming power cycle, then recovering excess waste heat contributing to heating demand onboard the cruise ship. The two design cases of hydrogen and ammonia operation has therefore considered two alternative waste heat recovery scenarios, to alternate the ratio of electricity generation and heat recovery. Scenario 1 for maximum electricity generation and scenario 2 prioritizing recovering 100% of the heating demand.

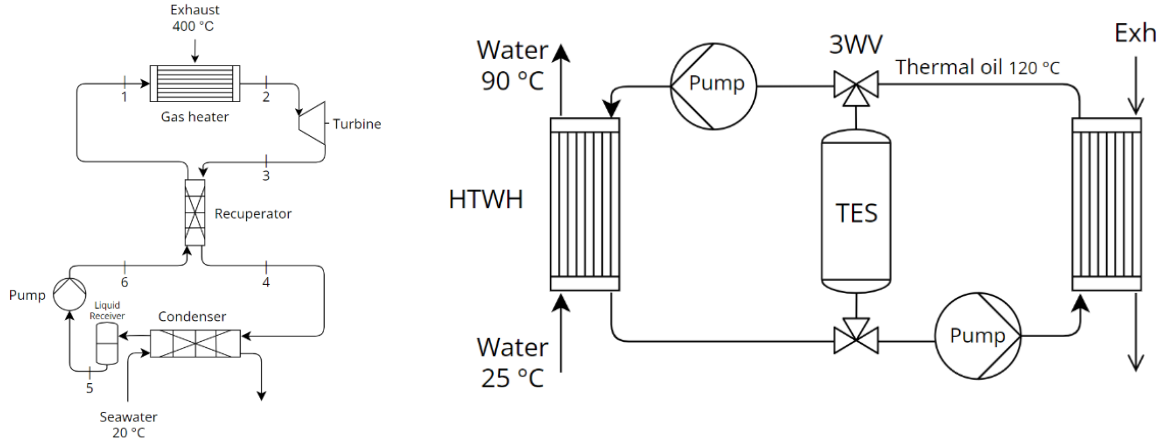

Figure 4. Waste heat recovery

2.4.1. Bottoming power cycle

Figure 4 presents the schematic of the transcritical CO_2 recuperative rankine cycle used for electricity generation. Exhaust gas superheat the working fluid in the gas heater in supercritical state. CO_2 then expands in a turbine with an isentropic efficiency of 0.9, further, pre-heating the high-side CO_2 in a recuperator with an effectiveness of 0.9. CO_2 is condensed in a condenser with a pinch point of 5 K, setting a condenser pressure of 64.34 bar. A liquid receiver was installed ensuring liquid-phase flow to the pump which lifts the pressure to 180 bar with an isentropic efficiency of 0.8. The mass flow of the working fluid was controlled manually in the pump, adjusted for optimal operational performance. The CO_2 cycle was compared to a subcritical isobutane cycle. Isobutane is a great alternative due to great thermophysical properties and low GWP, however is highly flammable and experience thermal instability at 300 ℃.[7] For comparison to the isobutane cycle, the recuperative CO_2 cycle was optimized with a gas cooler pinch point of 25 K.

2.4.2. Heat recovery

Exhaust waste heat was further recovered in the heat recovery unit. Therminol D-12 is heated to 120 ℃ which circulates providing thermal energy in the HTWH presented in Figure 4. Water with a temperature 25 ℃ is heated in a plate heat exchanger with a pinch point of 2 K, providing water of 90 ℃ for the heating demand onboard. When the heat recovery surpasses the heating demand provided in Figure 1, therminol is stored in a thermal storage tank. The amount of stored therminol is calculated using Eq.(1), where $\dot{Q}$ is the surpassed heat in kW, C_P is the specific heat capacity of therminol in kJ/kgK, and ΔT is the temperature range of heat transfer. For this study the C_P is assumed to be 2.304 kJ/kgK. With a pinch point of 2 K the ΔT is equal to 93 K. To calculate the required storage volume, a density of 723.2 kg/m^3 was assumed for Therminol D-12.

$$m = \frac{\dot{Q} \cdot 3600}{C_p \cdot \Delta T}$$

Eq.(1)

2.5. Cold recovery

The objective was to evaluate the potential of recovering cold energy from regasification of LH_2 when operating with hydrogen ICE's. Liquid hydrogen was stored onboard at -248.5 ℃ with a pressure of 3 bar for design case. The study assumes that the hydrogen ICE's require hydrogen fuel injection at conditions of 80 ℃ and 3 bar. Hydrogen must therefore be vaporized through heating to meet the engine operational criteria. The circulating water from the decentralized AHU's was then used to regasify LH_2. From Figure 5, water enters the first heat exchanger at a temperature of 12 ℃ and is cooled to 7 ℃ through regasification of LH_2. GH_2 is further heated to 80 ℃ using engine cooling water at 90 ℃. The cold energy was then circulated back to decentralized AHU's providing cool air during the summer season. Both heat exchangers assume a pinch point of 1 K.

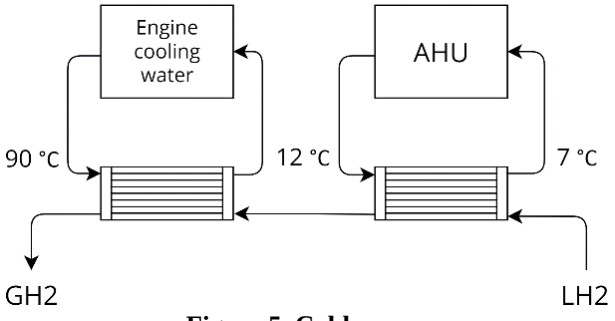

Figure 5. Cold recovery

2.6. Cold thermal energy storage

An alternative to the cold recovery through regasification of LH_2 was to integrate cold thermal energy storage (CTES). This allows cold thermal energy to be stored and later discharged during port stay. Water is chosen as phase-change material (PCM) for this application due to the easy accessibility and high latent heat of fusion of 335 kJ/kg. Assuming zero thermal losses, the CTES system is charged through regasification of LH_2 going to the main engines. The CTES system charges throughout the voyage and is designed to achieve

full charge before the port stay, with minimal subcooling of the ice. The objective was then to provide 2928 kWh of cooling during the 3-hour port stay.

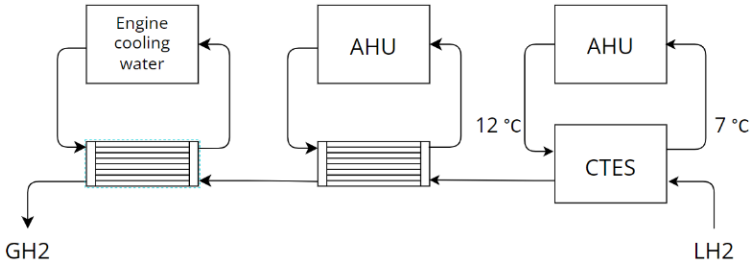

Figure 6. Cold recovery with CTES

Charging and discharging is achieved in a copper double bundle tube in tank system. LH_2 charge in one tube and water from decentralized AHU's discharge in a separate tube. The total required CTES storage volume is 57.1 m^3. Charging requires tubing with a heat transfer area of 17.3 m^2 and discharging requires heat transfer area of 1963.8 m^2.

3. RESULTS AND DISCUSSION

3.1. CO_2 refrigeration system

The subcritical R134a cycle achieved a COP of 3.258. The simple transcritical CO_2 cycle achieved a COP of 2.118 with a high-side pressure of 79.7 bar, significantly lower than the R134a cycle. The throttling losses reduce the performance of transcritical CO_2 cycles, however, the cycle experience substantially lower COP due to the low high-side pressure as well. With a constant gas cooler outlet temperature of 35 ℃, the gas cooler outlet temperature follows the 35 ℃ isothermal line as high-side pressure is increased. With the current high-side pressure, the expansion valve throttles down to a high steam mass fraction of 0.66 resulting in a low specific cooling capacity. Increasing high-side pressure will therefore increase cooling capacity resulting in increased COP. The integration of an internal heat exchanger significantly improved the COP of the refrigeration unit. The IHX pre-cools the refrigerant before the expansion valve, increasing the cooling capacity. The cycle then achieved a COP of 3.03, still outperformed by the R134a cycle. The greatest performance was achieved in the transcritical ejector cycle with a COP of 3.588. The ejector contributes to a pressure lift of 5.26 bar from the low-side to the intermediate pressure stage, reducing specific compressor work. The cycle achieves a 10.13% increase in COP compared to the R134a.

3.2. Waste heat recovery

The subcritical isobutane rankine cycle achieved a thermal efficiency of 0.196, the ratio of net power output and thermal input. Without a recuperator, the transcritical CO_2 cycle achieved a thermal efficiency of 0.1524. The cycle has substantially lower performance, yet positive attributes such as non-flammability and thermal stability. By integrating the recuperator, the thermal efficiency is improved to 0.271, 38.3% better than the isobutane cycle.

3.2.1. Electricity generation

For Scenario 1 of the hydrogen design case, the maximum and minimum electricity generation was 539 kW and 217 kW with a working fluid mass flow of 8.5 kg/s, respectively. The total electricity generation amounts to 5973 kWh with an average thermal efficiency of 0.194. Scenario 2 generates a total of 3938.3 kWh at an average thermal efficiency of 0.262. The maximum and minimum net power output was then 282.3 kW and 235 kW with a working fluid mass flow of 3.5 kg/s, respectively. Scenario 1 of the ammonia design case generates a maximum and minimum of 258 kW and 80 kW with working fluid mass flow of 4 kg/s, respectively. The total electricity generation amounts to 2652 kWh with an average thermal efficiency of 0.18. For scenario 2, the electricity generation amounts to 0. Prioritizing heat recovery, all the waste heat exhaust gas goes towards heat recovery bypassing the power cycle. This is because the total potential heat energy of the waste exhaust gas does not cover the heating demand onboard. The total electricity generation is summarized in Table 2.

Table 2. Total electricity generation

		Scenario 1	Scenario 2
Hydrogen design case	Electricity generation [kWh]	5973	3938.3
	% of total electrical demand	14.48%	9.54%
	Fuel saving [kg]	497.43	328
	% of total fuel	6.02%	3.97%
Ammonia design case	Electricity generation [kWh]	2652	0
	% of total electrical demand	6.42%	0
	Fuel saving [kg]	1256.2	0
	% of total fuel	2.71%	0

3.2.2. Heat recovery

Scenario 1 of the hydrogen design case recovered 22346 kWh of thermal energy, 61.9% of the total heating demand. For scenario 2, heat recovery was prioritized and 100% of the heating demand was covered. Scenario 1 of the ammonia design case only contribute 17.74% of the heating demand. In scenario 2, all waste heat exhaust gas was directed to the heat recovery unit with no electricity generation, yet only 56.13% of the heating demand was covered as presented in Table 3.

Table 3. Total heat recovery

		Scenario 1	Scenario 2
Hydrogen design case	Heat recovery [kWh]	22346	36107
	% of total heating demand	61.9%	100%
Ammonia design case	Heat recovery [kWh]	6407	20270
	% of total heating demand	17.74%	56.13%

3.2.3. Thermal energy storage

As presented Figure 7, the heat recovery surpassed the heating demand in scenario 1 and 2 of the hydrogen design case and scenario 2 of the ammonia design case. To prevent wasted thermal energy, this excess heat was stored in a TES tank. Using Eq.(1) and Therminol D-12 characteristics, the total required therminol storage volume was calculated. The hydrogen design case required storage volumes of 123.08 m^3 and 303 m^3 for scenario 1 and 2, respectively. Scenario 1 of the ammonia design case does not require TES but scenario 2 required a storage volume of 47.8 m^3. During the 3-hour port stay, 4417 kWh of heating is required. From Table 3, scenario 1 and 2 of the hydrogen design case can provide the heating demand during port stay. However, for the ammonia design case only 46.2% of the heating is contributed for scenario 2.

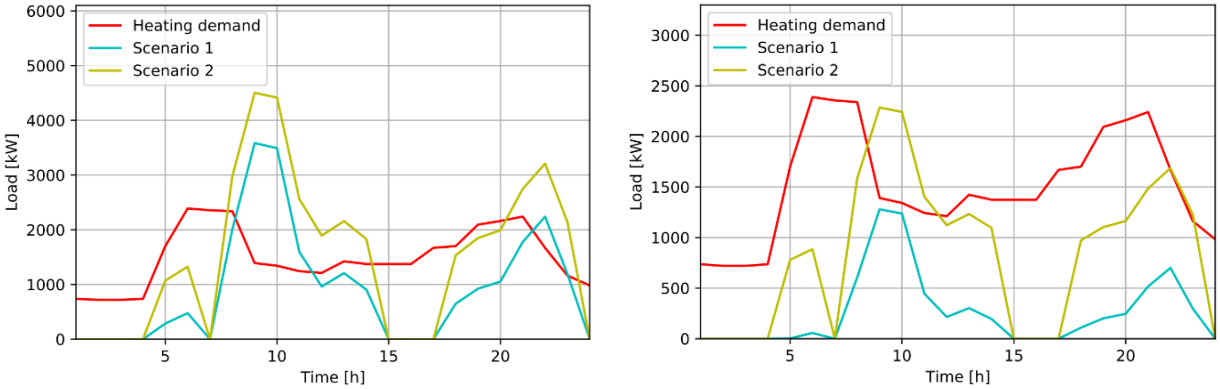

Figure 7. Electricity generation

3.3. Cold recovery

Figure 8 presents the amount of cold energy recovered at various LH_2 mass flow rates. The maximum cold recovery is 503.8 kW at a LH_2 mass flow of 0.1394 kg/s and minimum of 167 kW at a mass flow of 0.0456 kg/s. The total cold energy recovery throughout the whole voyage amounts to 4403.7 kWh, 17.22% of the total cooling demand. Considering a hydrogen auxiliary engine with a specific fuel consumption of 0.0833 kg/kWh, the total fuel saved amount to 102.22 kg assuming a COP of 3,588 in the refrigeration system. This corresponds to a NOx reduction of 4.17 kg, with respect to the IMO tier III NO_X regulation.

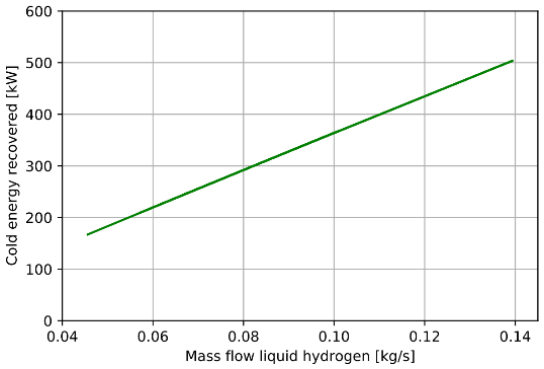

Figure 8. Cold recovery result

3.4. Cold thermal energy storage

The initial freezing in hour 0 represents start of charging after port stay in Stockholm of Figure 9. Complete charge is achieved after 20 hours and 41 minutes. The remaining 19 minutes before discharging, the ice is further subcooled to -3.25 ℃. After 3 hours, 31716.8 kg of ice is melted providing 2928.8 kWh of cooling to the decentralized AHU's as presented in Figure 9. Without CTES, this cold energy would otherwise be provided by the CO_2 refrigeration system. With a COP of 3.588, the refrigeration system consumes about 68 kg of hydrogen. With an energy-based NO_X emission of 3.4 g/kWh and a specific fuel consumption of 0.0833 kg/kWh, will the total emission saved amount to 2.774 kg during port stay.

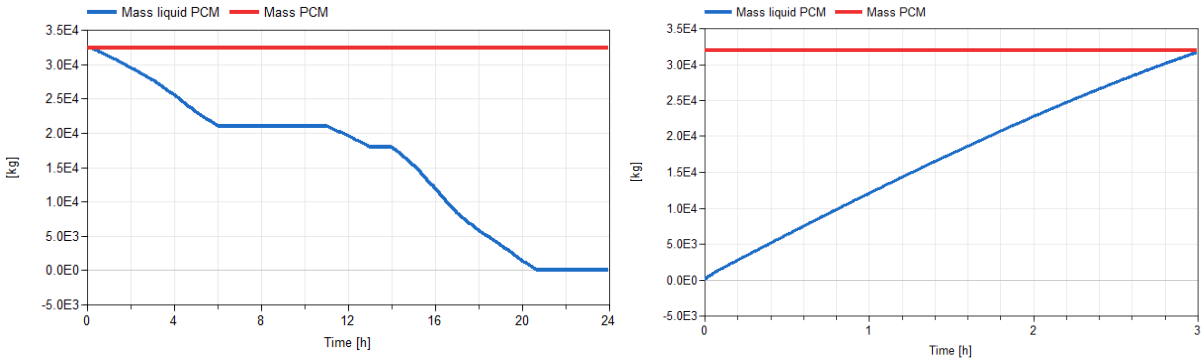

Figure 9. Charging and discharging CTES

3.5. Fuel and emission reduction

The hydrogen and ammonia auxiliary engines have a specific fuel consumption of 0.0833 kg/kWh and 0.474 kg/kWh, respectively. The total fuel saving of electricity generation and cold recovery can then be calculated and presented in Table 4.

Table 4. Total fuel reduction

		Scenario 1	Scenario 2
Hydrogen design case	Fuel saving [kg]	599.7	430.2
	% of total fuel	7.26%	5.21%
Ammonia design case	Fuel saving [kg]	1256.2	0
	% of total fuel	2.71%	0

Further, using the IMO tier III NO_X regulation and the fuel-based emission factors of Table 1, the total emission reduction can be calculated and presented in Table 5.

Table 5. Total emission reduction TES/CTES integrated

		Scenario 1	Scenario 2
Hydrogen design case	CO_2 [kg]	7693.4	12431.1
	NO_X [kg]	101.1	141.2
	SO_X [kg]	125.5	202.8
Ammonia design case	CO_2 [kg]	2205.83	6978.5
	NO_X [kg]	31	69.5
	SO_X [kg]	36	113.84

The two scenarios of waste heat recovery can then be compared in terms of fuel reduction and emission reduction. From Table 4, scenario 1 is more favourable in terms of reduced fuel consumption. From Table 5, scenario 2 is more favourable in terms of emission reduction. This includes emission reduction during port stay, one key objective of the IMO environmental regulations. Scenario 2 may therefore be found more attractive for the design cases examined.

4. CONCLUSIONS

The objective of this article was to simulate different thermal systems of hydrogen and ammonia driven cruise ships for increased energy efficiency and low emissions. A reference case by Baldi et al. was used to gather energy loads of a cruise ship travelling the Baltic Sea. Two design cases of hydrogen and ammonia operation was created. Simulations using Dymola found that a simple subcritical R134a refrigeration cycle achieved a COP of 3.258. The greatest performance of the CO_2 cycles was achieved in the transcritical ejector cycle with a COP of 3.588, which resulted in a performance increase of 10.13% in comparison to the R134a cycle. Further, the thesis investigated waste heat recovery of the main engine exhaust gas. The hydrogen design case achieved an electricity generation covering 14.48% and 9.54% of the total electrical demand for scenario 1 and 2, respectively. The waste heat exhaust gas further contributed to 61.9% and 100% of the heating demand in the heat recovery unit for scenario 1 and 2, respectively. The ammonia design case achieved an electricity generation of 6.42% of the electrical demand for scenario 1 but did not generate electricity in scenario 2. Scenario 1 only contributed 17.74% of the heating demand whereas 56.13% was contributed in scenario 2. The hydrogen design case required a TES tank volume of 123.08 m^3 and 303 m^3 for scenario 1 and 2, respectively. Scenario 1 of the ammonia design case did not require a TES. Scenario 2 required a TES volume of 47.8 m^3. Scenario 2 was found more favourable as the concept works towards achieving the emission regulation of zero emission during port stay. The thesis also investigated cold recovery of liquid hydrogen. Regasification of liquid hydrogen contributed to 17.22% of the cooling demand. This resulted in a fuel saving of 102.22 kg, corresponding to 4.17 kg NO_X reduction. Alternatively, by integrating CTES, the emission reduction could be shifted from seagoing to port stay. With a CTES tank containing ice with a total volume of 57.1 m^3, 2928 kWh of cooling could be provided during port stay. This resulted in a NO_X emission reduction of 2.774 kg amongst the harbour.

REFERENCES

1. SINTEF. CruiZE - Cruising towards Zero Emissions. Available from: https://www.sintef.no/en/projects/2020/cruize-cruising-towards-zero-emissions/ [Accessed on: 2021 Dec 16]

2. al JF et. Fourth IMO GHG Study 2020. Tech. rep. London, 2021

3. Ancona MA, Baldi F, Bianchi M, Branchini L, Melino F, Peretto A and Rosati J. Efficiency improvement on a cruise ship: Load allocation optimization. Energy Conversion and Management 2018; 164:42–58

4. Baldi F, Ahlgren F, Melino F, Gabrielii C and Andersson K. Optimal load allocation of complex ship power plants. Energy Conversion and Management 2016; 124:344–56

5. Xu X, Liu E, Zhu N, Liu F and Qian F. Review of the Current Status of Ammonia-Blended Hydrogen Fuel Engine Development. Energies 2022; 15:1023

6. Kl¨ussmann JN, Ekknud L, Ivarsson A and Schramm J. Ammonia application in CI engines. Special report, a report from the advanced motor fuels technology collaboration programme 2020

7. Astolfi M, Alfani D, Lasala S and Macchi E. Comparison between ORC and CO2 power systems for the exploitation of low-medium temperature heat sources. Energy 2018; 161:1250–61

Integrated thermal system for hydrogen and ammonia driven cruise ship

NTNU
Kunnskap for ei betre verd